PETROVIETNAM JOURNAL

An Official Publication of the Vietnam National Oil and Gas Group Vol 6 - 2016

ISSN-0866-854X

PETROVIETNAM JOURNAL IS PUBLISHED MONTHLY BY VIETNAM NATIONAL OIL AND GAS GROUP

CONTACT ADDRESS
Floor M2, VPI Tower, Trung Kinh street, Yen Hoa ward, Cau Giay district, Ha Noi
*Tel: (+84-4) 37727108 * Fax: (+84-4) 37727107 * Email: tapchidk@vpi.pvn.vn*
Mobile: 0982288671

Cover photo: Hon Rom, Mui Ne, Phan Thiet. Photo: Le Khoa

Publishing Licence No. 100/GP-BTTTT dated 15 April 2013 issued by Ministry of Information and Communications

PETROVIETNAM JOURNAL

FOCUS

PETROVIETNAM ATTENDS THE 20TH

St. Petersburg International Economic Forum

The delegation of the Vietnam Oil and Gas Group (Petrovietnam) attended the 20th St. Petersburg International Economic Forum (SPIEF 2016) from 18 - 20 June 2016. In the framework of this important event, Petrovietnam's leader had meetings and working sessions with the Russian partners, contributing to strengthening and promoting co-operation in the field of oil and gas. In particular, Rosneft has signed a contract to supply 96 million tons of crude oil to Petrovietnam Oil Corporation (PV OIL) from now to 2040.

Rosneft is expected to supply up to 96 million tons of crude oil to PV OIL from now to 2040. Photo: PV OIL

4

FOCUS

ENSURING THE CONSTRUCTION PROGRESS of Nghi Son Refinery and Petrochemical Complex

Deputy Prime Minister Trinh Dinh Dung on 21 June 2016 chaired a meeting with relevant ministries and agencies to seek solutions to a number of obstacles encountered during the process of construction of the Nghi Son Refinery and Petrochemical Complex. He stressed that Nghi Son complex is among the nation's key projects which contributes to ensuring the national energy security, creating jobs and producing a variety of products to cater for industries, especially domestic support industries.

Deputy Prime Minister Trinh Dinh Dung chaired a meeting with relevant ministries and agencies to seek solutions for accelerating the construction of the Nghi Son Refinery and Petrochemical Complex. Photo: Nhat Bac

Speaking at the meeting, Deputy Prime Minister Trinh Dinh Dung assigned the Ministry of Industry and Trade, other ministries and agencies concerned, and the People's Committee of Thanh Hoa province to closely work with the investors to ensure the construction progress of the complex.

He asked the Ministry of Finance, in co-ordination with the Ministry of Industry and Trade and the Ministry of Planning and Investment, to clearly determine the total rate of support and incentives for the complex for each year and each oil price scenario, and on that basis to make recommendations to the government and the Prime Minister for solutions to remove difficulties and obstacles to ensure the project's overall effectiveness.

Regarding product consumption, the Deputy Prime Minister asked the Ministry of Industry and Trade and relevant ministries and agencies to work with petroleum importing and distributing companies to develop plans for refined petroleum product distribution in the domestic market in order to ensure the consumption of products from domestic factories. The plans for consumption of petroleum products in the domestic market should ensure the harmonisation of the interests of the State, the investors and the people.

Deputy Prime Minister Trinh Dinh Dung assigned the Ministry of Science and Technology, in collaboration with the relevant

6

SCIENTIFIC RESEARCH

PETROLEUM EXPLORATION & PRODUCTION

FAULT SEAL CAPACITY EVALUATION IN BLOCK 04-3 OF NAM CON SON BASIN, OFFSHORE VIETNAM

Bui Huy Hoang[1], Nguyen Thanh Lam[1], Phung Van Phong[1] Nguyen Tuan Anh[1], Pham Xuan Son[2] Vu Tuan Anh[3], Nguyen Lam Anh[3], Pham Viet Au[3], Nguyen Van Thang[4]
[1]Vietnam Petroleum Institute
[2]Vietsovpetro
[3]PVEP Song Hong Company Limited
Email: hoangbh.epcdvpi.pvn.vn

Summary

The purpose of the study is to evaluate the fault seal capacity and hydrocarbon (HC) retention potential of the Miocene - Oligocene fault-bounded structures in Block 04-3, Nam Con Son basin, offshore southern Viet Nam. Seismic and well petrophysical interpretation data are used to build 3D fault model and stratigraphic model within the 6 selected structures. Parameters such as fault throw, bed thickness, Vshale, lithology, burial depth, and fluid density are incorporated into fault seal evaluation. The critical leak points at the Middle Miocene, Lower Miocene and Oligocene intervals on faults bounding the 6 structures are defined. Hydrocarbon column heights supported by the faults can be estimated using the empirical relationship between Shale Gouge Ratio and threshold pressure. The study predicts that the maximum gas column ranges from 136m to 252m in Middle-Lower Miocene reservoirs in the drilled structures and from 119m to 295m in Middle-Lower Miocene and Oligocene reservoirs in the undrilled structures.

Key words: *Fault seal analysis, prospect, Shale Gouge Ratio (SGR), Clay Smear Potential (CSP), gas column height, hydrocarbon column height, hydrocarbon density, threshold pressure, spill-point.*

1. Introduction

For fault-bounded structures, fault seal analysis is critical in evaluating risks, ranking prospects and optimising the drilling priority. The study aims to determine the seal capacity of the bounding faults, identify potential leak points on the faults, and calculate the theoretical maximum HC column height that can be supported by the fault. The 6 structures chosen for fault seal analysis are A, B, C, D, E and F in Block 04-3, among which structures A, B, and C are drilled, and structures D, E and F are undrilled. The targets of these structures are Oligocene clastic, Miocene clastic and Miocene carbonate reservoirs. The analysis from the drilled structures will be used to extrapolate and reduce uncertainties for the undrilled structures.

2. Geological overview

2.1. Structural geology

Block 04-3 is located in the northeast of the Nam Con Son basin (NCSB), offshore southern Vietnam. The structural map and the general stratigraphic column of Nam Con Son basin are illustrated in Figure 1. In Block 04-3, the western area is on the Mang Cau high (A2 in Figure 1), while the eastern area is in the Central trough (A3 in Figure 1).

The geological evolution of the basin can be divided into 3 episodes: pre-rift (Pre-Tertiary), syn-rift (Oligocene - Middle Miocene), and post-rift (Middle Miocene - Present) (Figure 2). The Oligocene formation is composed of interbedding sand-shale, deposited in fluvial, delta to lacustrine environment. The Early Miocene formation is composed of interbedding sand, shale and silt with occasional coal, and deposited in delta plain, coastal to shallow marine environment. The Middle Miocene formation can be divided into 2 parts: the lower part consists of interbedding sand, shale and silt with occasional carbonate; and the upper part consists of carbonate interbedding with sand, shale and marl (Figure 1 b).

In the 6 structures chosen for fault seal analysis, the main trend of the faults is NE-SW, and they were formed either during the intra-Middle Miocene, or at the end of Middle Miocene. A number of main bounding faults were active until the Late Miocene. The structures in this study formed either at the end of Middle Miocene (structures C and D) or Late Miocene (structures A, B, E and F) (Figure 2).

2.2. Hydrocarbon occurrences

The study area and adjacent areas have several gas and gas-condensate discoveries in Middle-Lower Miocene and Oligocene sandstone, and Middle Miocene carbonate.

8

FOCUS

NEWS

OIL AND GAS MARKET

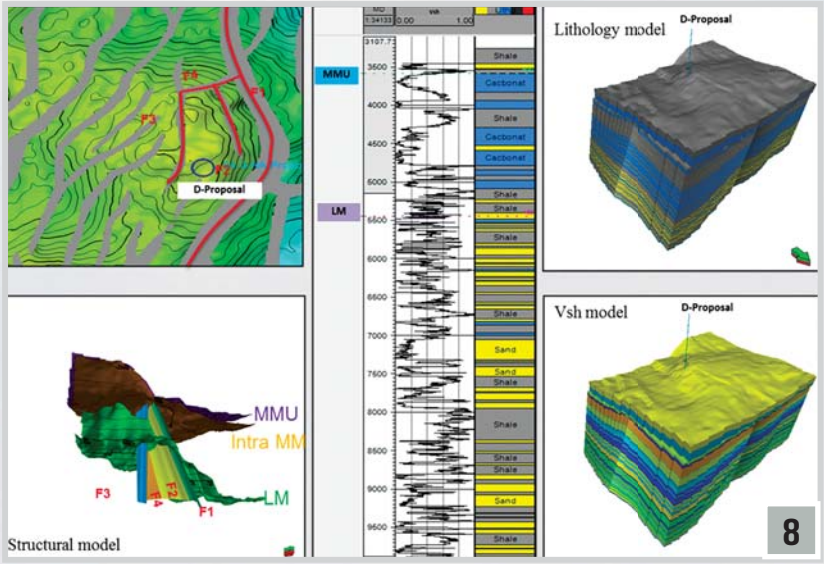

8

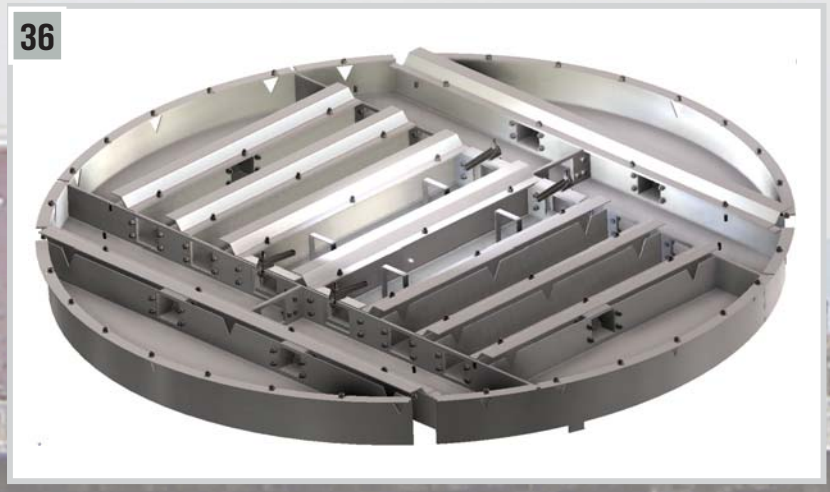

36

PETROVIETNAM ATTENDS THE 20TH St. Petersburg International Economic Forum

The delegation of the Vietnam Oil and Gas Group (Petrovietnam) attended the 20th St. Petersburg International Economic Forum (SPIEF 2016) from 18 - 20 June 2016. In the framework of this important event, Petrovietnam's leader had meetings and working sessions with the Russian partners, contributing to strengthening and promoting co-operation in the field of oil and gas. In particular, Rosneft has signed a contract to supply 96 million tons of crude oil to Petrovietnam Oil Corporation (PV OIL) from now to 2040.

Rosneft is expected to supply up to 96 million tons of crude oil to PV OIL from now to 2040. Photo: PV OIL

Dr. Phan Ngoc Trung, Member of Petrovietnam's Board of Directors, witnessed the signing of the contract between Rosneft and PV OIL. Photo: Nguyen Ban

Petrovietnam's delegation at the meeting with Zarubezhneft and Lukoil's leaders. Photo: Nguyen Ban

SPIEF, considered as Russia's Davos, is an annual economic forum which gathers many government leaders and chief executives of major companies around the world. With the theme "Capitalising on the new global economic reality", SPIEF 2016 attracted over 12,000 delegates from more than 100 countries. This event is evaluated as positively contributing to the building of macro-economic development models and promoting comprehensive co-operation between Russian companies and foreign partners.

In the framework of this important event, Petrovietnam's delegation joined the discussions on economy, oil and gas, and energy, and attended SPIEF 2016's special events such as the Plenary session "Capitalising on the new global economic reality" (with the participation of Russian President Vladimir Putin); the Energy Company Summit "World oil market at crossroads: Uncertainty investments or risk management?"; and the Global Energy Prize Award Ceremony, etc.

During the time of SPIEF 2016, Petrovietnam's leader also had meetings and bilateral working sessions with the senior leaders of Russia's major oil and gas corporations and international oil and gas companies. Dr. Phan Ngoc Trung, Member of Petrovietnam's Board of Directors, had a working meeting with Mr. Igor Sechin, Chairman of Rosneft's Management Board, and witnessed the signing of a contract to supply crude oil between Rosneft and Petrovietnam Oil Corporation (PV OIL). Accordingly, Rosneft is expected to supply up to 96 million tons of crude oil to PV OIL from now to 2040. According to Mr. Igor Sechin: "Successfully working with Petrovietnam in the exploration and production of hydrocarbons in Vietnamese offshore, Rosneft is interested in further expansion of its business in the country, including refining, petrochemicals, commerce and logistics. The new stage of co-operation will enable the company to get a new channel of marketing hydrocarbons in the Asia - Pacific market and create additional synergies due to refining in the region".

During this business trip to Russia, Petrovietnam's leaders had a working meeting with Mr. Sergey Kudryashov, General Director of Zarubezhneft. The two sides discussed the co-operation in the joint venture projects in both Vietnam and Russia, as well as the commitment of the two sides to continue efforts to promote co-operation in the coming period. The delegation also had a meeting with Zarubezhneft and Lukoil to exchange and seek possible co-operation in the field of construction of underground storages in Vietnam.

The Petrovietnam's delegation also paid a working visit to Gazpromviet during this business trip. Leaders of Gazpromviet reported to Dr. Phan Ngoc Trung and Petrovietnam's delegation on the implementation results and field development plan in 2016 - 2017 of two projects in Nagumanovskoye field (Orenburg province) and Severo-Purovskoye field (Autonomous Region of Yamal - Nenets). The Petrovietnam's leader requested Gazpromviet to continue to implement measures to improve investment efficiency, and ensure the interests of the staff of both parties of the projects.

Nguyen Ban - Thu Huyen

ENSURING THE CONSTRUCTION PROGRESS of Nghi Son Refinery and Petrochemical Complex

Deputy Prime Minister Trinh Dinh Dung on 21 June 2016 chaired a meeting with relevant ministries and agencies to seek solutions to a number of obstacles encountered during the process of construction of the Nghi Son Refinery and Petrochemical Complex. He stressed that Nghi Son complex is among the nation's key projects which contributes to ensuring the national energy security, creating jobs and producing a variety of products to cater for industries, especially domestic support industries.

Deputy Prime Minister Trinh Dinh Dung chaired a meeting with relevant ministries and agencies to seek solutions for accelerating the construction of the Nghi Son Refinery and Petrochemical Complex. Photo: Nhat Bac

Speaking at the meeting, Deputy Prime Minister Trinh Dinh Dung assigned the Ministry of Industry and Trade, other ministries and agencies concerned, and the People's Committee of Thanh Hoa province to closely work with the investors to ensure the construction progress of the complex.

He asked the Ministry of Finance, in co-ordination with the Ministry of Industry and Trade and the Ministry of Planning and Investment, to clearly determine the total rate of support and incentives for the complex for each year and each oil price scenario, and on that basis to make recommendations to the government and the Prime Minister for solutions to remove difficulties and obstacles to ensure the project's overall effectiveness.

Regarding product consumption, the Deputy Prime Minister asked the Ministry of Industry and Trade and relevant ministries and agencies to work with petroleum importing and distributing companies to develop plans for refined petroleum product distribution in the domestic market in order to ensure the consumption of products from domestic factories. The plans for consumption of petroleum products in the domestic market should ensure the harmonisation of the interests of the State, the investors and the people.

Deputy Prime Minister Trinh Dinh Dung assigned the Ministry of Science and Technology, in collaboration with the relevant

The construction site at Nghi Son Refinery and Petrochemical Complex. Photo: PVN

With the largest foreign direct investment (FDI) in Viet Nam so far (over USD 9 billion), the Nghi Son Refinery and Petrochemical Complex will robustly boost the socio-economic development of the area covering the south of Thanh Hoa province, the north of Nghe An province and the vicinities. The project is expected to create jobs for tens of thousands of people during the construction phase and for thousands of people during the operational phase. According to its schedule, the project will go on stream in 2017 and together with Dung Quat Refinery will meet two-thirds of the domestic demand for petroleum products.

agencies, to provide guidance on norms and standards for oil and gas products to be consumed domestically to meet the requirements of international commitments acceded to by Vietnam, as well as the requirements of environmental protection and response to climate change. The Ministry of Public Security directs the fire prevention and control agencies to study the proposal of the Vietnam Oil and Gas Group concerning the installation of automatic fire prevention and control system in parallel with the process of commissioning and inspection before commercial operation.

Built on an area of 400ha at Nghi Son Economic Zone (Thanh Hoa province), with construction commencing in 2013, the Nghi Son Refinery and Petrochemical Complex is a key petroleum project of political, economic and social importance in the cause of development of the country, contributing to ensuring energy security for the nation. The success of this project will be an important factor to attract further foreign investors into Vietnam, especially investors from Japan and Kuwait. The Complex, which is scheduled to start commercial operation in 2017 with a refining capacity of 200,000 barrels per day (equivalent to 10 million tons per year), will supply about 40% of Vietnam's petroleum products demand.

Nguyen Hoang

FAULT SEAL CAPACITY EVALUATION IN BLOCK 04-3 OF NAM CON SON BASIN, OFFSHORE VIETNAM

Bui Huy Hoang[1], Nguyen Thanh Lam[1], Phung Van Phong[1] Nguyen Tuan Anh[1], Pham Xuan Son[2]
Vu Tuan Anh[2], Nguyen Lam Anh[2], Pham Viet Au[2], Nguyen Van Thang[3]
[1]*Vietnam Petroleum Institute*
[2]*Vietsovpetro*
[3]*PVEP Song Hong Company Limited*
Email: hoangbh.epc@vpi.pvn.vn

Summary

The purpose of the study is to evaluate the fault seal capacity and hydrocarbon (HC) retention potential of the Miocene - Oligocene fault-bounded structures in Block 04-3, Nam Con Son basin, offshore southern Viet Nam. Seismic and well petrophysical interpretation data are used to build 3D fault model and stratigraphic model within the 6 selected structures. Parameters such as fault throw, bed thickness, Vshale, lithology, burial depth, and fluid density are incorporated into fault seal evaluation. The critical leak points at the Middle Miocene, Lower Miocene and Oligocene intervals on faults bounding the 6 structures are defined. Hydrocarbon column heights supported by the faults can be estimated using the empirical relationship between Shale Gouge Ratio and threshold pressure. The study predicts that the maximum gas column ranges from 136m to 252m in Middle-Lower Miocene reservoirs in the drilled structures and from 119m to 295m in Middle-Lower Miocene and Oligocene reservoirs in the undrilled structures.

Key words: *Fault seal analysis, prospect, Shale Gouge Ratio (SGR), Clay Smear Potential (CSP), gas column height, hydrocarbon column height, hydrocarbon density, threshold pressure, spill-point.*

1. Introduction

For fault-bounded structures, fault seal analysis is critical in evaluating risks, ranking prospects and optimising the drilling priority. The study aims to determine the seal capacity of the bounding faults, identify potential leak points on the faults, and calculate the theoretical maximum HC column height that can be supported by the fault. The 6 structures chosen for fault seal analysis are A, B, C, D, E and F in Block 04-3, among which structures A, B, and C are drilled, and structures D, E and F are undrilled. The targets of these structures are Oligocene clastic, Miocene clastic and Miocene carbonate reservoirs. The analysis from the drilled structures will be used to extrapolate and reduce uncertainties for the undrilled structures.

2. Geological overview

2.1. Structural geology

Block 04-3 is located in the northeast of the Nam Con Son basin (NCSB), offshore southern Vietnam. The structural map and the general stratigraphic column of Nam Con Son basin are illustrated in Figure 1. In Block 04-3, the western area is on the Mang Cau high (A2 in Figure 1), while the eastern area is in the Central trough (A3 in Figure 1).

The geological evolution of the basin can be divided into 3 episodes: pre-rift (Pre-Tertiary), syn-rift (Oligocene - Middle Miocene), and post-rift (Middle Miocene - Present) (Figure 2). The Oligocene formation is composed of interbedding sand-shale, deposited in fluvial, delta to lacustrine environment. The Early Miocene formation is composed of interbedding sand, shale and silt with occasional coal, and deposited in delta plain, coastal to shallow marine environment. The Middle Miocene formation can be divided into 2 parts: the lower part consists of interbedding sand, shale and silt with occasional carbonate; and the upper part consists of carbonate interbedding with sand, shale and marl (Figure 1b).

In the 6 structures chosen for fault seal analysis, the main trend of the faults is NE-SW, and they were formed either during the intra-Middle Miocene, or at the end of Middle Miocene. A number of main bounding faults were active until the Late Miocene. The structures in this study formed either at the end of Middle Miocene (structures C and D) or Late Miocene (structures A, B, E and F) (Figure 2).

2.2. Hydrocarbon occurrences

The study area and adjacent areas have several gas and gas-condensate discoveries in Middle-Lower Miocene and Oligocene sandstone, and Middle Miocene carbonate.

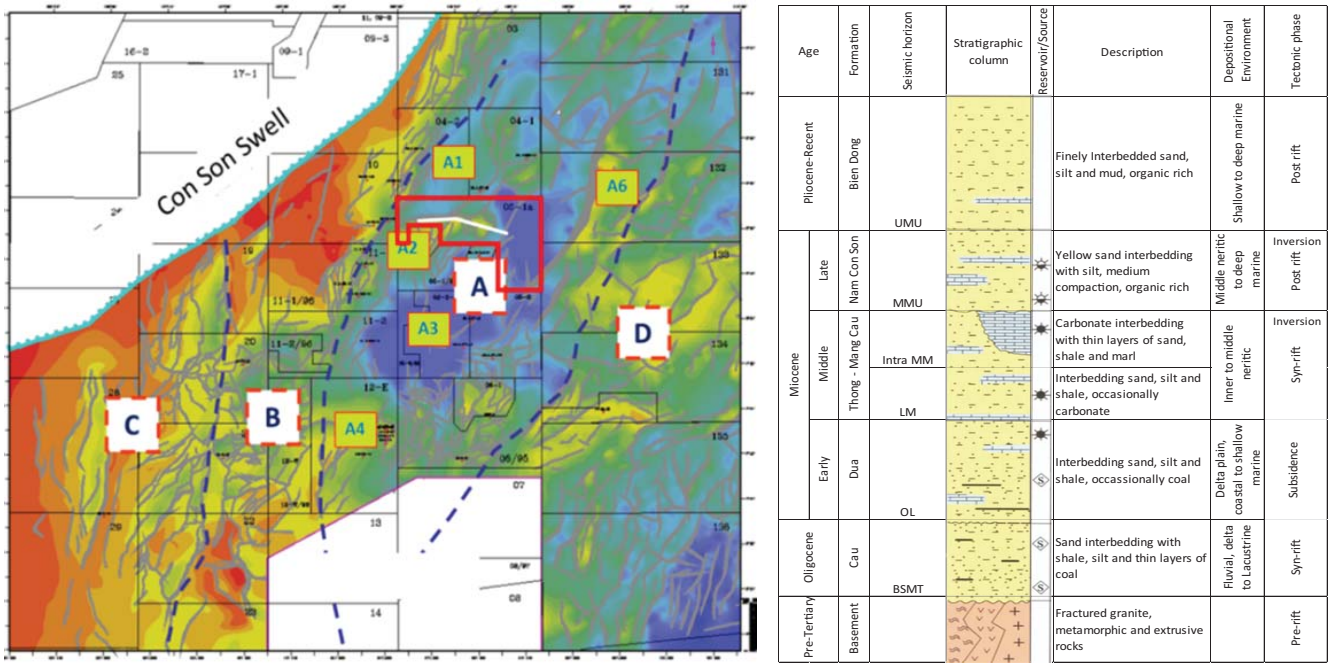

(a) (b)

Figure 1. *The structural map with major structural components (a) and the general stratigraphic column (b) of the Nam Con Son basin [1]. The study area is highlighted. The white line in the study area is the position of the seismic profile in Figure 2*

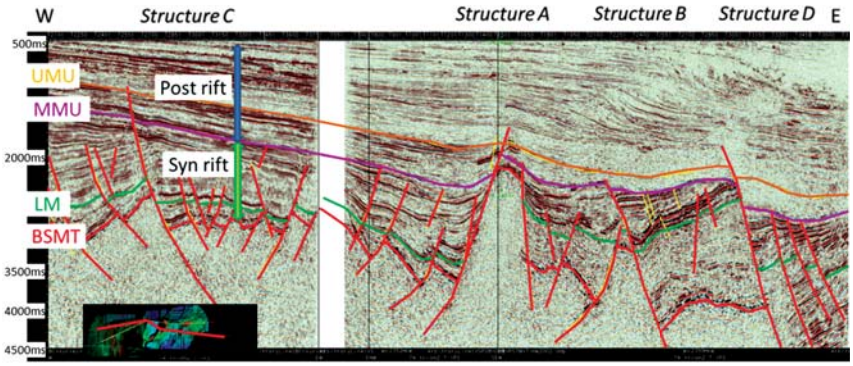

UMU = Upper Miocene Unconformity, MMU = Middle Miocene Unconformity, LM = Lower Miocene, BSMT = Basement

Figure 2. *A seismic cross-section through the study area [2]*

2.3. Reservoir engineering

Available data are not sufficient to determine HC-water contacts, as well as pressure regimes on both sides of the faults. However, available DST (Drill-stem Test) data can be used to estimate gas density at reservoir condition. In the Early Miocene reservoir, the estimated HC density is 0.24g/cc, while in the Middle Miocene reservoir the density ranges from 0.27 to 0.28g/cc. These gas densities are essential to predict the maximum HC column height using the methodology in section 3.

3. Methodology

There are 2 kinds of seal at a given point on a fault:

- Seal by juxtaposition: it happens through juxtaposition of one interval against an impermeable interval, most commonly shales;

- Seal by fault deformation zone: fault deformation creates fault rocks that are significantly reduced in porosity and permeability. For this type of seal, the dominating seal mechanism is capillary seal [3, 4].

For an interval of interest, the fault can seal if any of the above seal conditions are satisfied, and the fault has not been reactivated after the trap formed [5].

Seal by juxtaposition can be evaluated with a juxtaposition diagram, whereas seal by fault deformation zone needs to be evaluated using various parameters such as SGR, CSP and threshold pressure. The following sections present the methodologies involved in evaluating seal capacity of fault deformation zone.

The most common method to characterise fault zone deformation products is the Shale Gouge Ratio (SGR) method, which approximates the clay content of the fault zone. It is based on the assumption that the clay content of the host rock along the fault is evenly distributed on the fault plane. The basic formula for SGR [6] is:

$$SGR = \frac{\sum(Layer\ clay\ content\ \times Bed\ thickness)}{Throw} = \frac{\sum(Vcl\ \times \Delta z)}{Throw}$$

The higher the SGR value, the higher the clay content along the fault is, and therefore the higher the sealing capacity. If the shale layers in the study area are thick, then the shale layers can be smeared along the fault and impeded HC flow. In such cases, we need to consider other methods such as Clay Smear Potential (CSP) and Shale Smear Factor (SSF) [7, 8]. The formulas for CSP and SSF are:

$$CSP = \frac{\sum(Shale\ bed\ thickness)^2}{Distance\ from\ source\ bed}$$

$$SSF = \frac{Fault\ throw}{Shale\ layer\ thickness}$$

Fault seal potential can be further enhanced through diagenesis process, whereby cementation at great burial depth can reduce the porosity and permeability at the fault zone [9, 10].

After calculating SGR, we can calculate the threshold across fault pressure difference that the fault can sustain before being breached based on the empirical relationship from Bretan et al. [11]:

$$\Delta P = 10^{(\frac{SGR}{27} - C)}$$

In which ΔP is threshold pressure in bar, C is a constant varying based on the depth of the interval of interest: C = 0.5 at depth < 3km, C = 0.25 at depth between 3 and 3.5km, and C = 0 at depth > 3.5km.

SGR sealing threshold for HC-HC juxtaposition is SGR > 0.4, while for HC-water juxtaposition it is at least 0.2. The threshold pressure does not increase in the SGR range of 0.4 - 1, therefore the maximum column height does not increase in that range [11].

Based on the above threshold pressure, we can calculate the maximum HC column height corresponding to an SGR value by the following formula [11]:

$$H_{max} = \Delta P/\Delta\rho g = 10^{(\frac{SGR}{27} - C)/\Delta\rho g}$$

Where H_{max} is the maximum column height (m), ΔP is the threshold pressure (Pa), Δρ is the density difference between water and HC (kg/m³), and g is the gravitational acceleration constant. As mentioned above, ΔP has a limit at around SGR = 0.4, therefore H_{max} will also has a limit at the respective value.

Since fault properties vary vertically and laterally along the fault surface, H_{max} will also vary accordingly. To account for such heterogeneity, we need to calculate H_{max} for every node on the fault model, and convert them into contact depth by adding the depth of the structural crest. Then the actual maximum HC column height supported by the fault is determined by the point with the shallowest contact depth.

In addition, the determined HC contact depth must not be deeper than the structural spill-point, and the maximum column height does not increase in the SGR range of 0.4 - 1. Therefore, the steps involved in determining the maximum HC column height are as follow:

- Calculate H_{max} and the corresponding contact depth for every possible leak point on the fault model interval where SGR < 0.4. The contact depth will be limited by the spill-point depth;

- The deepest fluid contact depth supported by the fault will be the minimum value of the every possible leak point's contact depth.

4. Fault seal capacity evaluation

This study focused on 6 structures in Block 04-3, 3 of which are drilled (structures A, B, and C) and 3 are undrilled (structures D, E and F).

All the drilled structures are on the Mang Cau high (Figure 3). In this area, the Miocene sediments are deposited directly on the Pre-Tertiary basement. Among the undrilled structures, structure D is on the Mang Cau high, and structure E and F are in the central trough zone of the Nam Con Son basin. The study focused on major faults that can affect the structural closure of the prospect.

To construct a 3D model of the subsurface structure, fault sticks and horizon picks are imported into Petrel modelling software. Well log data (Lithology and Vshale) are used to populate the 3D model, so that fault plane properties can be extracted for further analysis. For undrilled exploration targets, a hypothetical well will be determined with its well data inferred from nearby wells and from the depositional environment trend.

There are no published articles on fault seal for carbonate, therefore in this study we use the following threshold values for determining reservoirs: The Vshale (Vsh) cutoff for reservoir is < 0.4 and non-reservoir is > 0.4 for both clastic and carbonate, and an additional effective porosity cutoff of > 5% is applied to the carbonate reservoir. This porosity cutoff

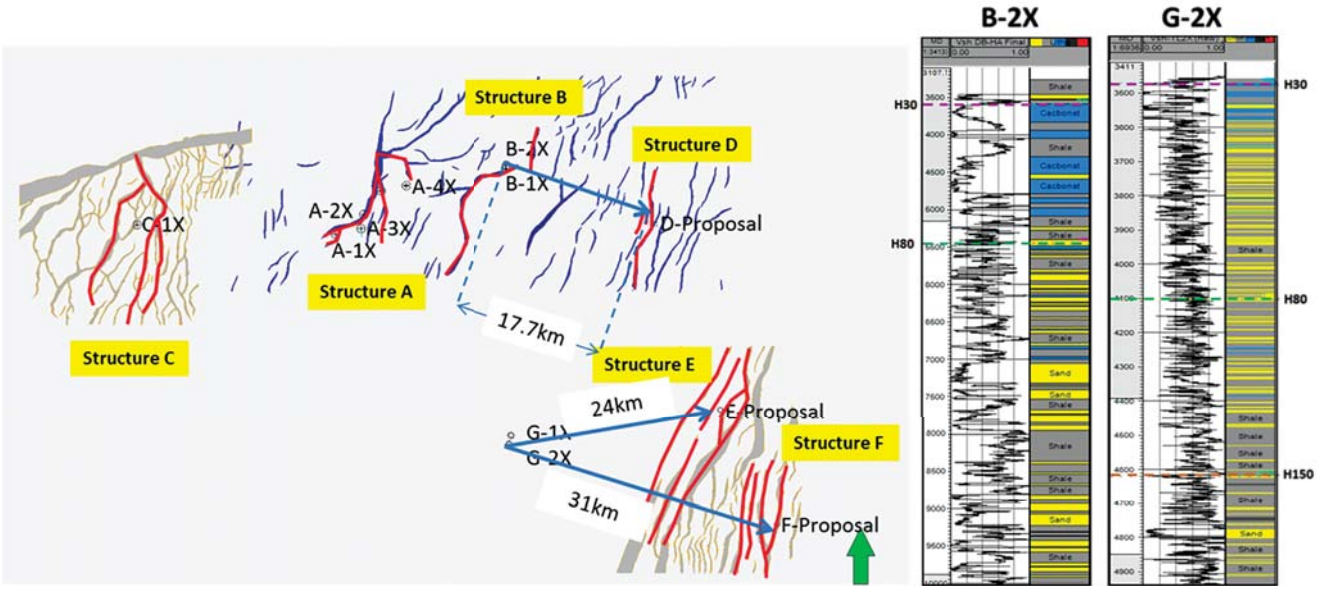

Figure 3. *Structures and their chosen faults for fault seal analysis study in Block 04-3. Arrows indicate the wells used as lithology model for the proposal wells. The distances from the model well to the proposal well are also indicated*

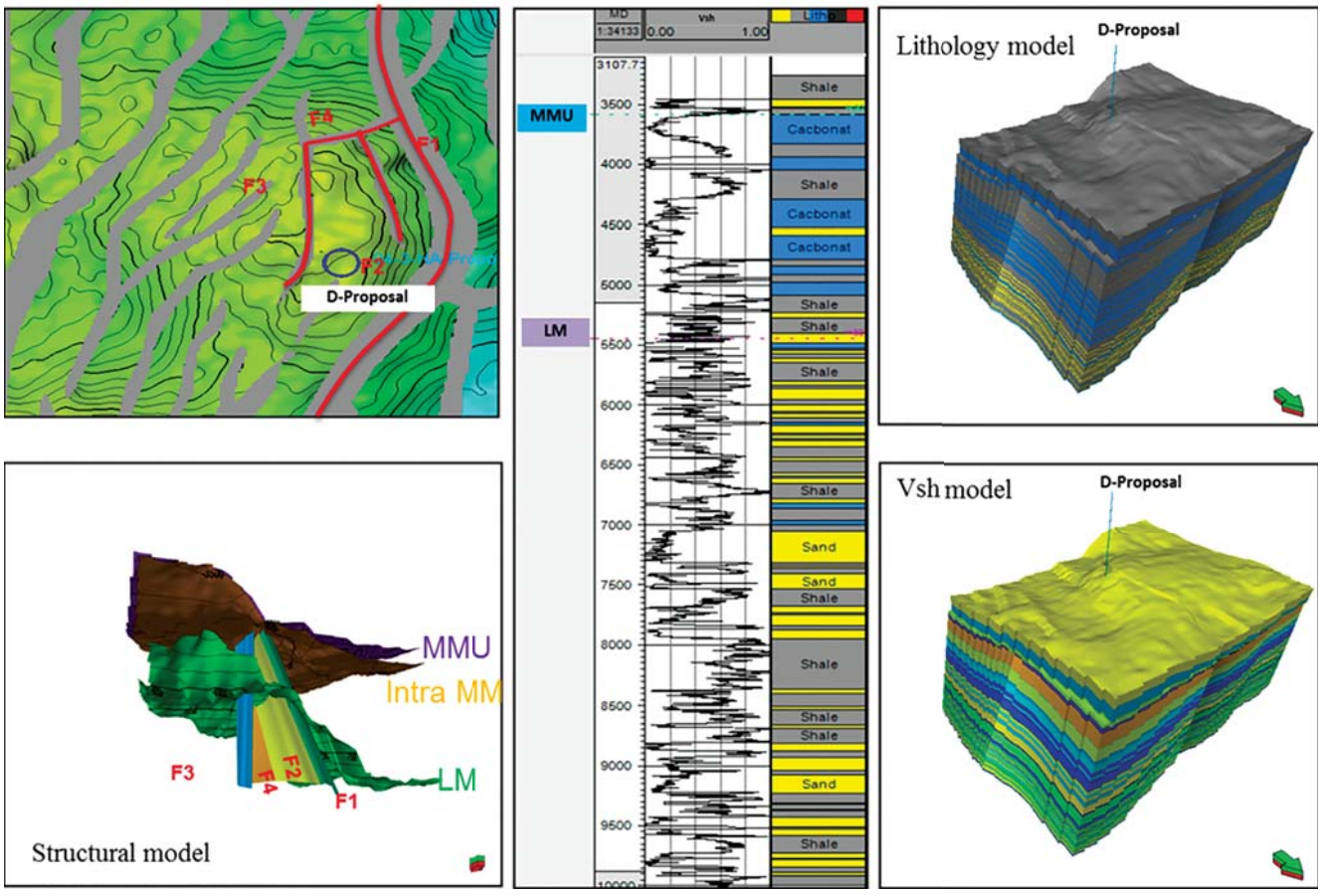

Figure 4. *Lithological and Vshale models for the undrilled structure D are based on well B-2X*

has been used for evaluating carbonate reservoirs in the Nam Con Son basin [12].

From the discussion in section 2.2, the Vshale, porosity and lithological model for the undrilled prospects are based on nearby wells as follow: structures E and F are based on well G-2X, and structure D is based on well B-1X (Figure 3, 4). Since the reservoirs are mainly silty sands, clay mixing along the fault zone is probably the dominant fault seal mechanism. Therefore, SGR is chosen as the main algorithm.

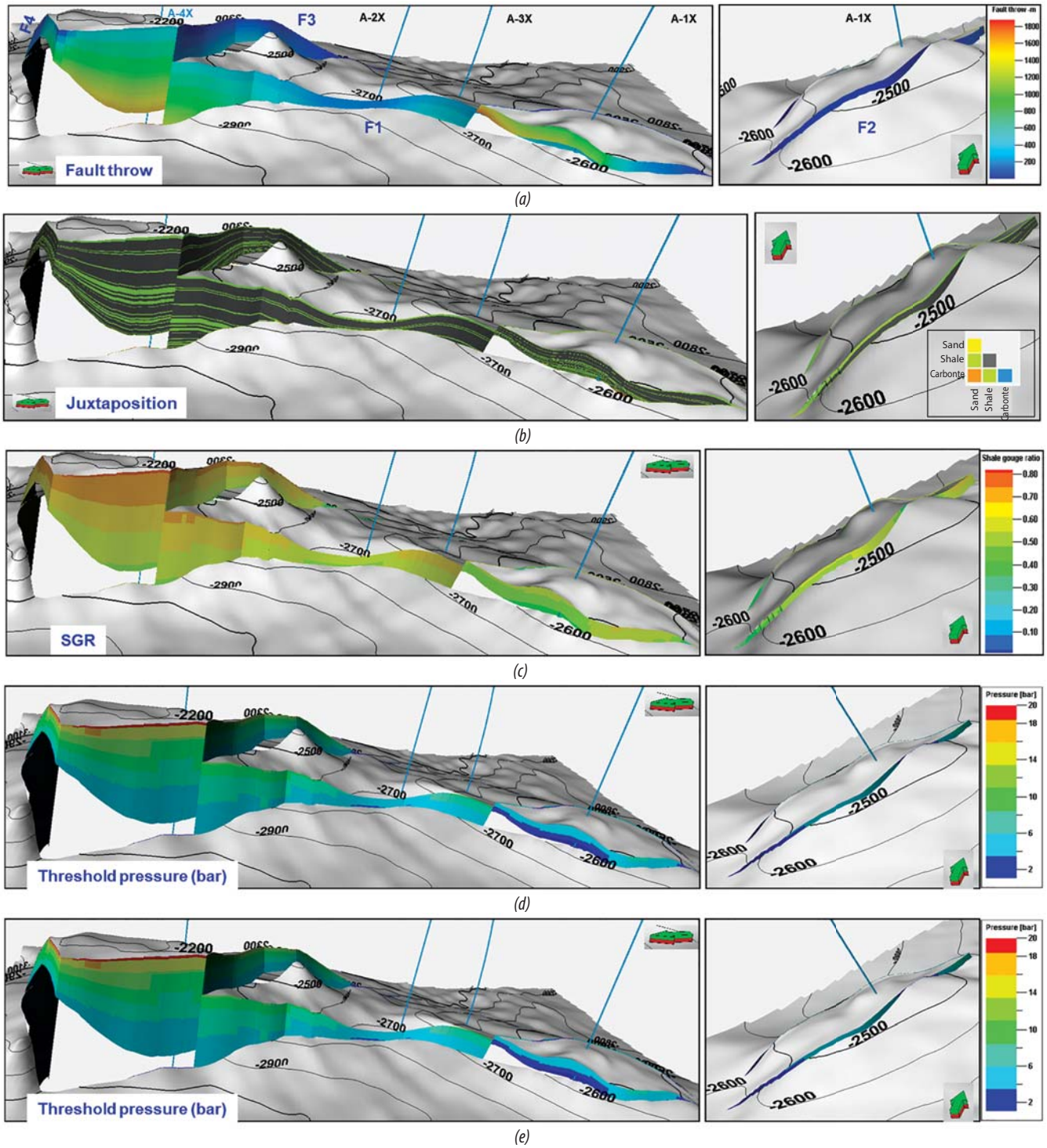

Figure 5. *Fault throw, lithological juxtaposition, SGR, threshold pressure and predicted HC column height for structure A, illustrated on MMU horizon map*

Lithological juxtaposition diagrams express the juxtaposition of various lithologies on the fault surface. It provides a quick look on the possible leak points on the faults, which are sand on sand, sand on carbonate, and carbonate on carbonate juxtapositions. Most of the structures have multiple leak points in each interval, therefore an analysis of fault rock processes based on SGR and CSP is critical in accurately evaluating the fault seal capacity.

Fault throws in the study area vary according to structural trend. Structures on the Mang Cau high (A, B, C, and D) have large throw (maximum throw can be over 1,600m), while in the Nam Con Son basin central trough (structures E and F) the throw is smaller (maximum throw 200 - 450m) (Figure 5a, Table 1).

SGR calculations for all faults bounding the structures are illustrated in Table 1. In the drilled structure A, DST

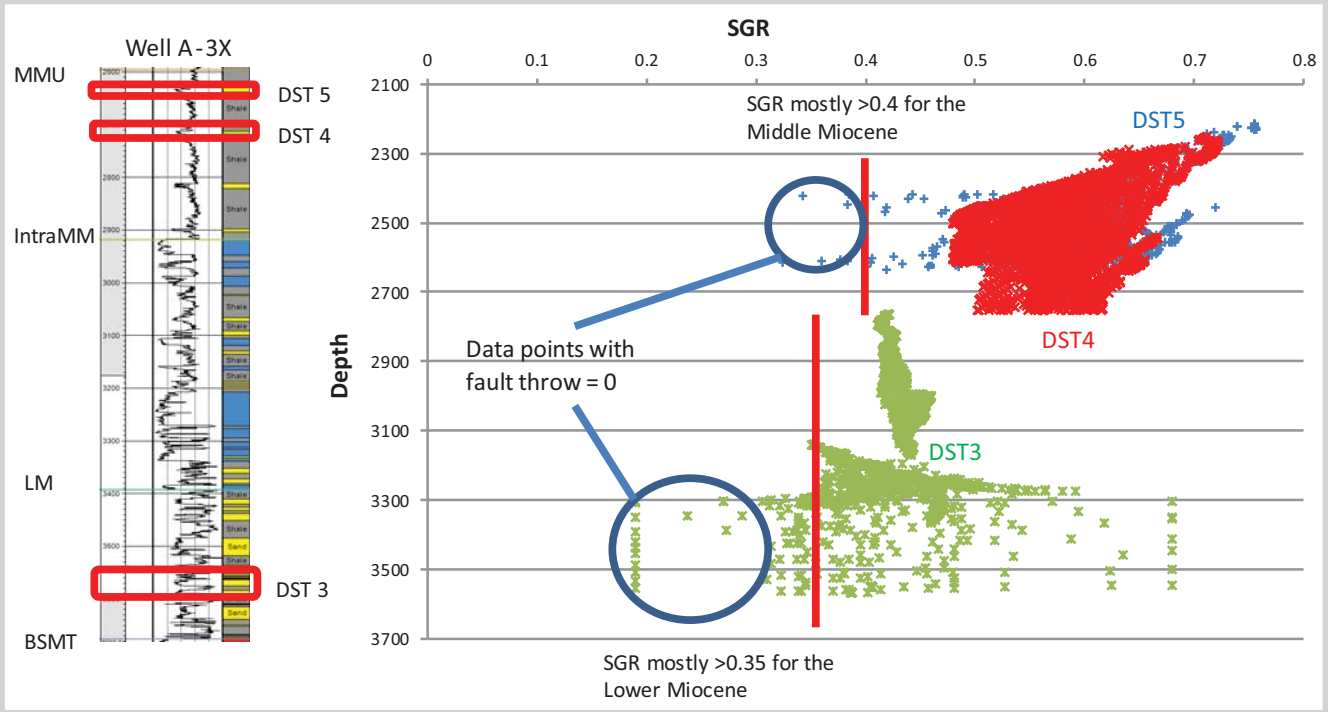

Figure 6. *DST tests for clastic sections in well 3X of structure A. Gas discoveries intervals have SGR > 0.4 in the Middle Miocene and SGR > 0.35 in the Lower Miocene*

Table 1. *Predicted maximum gas column height and percentage of trap fill along faults. The trap fill percentage is calculated by dividing the HC column height by the vertical closure of the structure from crest to spill-point*

Structure	Interval	Fault throw	SGR	HC column height	Vertical closure (crest to spill-point)	Trap fill along faults
		m		m	m	%
A	MMU - Intra MM	10 - 1600	0.5 - 0.8	136	377	37
	Intra MM - LM	10 - 1800	0.5 - 0.6	140	663	21
	LM - Top BSMT	Juxtaposed with basement, not evaluated				
C	Intra MM - LM	10 - 400	0.3 - 0.5	166	220	75
	LM - Top BSMT	10 - 500	0.3 - 0.6	252	344	74
D	MMU - Intra MM	50 - 250	0.2 - 0.3	174	200	87
	Intra MM - LM	10 - 600	0.2 - 0.8	136	151	90
F	MMU - LM	0 - 400	0.3 - 0.55	252	326	77
	LM - OL	0 - 300	0.5 - 0.75	292	648	45
	OL - Top BSMT	0 - 250	0.45 - 0.75	295	580	50

tests for clastic sections show gas bearing intervals with mostly SGR > 0.4 for the Middle Miocene formation and mostly SGR > 0.35 for the Lower Miocene formation (Figure 5c). The Lower Miocene formation has lower SGR yet it still seals. This is probably due to diagenesis effect by sediment burial, which in this case is 3,300m in burial depth. The deeper the burial, the more significant the mechanical compaction and chemical pressure solution processes will be, which will reduce the porosity and permeability of the fault zone, thus enhancing the fault seal capacity.

Calculated maximum HC column heights are shown in Table 1. In the Middle Miocene section, the drilled structures (structures A and C) have the column heights in the range of 136 - 166m, while the undrilled structures have the column height in the range of 136 - 252m. In the Lower Miocene section, the drilled structure C has the column height of 252m, while the undrilled structures have the column heights in the range of 252 - 292m. In the Oligocene section, which is present in the undrilled structures only, the column heights are in the range of 251 - 295m.

5. Conclusion

SGR thresholds determined from drilled structures can be used for undrilled ones. SGR for DST intervals with

discoveries are greater than 0.4 for the Middle Miocene interval and greater than 0.35 for the Lower Miocene interval.

In case reservoir engineering data on both sides of the faults are lacking, the published empirical equation from Bretan et al. [11] can be used to evaluate sealing threshold pressure across faults. Calibration with known fields and discoveries in the Nam Con Son basin is necessary to get a reasonable maximum HC column height.

The predicted HC column heights and trap fill for drilled structures are 136 - 252m and 21 - 75% respectively, and for undrilled structures are 136 - 295m and 45 - 90% respectively. Trap fill is variable due to differences in vertical closure and clay content along faults.

HC column height is also dependent on the seal capacity of the cap rock, which is not considered in this study.

References

1. L.V.Hien. *Structural characteristics and petroleum potential of synrift targets in the Nam Con Son Basin*. VPI. 2012.

2. VSP. *G&G, RE and Final well reports*. 2002 - 2014.

3. Brown, Alton. *Capillary effects on fault - fill sealing*. AAPG Bulletin. doi:10.1306/08010201127. 2003; 87 (3): p. 381 - 395.

4. Al-Busafi, Bader. *Incorporation of fault rock properties into production simulation models*. http://etheses.whiterose.ac.uk/190/. 2005.

5. Richard M.Jones, and Richard R.Hillis. *An integrated, quantitative approach to assessing fault - seal risk*. AAPG Bulletin. doi:10.1306/10100201135. 2003; 87 (3): p. 507 - 524.

6. G.Yielding, B.Freeman and D.T.Needham. *Quantitative fault seal prediction*. AAPG Bulletin. doi:10.1306/522B498D-1727-11D7-8645000102C1865D. 1997; 81(6): p. 897 - 917.

7. N.G.Lindsay, F.C.Murphy, J.J.Walsh and J.Watterson. *Outcrop studies of shale smears on fault surfaces*. The geological modelling of hydrocarbon reservoirs and outcrop analogues. doi:10.1002/9781444303957.ch6. 1992. 15: p. 113 - 123.

8. J.D.Bouvier, C.H.Kaars-Sijpesteijn, D.F.Kluesner, C.C.Onyejekwe, and R.C.Van Der Pal. *Three - Dimensional seismic interpretation and fault sealing investigations, Nun River Field, Nigeria*. AAPG Bulletin. 1989; 73(11): p. 1397 - 1414.

9. Susanne Sperrevik, Paul A Gillespie, Quentin J.Fisher, Trond Halvorsen, and Rob J.Knipe. *Empirical estimation of fault rock properties*. Norwegian Petroleum Society Special Publications. doi:10.1016/S0928 - 8937(02)80010 - 8. 2002; 11: p. 109 - 125.

10. Q.J.Fisher, and R.J.Knipe. *Fault sealing processes in siliciclastic sediments*. Geological Society, London, Special Publications. 1998. 147 (1): p. 117 - 134.

11. Bretan, Peter, Graham Yielding, and Helen Jones. *Using calibrated shale gouge ratio to estimate hydrocarbon column heights*. AAPG Bulletin. doi:10.1306/08010201128. 2003; 87 (3): p. 397 - 413.

12. PVN. *G&G, RE and Final well reports*. 1979 - 2001.

METHODS FOR ENHANCING PRODUCTION EFFICIENCY OF GAS LIFT WELLS IN VIETSOVPETRO OIL FIELDS

Tong Canh Son, Pham Ba Hien, Nguyen Huu Nhan
Vietsovpetro
Email: sontc.rd@vietsov.com.vn

Summary

Research for solutions to improve the efficiency of oil production from wells with low production rates and/or flooding is a goal and strategy of the oil companies of Petrovietnam in general and Vietsovpetro in particular. This paper presents the effects of physical and chemical methods on the product flow of gas lift-based production wells both on laboratory and industrial scale in Bach Ho oil field. Chemical mixtures containing paraffin inhibitors and demulsifiers were pumped into the production flow of several wells using the gas lift production method in Bach Ho oil field. Initial results indicate that the output increased by about 7.1 - 80.0%, lift gas volume reduced by 5.6 - 32.7%, and paraffin deposition decreased by 12.1 - 14.1%. These results illustrate the effectiveness and feasibility of aforementioned technique. It is believed that the application of this technique over a broader range would bring increased profit for Vietsovpetro.

Key words: *Bach Ho oil field, gas lift, chemical mixture, foam.*

1. Background

Oil production by gas lift method has been implemented in the oil and gas fields of Vietsovpetro since 1997. So far, the results have confirmed the correct choice of mechanical production methods. In Bach Ho and Rong fields, oil is produced from many different areas having different geological parameters, hence requiring different optimum production methods. The production rates of the gas lift wells vary widely, ranging from 5 to 100 tons/well/day. The wells that have production rates greater than 60 tons/day are less complex than those having low production rates (less than 30 - 40 tons/day). For the latter, in the production process, paraffin/wax deposition often occurs on the wall of the pipe/tube leading to tube blockage. As a result, the oil and gas flow rate of these wells gradually reduces, leading to complete blockage and lost production. These wells are periodically shut in for removal of the paraffin deposited on the pipe walls. The frequency of the cleaning procedure is every week, and it takes from 3 to 4 hours each time. The deposited paraffin can be cleared by directly pumping steam into the tubing to melt the deposits. This technique is simple and easy to implement but it does have some disadvantages, including:

- The well needs to be shut in causing loss of production;
- Effect is seen normally with only the paraffin deposited at the wellhead;
- High temperature steam can cause problems for the flanges of the equipments located in the wellhead, probably leading to damage.

One of the possible methods that can overcome the above drawbacks of the thermal method is to pump a suitable chemical mixture into the well produced fluids. This chemical method might help not only by reducing paraffin deposition but also by decreasing the volume of gas used for gas lift.

2. Factors affecting oil production in gas lift wells

Effective working of the gas lift wells in Bach Ho oil field depends heavily on the flow capacity of the oil-gas-water mixture in the lift tubing, creating gas in the oil level and the ability to diffuse them into the fluid flow.

Oil produced in all areas of Bach Ho field has a high paraffin content (22 - 27%). Oil paraffin crystallisation temperature is in the range of 59 - 61°C and its freezing point is 29 - 36°C. Meanwhile, the temperature at the wellhead of nearly all the wells utilising the gas lift technique in Bach Ho field is about 25 - 40°C. This leads to problems of paraffin deposition in the production tubing, and the low lifting of oil. With time, the deposition layer increases and eventually causes blockage. This problem is particularly serious in the case of high water content wells.

The following formula can be used to evaluate the performance of the wells:

$$\eta = \frac{1}{\frac{fC_s}{q}\frac{p_z - p_y}{h\rho g} + 1}$$

Where:

η: The effective lift coefficient;

C_s: The relative velocity of the gas phase, m/s;

q: The fluid flow, m^3/s;

f: The cross sectional area of tube, m^2;

p_z: The working gas pressure after the valve, Pa;

p_y: The wellhead pressure, Pa;

h: The length of the lift, m;

ρ: The average density of the oil and gas system, kg/m^3;

g: Gravitational acceleration, m/s^2.

Based on the above equation, it is recommended that a chemical mixture having the ability to inhibit paraffin deposition combined with surface active properties should be pumped into the product flow for improved oil production.

3. Laboratory Studies

3.1. Information of chemical additives and study methods

The chemical additives used for crude oil treatment must satisfy the "Technical requirement on pour point depressant and demulsifier for treatment of crude oil produced from Vietsovpetro oil fields". The physical and chemical properties of some chemical reagents are presented in Table 1.

The modelling processes were conducted on laboratorial equipments in the Laboratory for Oil and Gas Treatment and Transportation of Vietsovpetro Research and Engineering Institute.

3.2. The effect of demulsifier on the ability to create gas bubbles in the produced fluids

Experimental study results presented in Figures 1 - 3 show that the use of a demulsifier at dosage of 200ppm increases the ability to create gas bubbles and their suspension in oil. When the water cut of the produced fluids increases, the ability to maintain the gas bubbles dispersed in the oil phase decreases. When using a chemical mixture, the surfactant disperses to the interface between oil and water phases reducing the surface tension; when the bubble is big enough it will be broken into smaller gas bubbles dispersed in the oil phase. Should the chemical mixture be "overdosed", this will facilitate a change in the emulsion type from "water in oil" to "oil in water", maintaining the level of suspension of gas bubbles in the oil. As a result, the density and viscosity of the oil-gas-water mixture in the tubing reduces, the

Table 1. *The physical and chemical properties of some chemical reagents*

Product name	Application	Composition	Physical and chemical properties
VX-7484	Paraffin inhibitor	Heavy aromatic naphtha, xylene...	Flash point: 63°C Density: 0.88 @ 15.5°C Pour point: 6°C
PAO-80033	Pour point depressant	Heavy aromatic naphtha, xylene...	Flash point: 32°C Density: 0.88 @ 50°C Pour point: 21°C
REPA-61V	Paraffin inhibitor	Heavy aromatic naphtha, xylene...	Flash point: 32°C Density: 0.9 @ 25°C Pour point: < -10°C
EC-6509A	Paraffin inhibitor	Heavy aromatic naphtha, xylene...	Flash point: 60.5 - 93.3°C Density: 0.881 at 15°C Pour point: 7°C
EC-6002A	Paraffin inhibitor	Heavy aromatic naphtha, xylene...	Flash point: > 50°C Density: 0.81 at 15°C Pour point: 6°C
DMC D-6	Demulsifier	Polymer surfactant and aromatic solvent	Flash point: > 50°C Density: 0.89 ± 0.03 at 25°C Pour point: < -20°C
DMO-86318	Demulsifier	Naphthalene, alkyl (C3 - 5) benzenes, alkyl benzenes (C9 - 10)...	Flash point: 62°C Density: 0.941 - 1.011 at 25°C Melting point: < -27°C
MA-195	Demulsifier	Mixture of non ionic derivatives in aromatic solvent	Flash point: 62°C Density: 0.950 - 0.965 at 25°C Freezing point: -25°C

lifting ability increases and eventually the fluid flow will be improved.

Research results (Figures 1 - 3) showed that DMC D-6 has better foaming ability than other tested chemicals.

3.3. The effect of chemical inhibition on paraffin deposition and kinematic viscosity of oil

As published in the results of study [1 - 3], oil produced from Bach Ho field has a high paraffin content and freezing point. When the temperature drops below the crystallisation temperature of the paraffin, crystallisation begins to occur. Meanwhile, as noted above, the wellhead temperature of nearly all the wells in Bach Ho field is much lower than the crystallisation temperature of paraffin and even lower than the freezing point of the oil. We have investigated the effects of chemical mixtures on viscosity reduction of the oil/water emulsion, thus improving the rheology of the product flow, as well as limiting paraffin deposition using the Rotovisco type RV-20 and "cold finger" equipment. The results obtained are displayed in Figure 4 and Table 2 and showed that using chemicals can significantly reduce paraffin deposition by 31 - 33%.

3.4. The ability of chemical demulsifier and paraffin inhibitor mixture to create gas bubbles in the oil water

Results of laboratory studies on the influence of the chemical mixture of demulsifier and paraffin inhibitor to form emulsion of water and oil from MSP-5 and MSP-7 of Bach Ho field are presented in Table 3.

Laboratory study results in Table 3 show that demulsifier DMC D-6 has the best result of foaming tendency and foam stability in comparison with other tested chemicals. If chemical DMC D-6 mixes with paraffin inhibitor VX-7464 with ratio 2:5, the results of foam tendency and foam stability will be better.

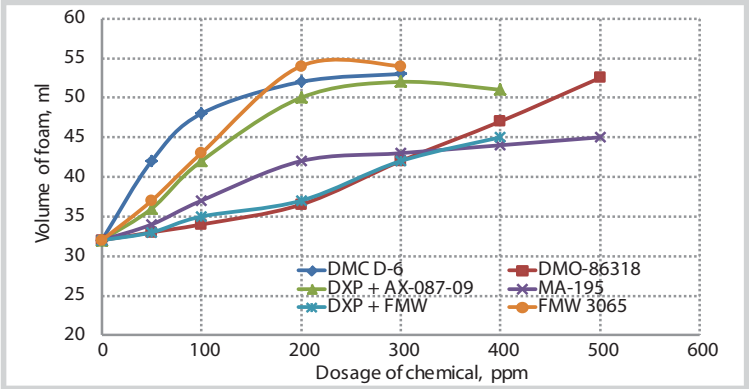

Figure 1. *The foaming ability of the oil-water emulsion from well No 507, rig platform #5 (MSP-5) (water content 15%) when using certain chemical demulsifiers*

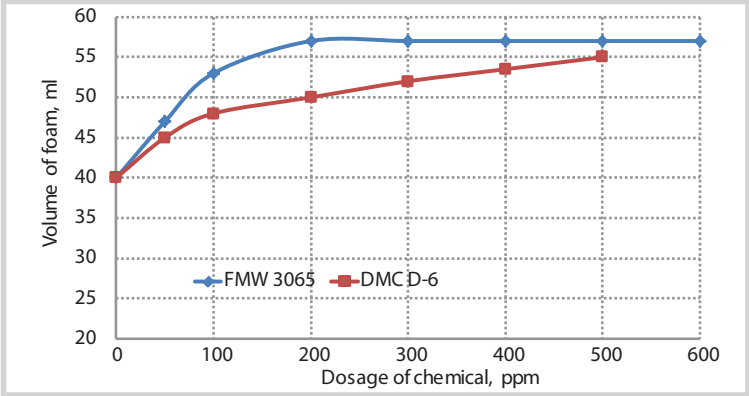

Figure 2. *The foaming ability of the oil-water emulsion from wells No 507 and 510, MSP-5 (water content 8%) when using certain chemical demulsifiers*

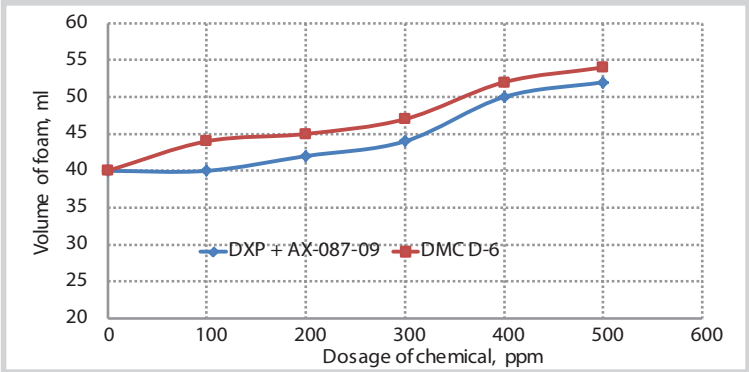

Figure 3. *The foaming ability of a mixture of oil-water emulsion from wells No 507, 509 and 108 (water content 25%), MSP-5 when using certain chemical demulsifiers*

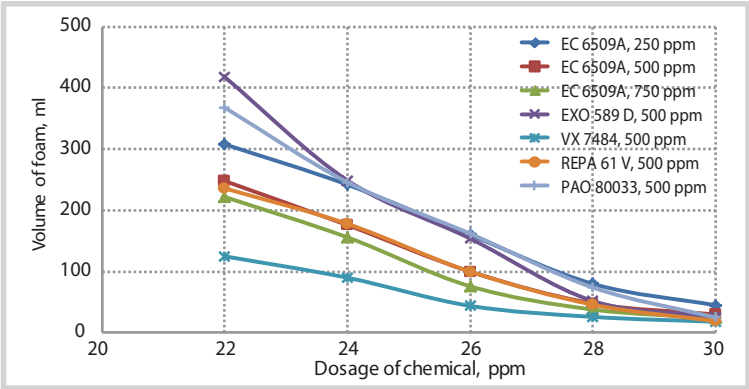

Figure 4. *The effect of the chemical on the kinematic viscosity of the oil from MSP-5*

Table 2. *The effect of chemicals in reducing the freezing temperature to inhibit paraffin deposition of Bach Ho field's crude oil*

No	Oil temperature (°C)	Test chemicals (g/t.)	Test time, hour	Paraffin deposition rate (g/m²/day)	Ability to inhibit deposition (%)
		Cold finger method (temperature of 22 °C)			
1	60	0	8	3538	-
2	60	500	8	2433	31.2
3	60	1000	8	2354	33.5

Table 3. *Oil emulsion foaming ability of water treated with the studied chemical mixture*

Mixtures of chemicals	Volume of foam created (ml)	Time to foam dissolved (s)
Mixture of oil in wells No 507 and 104, MSP-5, 8% water content		
No chemicals	38.3	34.7
DMC D-6 200ppm	46.7	49.0
DMC D-6 200ppm + VX-7484 500ppm	50.0	43.0
DMC D-6 200ppm + EXO 589D 500ppm	53.3	49.7
DMC D-6 200ppm + RE 5942 PAO 500ppm	48.3	47.7
DMC D-6 200ppm + RE 5943 PAO 500ppm	46.7	50.0
Mixture of oil in wells No 702 and 705, MSP-7, 11% water content		
No chemicals	61.7	71.3
DMC D-6 200ppm	73.3	78.7
REPA 61V 200ppm	70.0	72.7
DMC D-6 200ppm + VX-7484 500ppm	81.7	70.3
DMC D-6 200ppm + EC 6002 A 500ppm	60.0	68.3
DMC D-6 200ppm + RE 5942 PAO 500ppm	65.0	68.0
DMC D-6 200ppm + RE 5943 PAO 500ppm	65.0	67.7
Mixture of oil in wells No 507, 108, 705, 707 and 710, MSP-5 and MSP-7, 16% water content		
No chemicals	63.3	84.7
DMC D-6 200ppm	68.3	90.0
DMC D-6 200ppm + VX-7484 500ppm	70.0	82.3
DMC D-6 200ppm + EXO 589D 500ppm	56.7	72.0
DMC D-6 200ppm + EC 6509A 500ppm	60.0	39.0
DMC D-6 200ppm + RE 5942 PAO 500ppm	63.3	84.3
DMC D-6 200ppm + RE 5943 PAO 500ppm	61.7	86.0
DMC D-6 200ppm + EC 6002A 500ppm	70.0	96.7

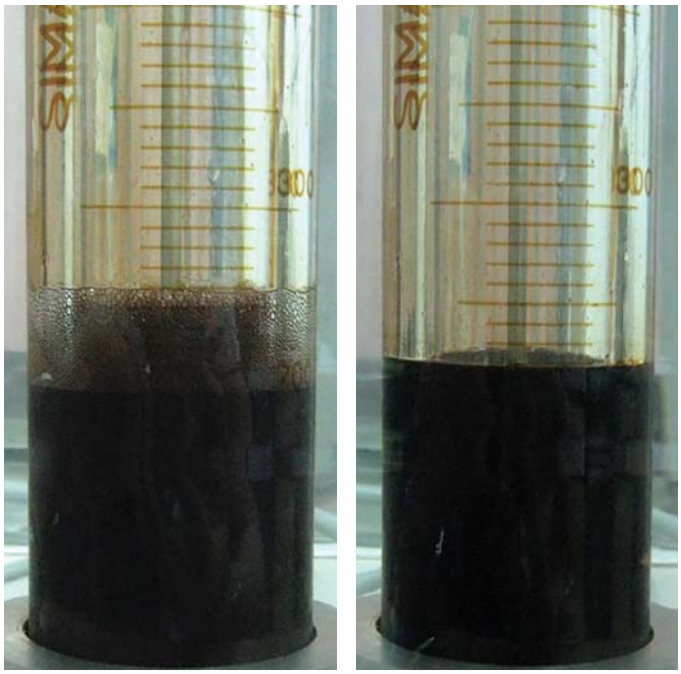

Figure 5. *The formations of foam without and with chemical*

4. Industrial tests on the gas lift wells of Bach Ho field

To test the results of the laboratory studies, Vietsovpetro conducted field tests in wells 104 and 510 on the MSP-5 platform and wells 75, 145, 702, 704 and 715 on the MSP-7 platform. Test results are presented in Table 4.

The results show that although there was very low oil temperature at the wellhead (about 26 - 32°C), after chemical injection, the speed of paraffin deposition was decreased by 12.1 - 14.1% (determined by mechanical methods), and the cost of lift gas consumption reduced by 21 - 32%. The average production of wells 104 and 510 increased by 7.5 tons/day and 14.5 tons/day, respectively. It means after chemical treatment, oil production in gas lift well of MSP-5 will increase to 59% for well 104, 52% for well 510 and about 7.1 - 80.0% for tested wells of MSP-7.

Table 4. *Industrial tests on gas lift wells of Bach Ho field*

Gas lift well	Working gas costs (m^3/m^3)		Costs of chemical products (kg/day)	Reduced paraffin deposition (%)	Fluid flow (ton/day)	
	Before chemical treatment	After chemical treatment			Before chemical treatment	After chemical treatment
Field tests on MSP-5						
104	450	303	12 - 24	12.1	12.6	20.1
510	168	133	28 - 54	14.1	28.1	42.6
Field tests on MSP-7						
75	144	136	16	-	49	54
145	228	143	30	-	10 - 13	15
702	57	53	45	-	126	135
704	381	265	8.0	-	15	21.4
715	326	246	15	-	15.0	27

5. Conclusions

- The use of pour point depressant for oil-gas-water treatment of gas lift wells will effectively reduce fluid viscosity, paraffin deposition rate in the tube and pressure to lifting well production. In this result the production flow rate of gaslift wells will be increased;
- Using chemical demulsifier for oil-gas-water treatment of gas lift wells will reduce lift gas cost, maintain the bubble formation ability and increase the lift coefficient;
- To improve the flow rate of gas lift wells, a mixture of depressant VX-7484 and demulsifier DMC D-6 (ratio 5:2) with a dosage of 700 - 1,000ppm should be injected into gas lift gas flow.

References

1. V.P.Vugovskoi, Tong Canh Son, Ha Van Bich, Le Dinh Hoe, Phung Dinh Thuc. *Problem restarting flow submarine pipeline.* Proceedings of the International Conference on Engineering Mechanics. Hanoi. 1995; 2: p. 342 - 348.

2. Фунг Динв Тхык, Ха Ван бик, Тонг Канв Шон. *Проблемы транспорта нефтей месторождений белый Тигр и Дракон по подводвам*. Азербайджанское нефтяное хозяйство. 1999; 6: с. 56 - 59.

3. Phung Dinh Thuc, Ha Van Bich, Tong Canh Son, Le Dinh Hoe and V.P.Vygovskoy. *The problem in transportation of high waxy crude oils through submarine pipelines at JV Vietsovpetro oil fields, offshore Vietnam*. Journal of Canadian Petroleum Technology. June 2003; 42(6): p. 15 - 18.

COMBINING SONIC WHILE DRILLING AND FORMATION PRESSURE WHILE DRILLING FOR PORE PRESSURE ANALYSIS TO REDUCE DRILLING RISK: A CASE STUDY IN OFFSHORE VIETNAM

Nguyen Dac The[1], Doan Thi My Dung[1], Aqil Ahmed[1], Phung Thai Ha[1], Sadu-ur Rehman[1], Nguyen Truong Son[2], Khuc Hong Giang[2]
[1]*Schlumberger*
[2]*Bien Dong Petroleum Operating Company*
Email: tdac@slb.com

Summary

The accurate prediction of pore pressure is important for safe drilling and can significantly reduce financial risk. The major focus during drilling in a high-temperature/high-pressure (HP/HT) environment is optimising the drilling operation to mitigate risk by utilising data such as sonic logging-while-drilling (LWD) and offset well information.

An offshore exploration well was being drilled in offshore Vietnam with drilling challenges of abnormally high formation pressure. In normally compacting sediments, water escapes through permeable sands or along fractures as overburden sediments build up, and fluid or pore pressure remains close to hydrostatic pressure. In such normally compacting sediments, under increasing effective pressure, porosity decreases and compressional velocity increases. However, if formation fluids cannot escape, for example due to the low permeability of overlying shales, then they bear part of the overburden load and hence become overpressured. These formations are called undercompacted, meaning they have a higher porosity than normally compacted shales. In overpressured shales, which contain pressured water, density is lower, porosity is higher, and compressional velocity is lower than normal.

Formation pressure can be the major factor affecting the success of drilling operations. If pressure is not properly evaluated, it can lead to drilling problems such as lost circulation, kick, stuck pipe, hole instability, and excessive costs. Therefore, knowledge of the pore pressure is of considerable value because it provides the means for improving drilling operations and designing better casing programmes to reduce those risks. Using the data gathered from well logs, it is possible to predict the probable pressure profile that will be encountered while drilling. LWD data enable monitoring pore pressure very effectively; this pore pressure prediction can be continuously updated using LWD sonic and formation pressure while drilling (FPWD) to make optimal decisions for the drilling operation. Once a suitable predrill pressure profile is established, it is monitored on the current wells with logging while drilling sonic and directly calibrated with formation pressures taken in sands.

In the offshore Vietnam well, pore pressure monitoring by LWD formation pressures and estimated pore pressure from LWD sonic data allowed drilling operations to be optimised. Employing this technique led to successful drilling without any incidences related to pore pressure. The computed pressures from LWD sonic matched the measured pressures obtained from FPWD. The real-time sonic matched the recorded-mode sonic closely. This technique could apply not only to the wells in this basin but also to the other wells in the locations with abnormal high formation pressure.

Key words: *Pore pressure prediction, sonic while drilling, formation pressure while drilling, LWD sonic, casing optimisation.*

1. Introduction

The subject well is located in Nam Con Son basin, offshore Vietnam. This basin is one of a series of Tertiary rift basins created on Vietnam's continental shelf as a consequence of the East Sea seafloor spreading. The formation pressure profiles in central Nam Con Son basin are characterised by overpressure beneath the late Pliocene-Quaternary sedimentary section. Predicted bottom hole static temperature of this high-pressure/high-temperature (HP/HT) well is about 172°C (most likely) and may vary from 165°C to 177°C.

There are many drilling challenges in the Nam Con Son basin due to the complex sedimentary environment and complex geological structures. This increases the challenges in drilling exploration wells, especially in the HP/HT environment. In addition, the safe mud weight is within a very narrow window between the pore pressure and formation breakdown, increasing the drilling risk [1].

Generally, to better reduce the drilling risk, pore pressure analysis is usually undertaken using available offset well information together with the surface seismic data prior to drilling the well. As an important input for

pore pressure analysis, sonic data is acquired during or after drilling to provide an estimate for safe mud window and drilling risk evaluation for the current well. This information can be utilised for subsequent nearby wells.

In projects with high risk, real-time data provide the information required to perform instantaneous analysis and update models that can assist in both drilling and reservoir evaluation. Real-time sonic data together with real-time FPWD data can be used to tackle the issue of unknown pore pressure with a narrow mud weight window [1].

Acquiring good quality LWD sonic data and other measurements such as gamma ray, density, resistivity, and FPWD, as well as monitoring the equivalent circulating density (ECD) and downhole parameters, were the keys to success in this HP/HT well. Predrill pore pressure provided early drilling hazard prediction in the job planning and was updated in real time to reduce uncertainties due to the complexity of geological structure.

Basic data acquisition (i.e., LWD gamma ray and resistivity) were required to assist lithology interpretation. LWD sonic was required for overpressure detection in real time and for geophysical evaluation. FPWD was required for formation pressure evaluation and pore pressure validation in the sand reservoir.

2. Case study

Pore pressure is the fluid pressure in the pore space of the formation. Pore pressure values range from hydrostatic pressure to severe overpressure (48% to 95% of the overburden stress). Pore pressure analyses include three aspects: predrill pore pressure prediction (PPP), PPP while drilling, and post-drilling pore pressure analysis. Predrill pore pressure can be predicted by using surface seismic interval velocity data in the planned well location, and by using geological, well logging, and drilling data in offset wells.

The purpose of pore pressure modelling is to create a safe operating window of mud weight such that the designed mud density will be high enough to ensure wellbore stability and low enough that drilling mud losses will not occur (Figure 1).

Figure 2 relates the mud weight (MW) to wellbore failures. The safe MW window should be higher than pore pressure and lower than mud losses. MW less than shear failure can lead to wellbore breakout; MW less than the pore pressure can lead to wellbore kicks or cavings. On the other hand, MW higher than mud losses can lead to partial loss and severe lost circulation if the MW is higher than breakdown.

The FPWD is a direct pore pressure measurement in permeable formations where a draw-down can be achieved, normally sands.

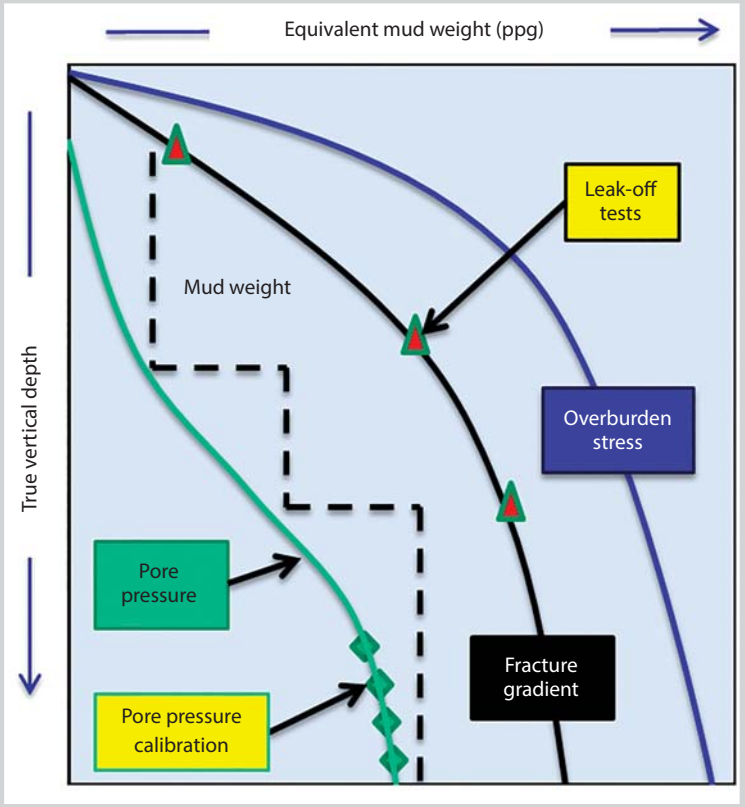

Figure 1. *Simple mud weight window*

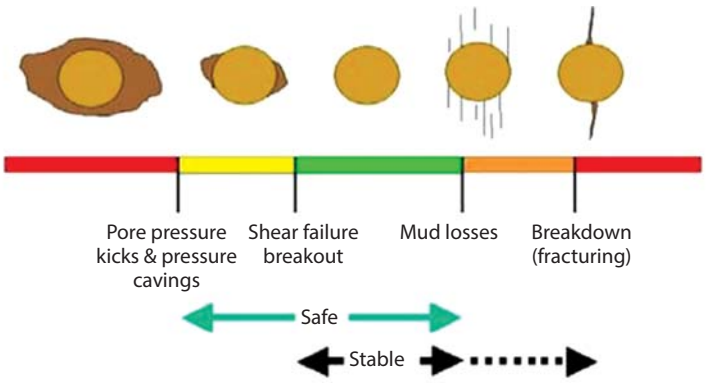

Figure 2. *Schematic relationship of mud weight and wellbore failures*

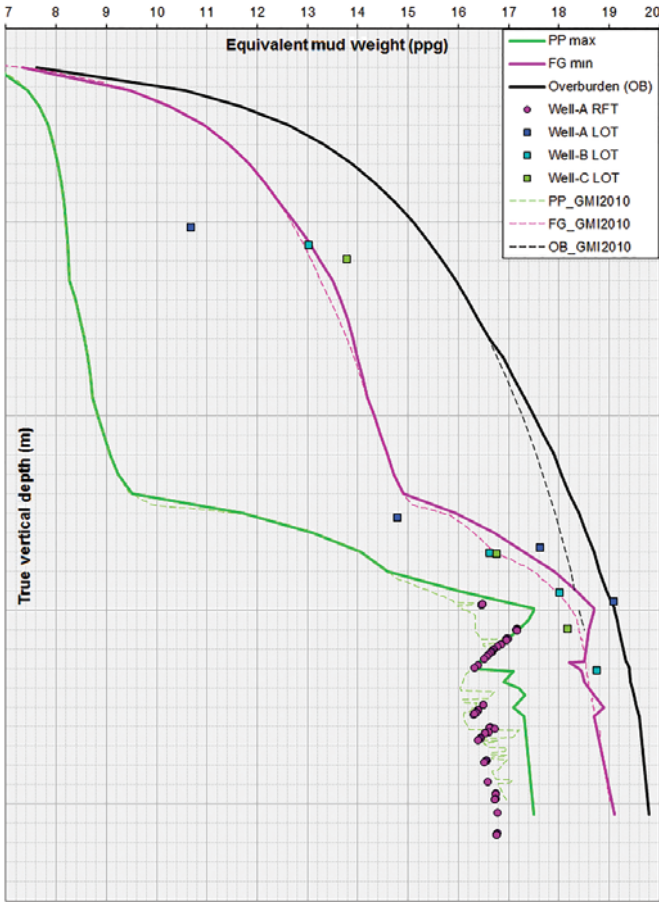

Figure 3. *Predrill pore pressure model*

2.1. Before drilling

A predrill pore pressure model must be built before drilling by using all available well-log data. In some sedimentary basins where undercompaction is the major cause of overpressure, the well-log-based resistivity method [2] can be used to predict pore pressure. Based on this relationship, pore pressure can be obtained from seismic interval velocity.

In this study, pore pressure was estimated from the sonic data using Eaton's method [2], and it compared well to pore pressure obtained from interval velocity and resistivity. This estimated pore pressure was calibrated by the direct formation pressure measurement from offset wells. The predrill pore pressure model is shown in Figure 3.

2.2. While drilling

To determine the minimum mud weight for drilling operations, the workflow described in Figure 4 was used for the pore pressure analysis and real-time monitoring.

There are always some uncertainties existing when pore pressure has been calculated and validated. The

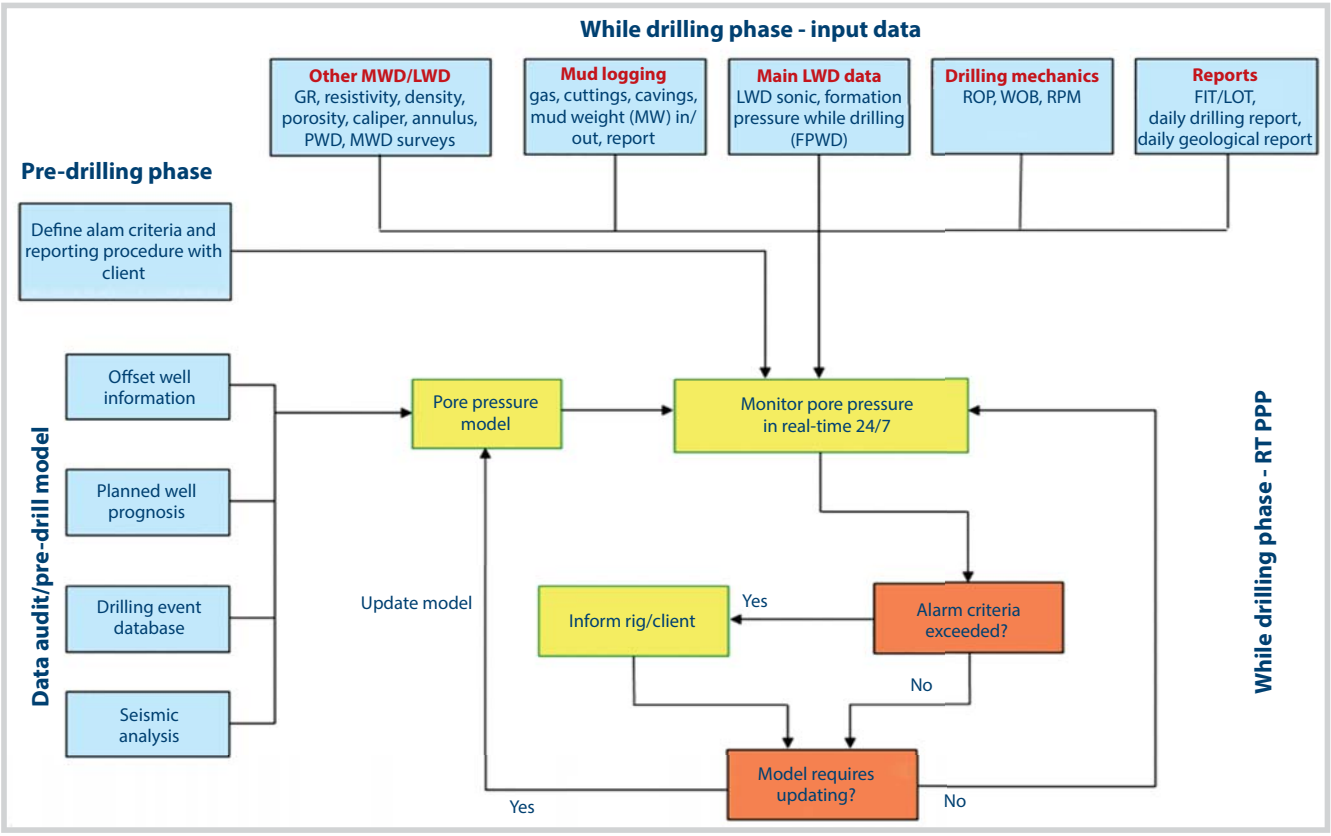

Figure 4. *Real-time pore pressure analysis and monitoring workflow [3]*

predrill pore pressure was planned based on the available offset well log data along with assuming similar lithology and little structural complexity. Thus, monitoring and updating pore pressure in real time are the keys to success when there is a high risk of wellbore instability.

In this HP/HT well, there was an extremely challenging narrow mud weight window and hence, low tolerance for MW uncertainty. Therefore, LWD logging data, LWD sonic measurement, and FPWD were acquired for three hole sections (16.5-in., 12.25-in. and 8.5-in.) for pore pressure monitoring in real time. In this case, the pore pressure was updated to total depth (TD) of the well to reduce the prediction uncertainties. The following steps were used to monitor and update the pore pressure in real time.

Monitoring and quality check (QC) of the LWD data compressional slowness (DTCO), density, and resistivity were done to make sure the acquired data were of good quality.

The formation lithology was correlated between the acquired LWD data and the offset well data, and the predrill PPP was adjusted immediately based on the changes of formation lithology [4].

The pore pressure was calculated in real time from LWD sonic and well calibrated by FPWD, and then used to calibrate the predrill PPP.

In general, the quality of LWD sonic data acquired in real time was good. The pore pressure was calculated from the compressional slowness (P slowness) and then calibrated by FPWD points in sand formation. The MW window was updated from the calculated pore pressure profile for safe drilling.

Figures 5 - 7 show the quality of real-time LWD sonic data and recorded-mode data for the 16.5-in., 12.25-in., and 8.5-in. sections. The real-time LWD sonic data was matched very well with the recorded-mode LWD sonic and pump-off measurement over the entire interval in all three sections.

Figures 8 - 10 show the pore pressure calculation in real time using LWD sonic and FPWD data. The main challenge was to manage the MW in the 16.5-in., 12.25-in., and 8.5-in. hole sections where the pressure was increased rapidly by depth. The mud weight window was updated based on the calculated pore pressure, and the predrill model was updated in real time for the 16.5-in., 12.25-in., and 8.5-in. sections.

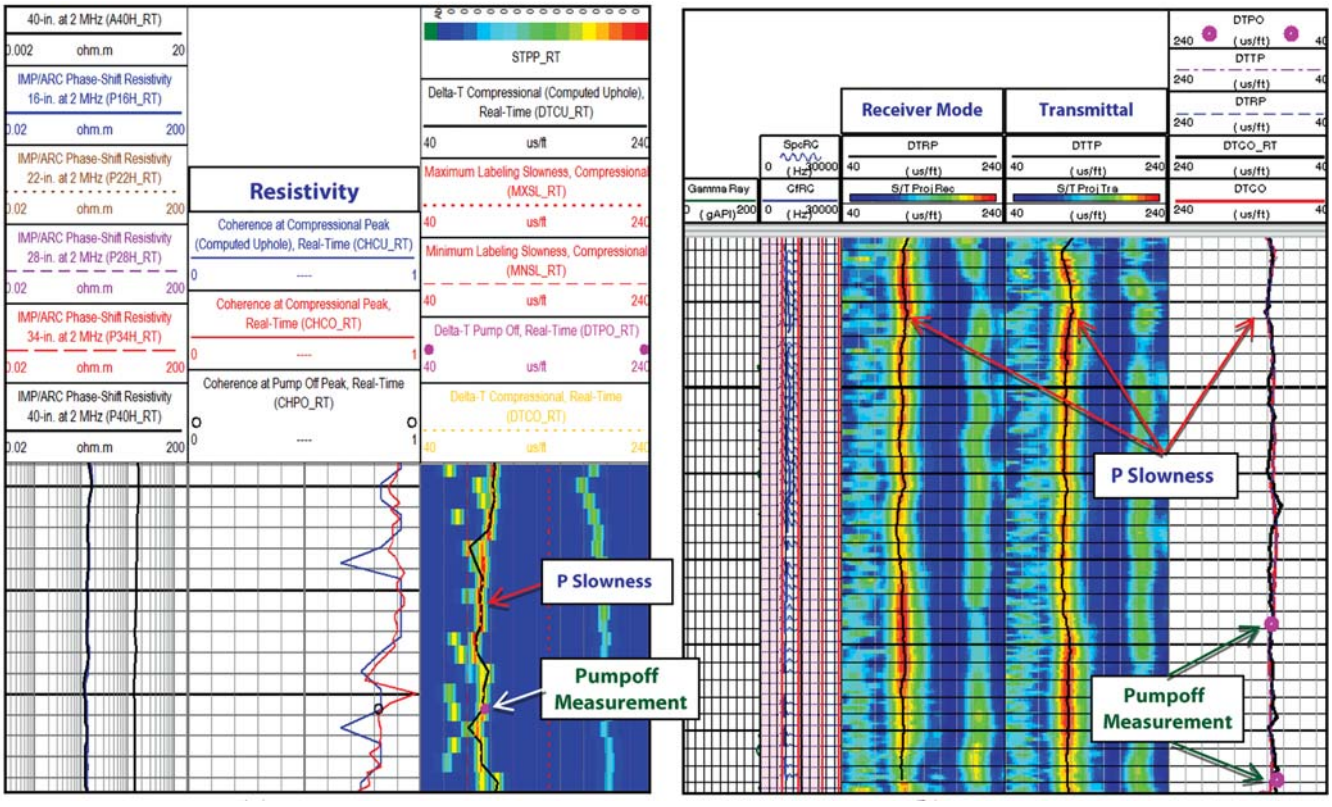

(a) (b)

Figure 5. *LWD sonic real-time (a) and recorded-mode (b) data in 16.5-in. section*

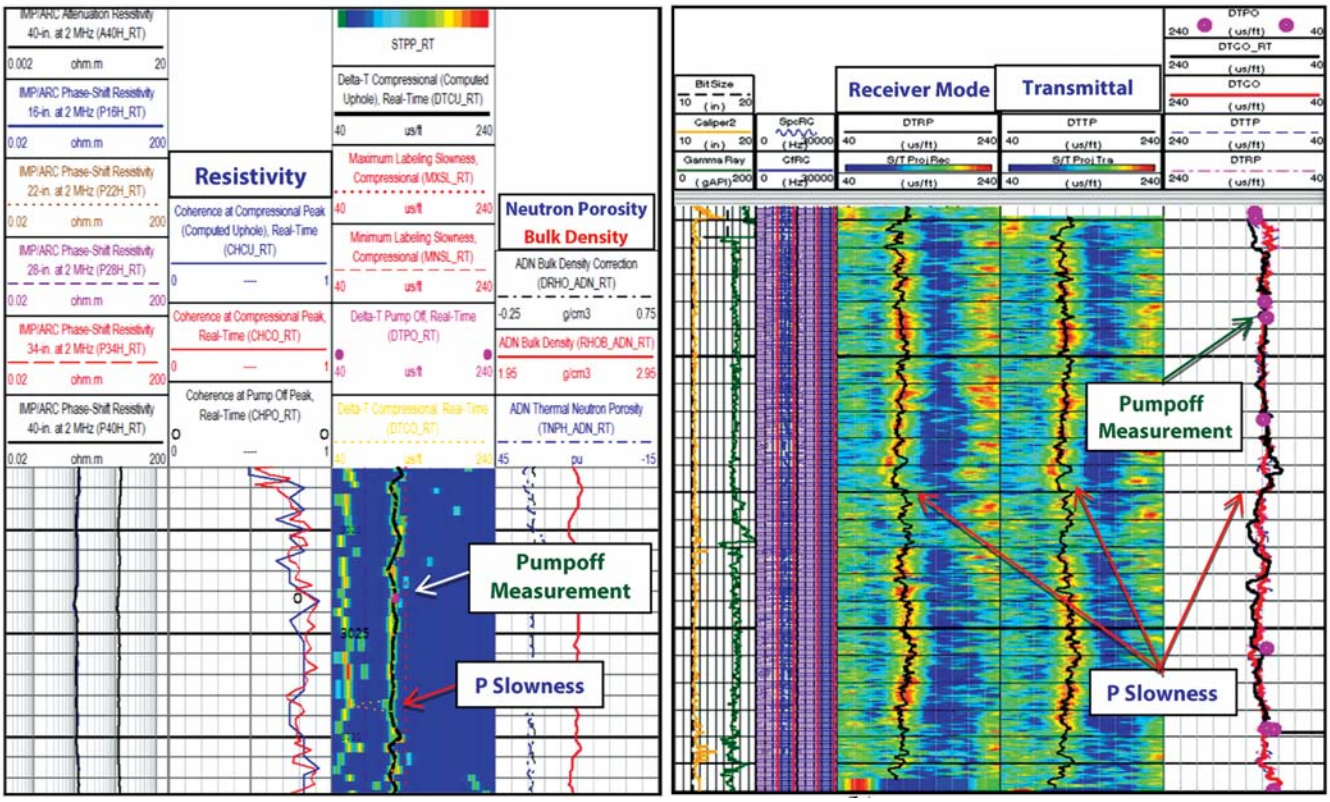

(a) (b)

Figure 6. *LWD sonic real-time (a) and recorded-mode (b) data in 12.25-in. section*

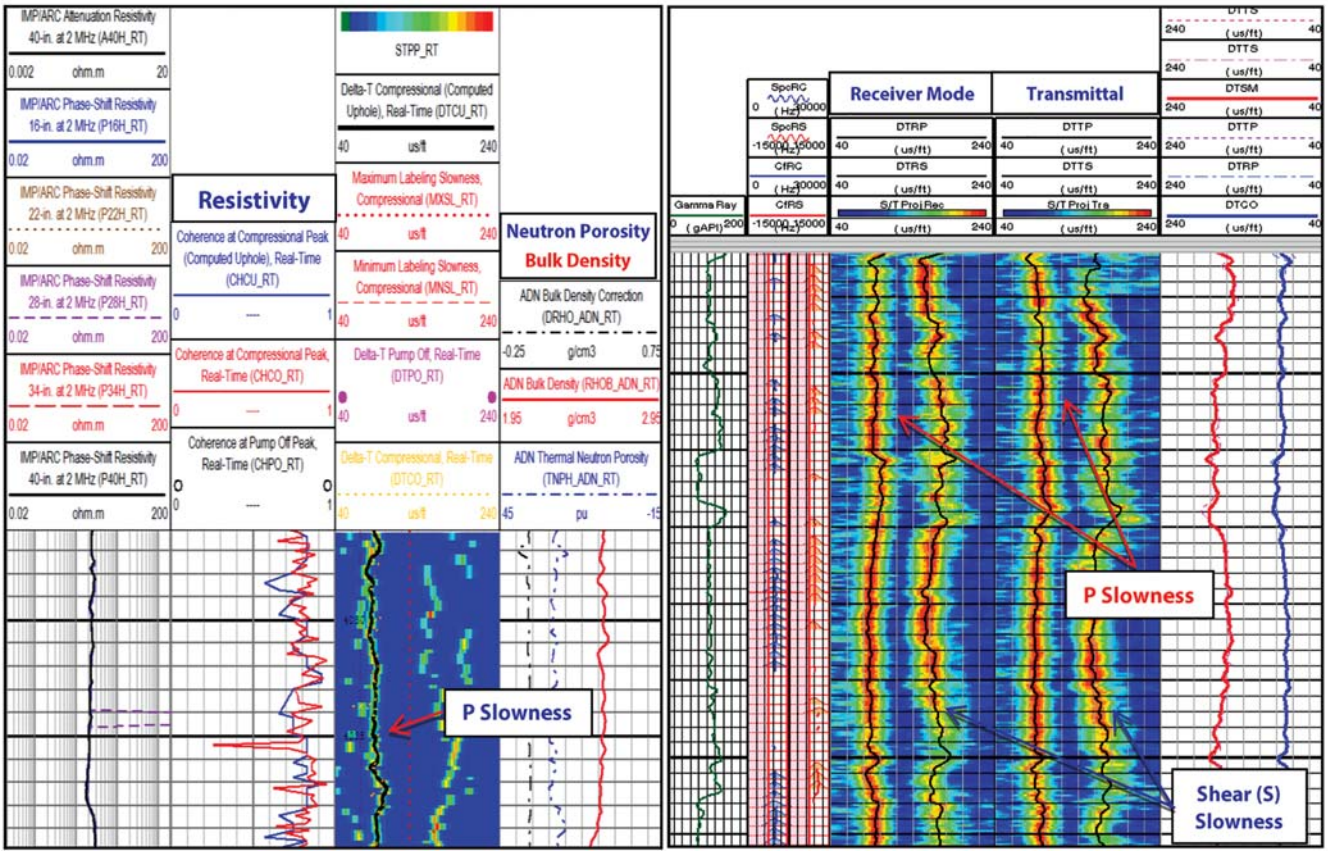

(a) (b)

Figure 7. *LWD sonic real-time (a) and recorded-mode (b) in 8.5-in. section*

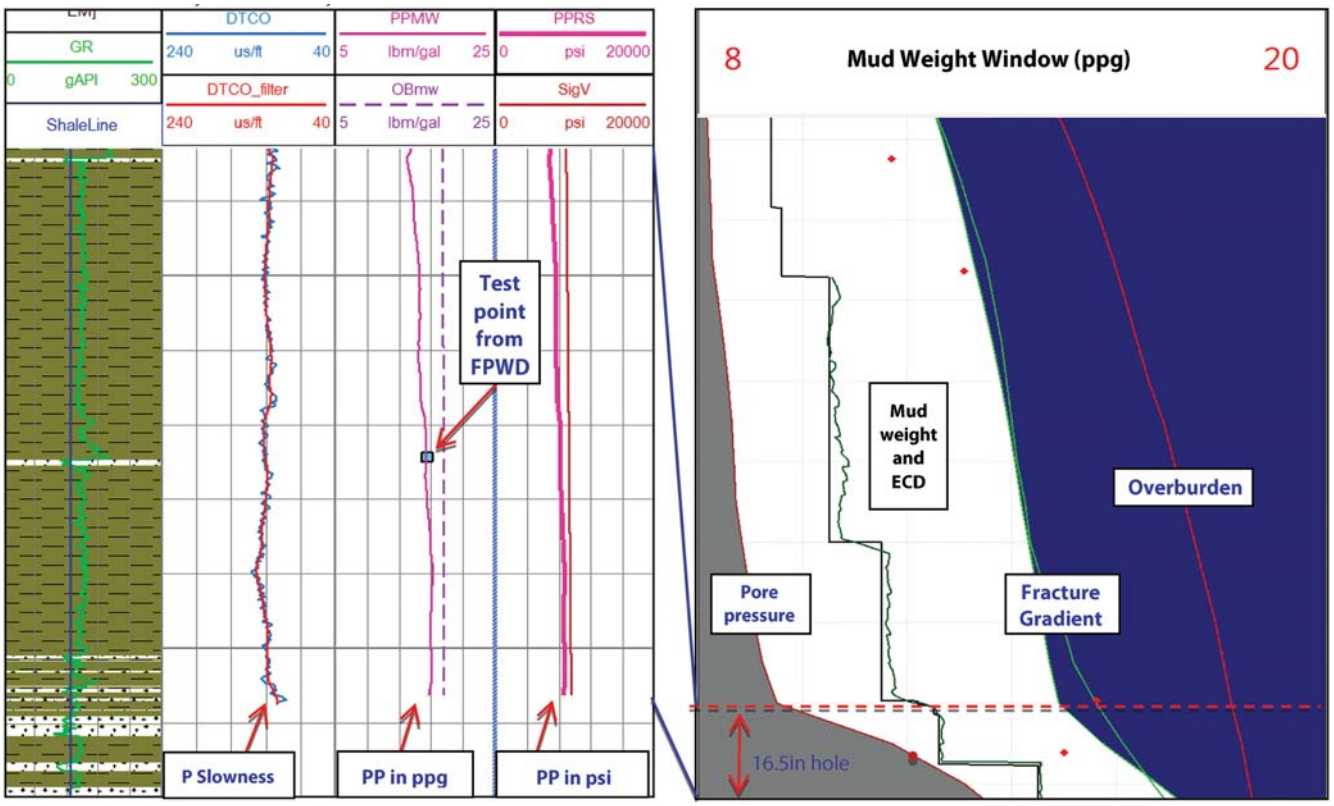

(a) (b)

Figure 8. *Real-time pore pressure calculation using LWD sonic and FPWD data (a) and the updated predrill model (b) in 16-in. hole*

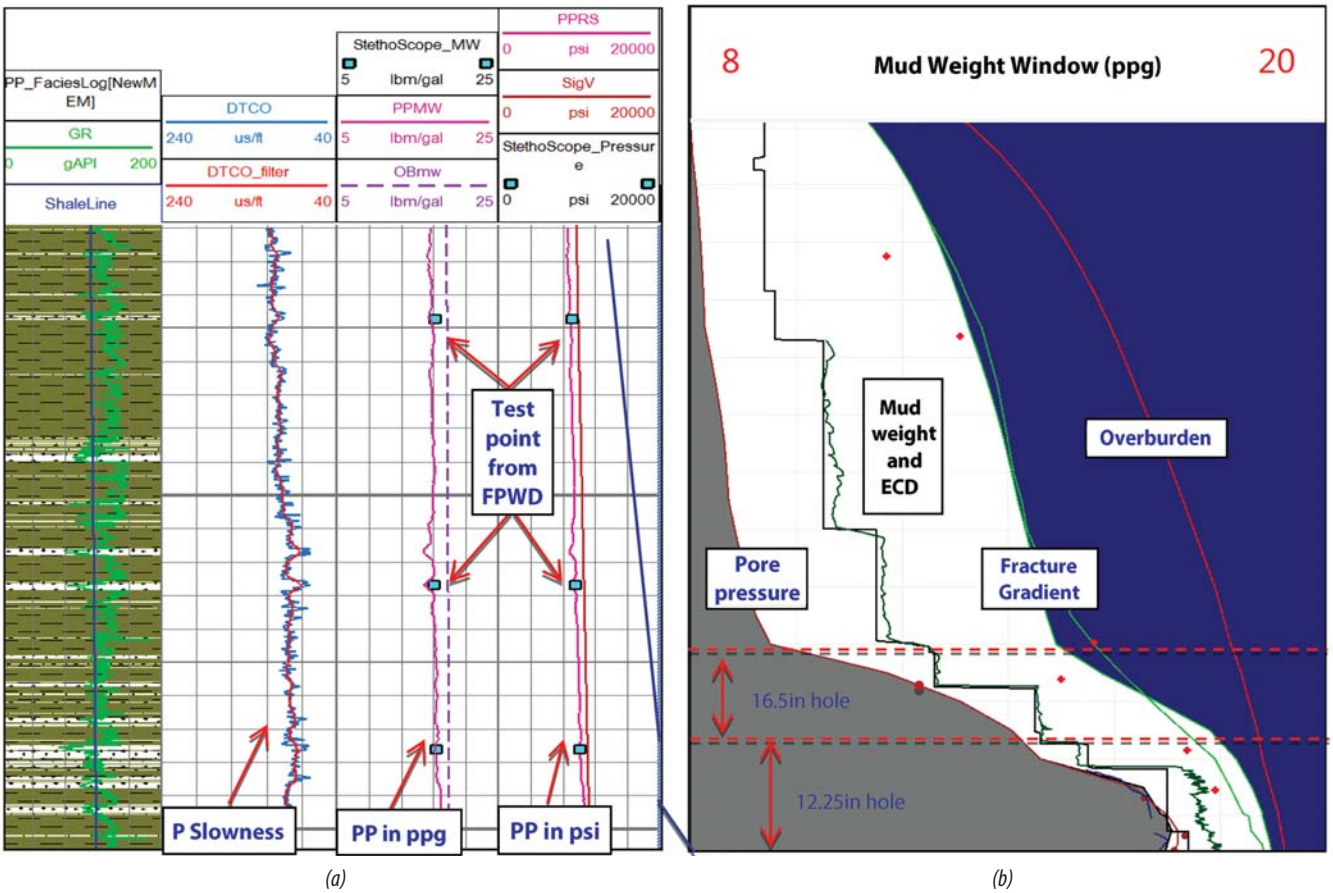

(a) (b)

Figure 9. *Real-time pore pressure calculation using LWD sonic and FPWD data (a) and updated predrill model (b) in 12.25-in. hole*

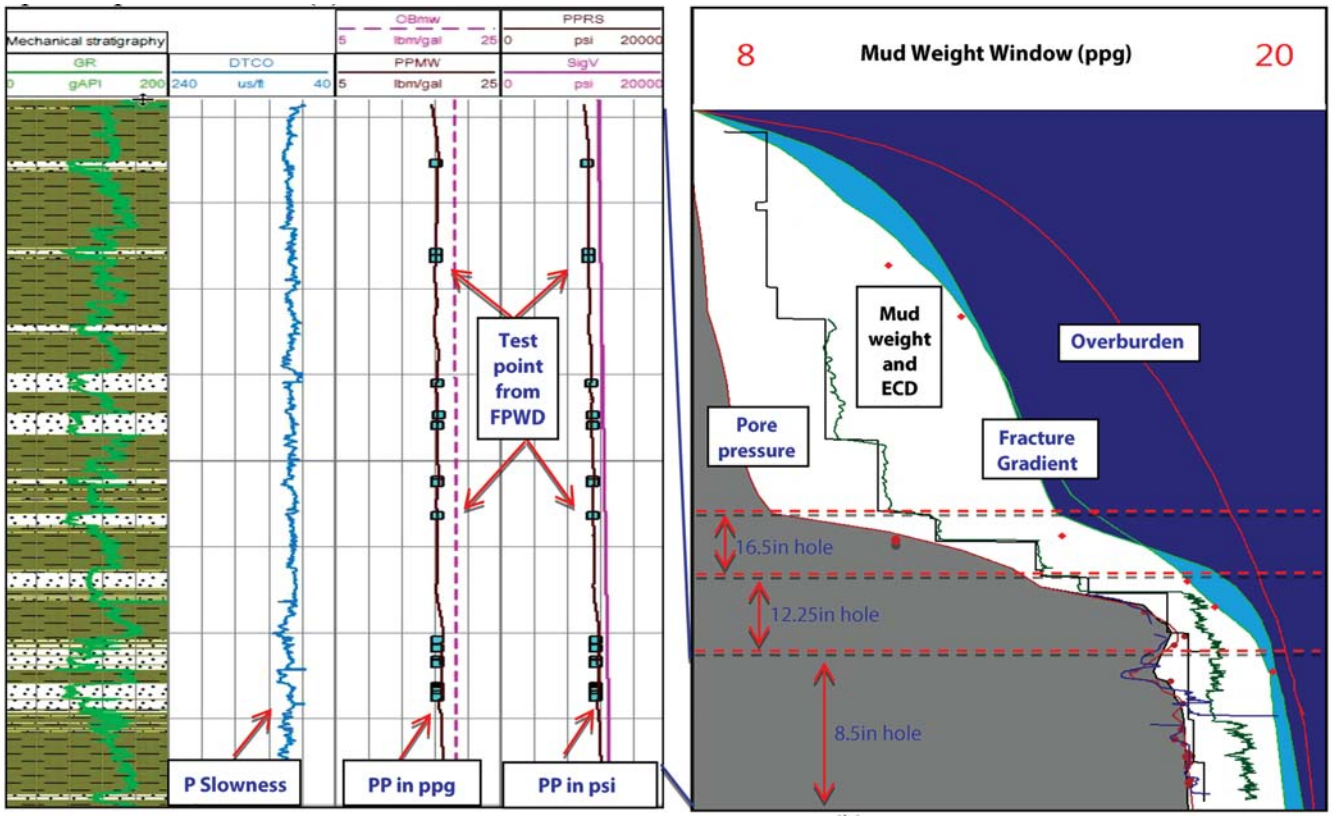

(a) (b)

Figure 10. *Real-time pore pressure calculation using LWD sonic and FPWD data (a) and updated predrill model (b) in 8.5-in. hole*

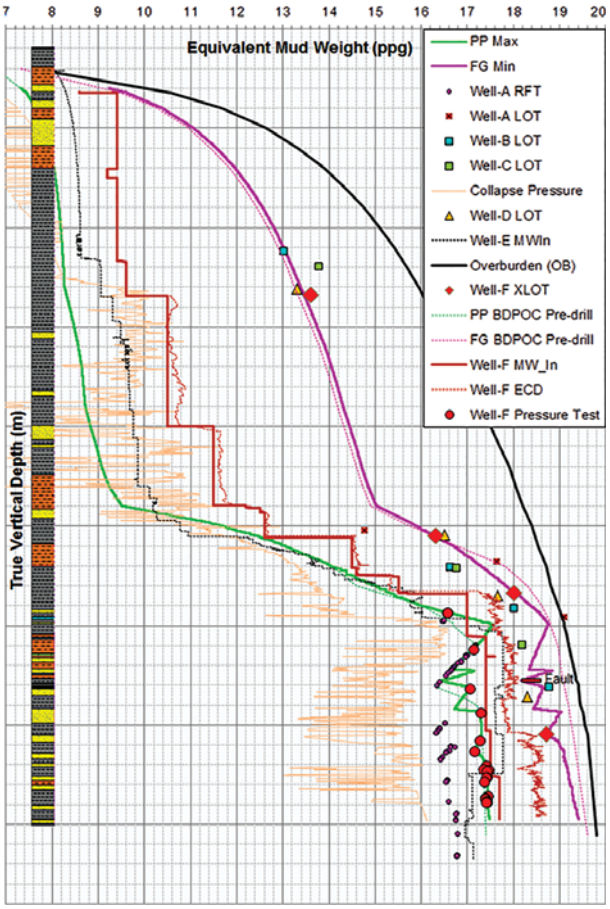

Figure 11. *Post-drilling model*

By using this technique, this well was successfully completed; drilling to TD of the well was accomplished without any pore pressure related incident.

2.3. Post-Drilling model

The real-time LWD sonic data matched well with recorded-mode and pump-off measurements for all three sections. The calculated pore pressure and fracture gradient matched the drilling observations; this indicates a correctly calibrated model that could be used for modelling and planning future wells in the same area. The post-drilling model is displayed in Figure 11.

3. Conclusions

The acquired real-time P slowness showed good agreement with the recorded-mode P slowness in this study. The calculated pore pressure from LWD sonic was matched with FPWD points in the sand formation. The MW window defined from calculated pore pressure in real time helped to improve well planning, prevented wellbore stability problems, and reduced drilling risks.

Accurate predrill PPP is the key to improving drilling efficiency and reducing risks and costs. Seismic data, regional geology data, formation pressure measurement, and well log data from offset wells can be used for predrill PPP.

The pore pressure profile, caliper log, and drilling events in offset wells were used to obtain a valid wellbore stability solution for predrill wells. Real-time analysis was performed while drilling to update the predrill model, reduce uncertainty, avoid drilling incidents, and increase drilling efficiency.

The good integration among petrophysics, geomechanics, acoustic, and the drilling domain helped to optimise the drilling performance in this well. As the result of this integration, the well was drilled successfully without major pore pressure related issues.

4. Discussion

LWD sonic data was combined with FPWD data to give a very good monitoring of pore pressure in real time. However, this method still has its own limitations, only pore pressure and fracture gradient boundaries are available, there are no information about the shear failure and mud loss boundaries. Therefore, real-time pore pressure and wellbore stability monitoring are recommended to provide four boundaries (pore pressure, shear failure, mud losses, breakdown) to avoid wellbore failures and reduce nonproductive time in the planned well, particularly for wells with high risk and when drilling in difficult geologic conditions/formations. The wellbore stability model (Figure 12) should be conducted before planning the well to recommend the MW and casing program.

The safe MW window can be determined between the shear failure (minimum MW) and mud losses (maximum MW). Real-time prediction helps to constrain and update the predrill model while providing real-time advice for making decisions in drilling operations.

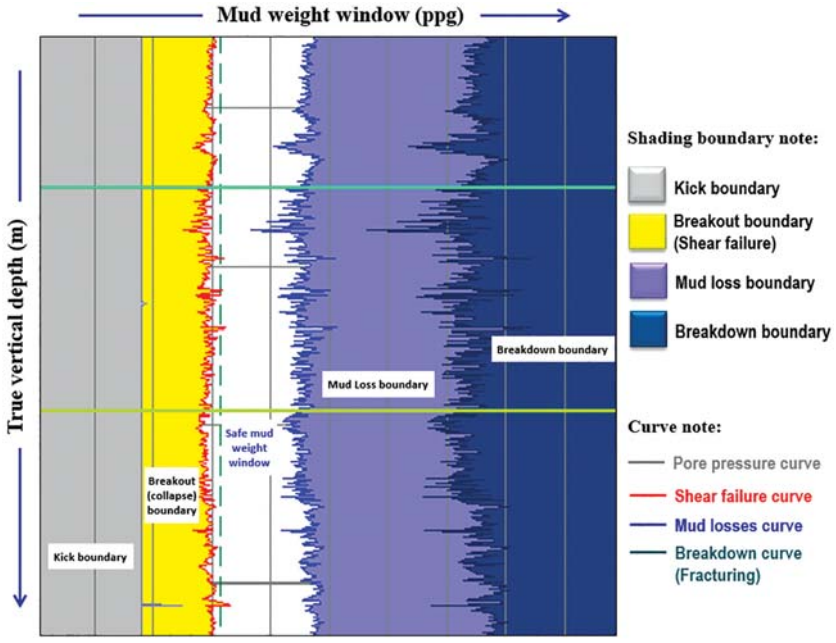

Figure 12. *Wellbore stability model predicts safe mud window with four boundaries (kick, breakout, mud loss, and breakdown)*

This paper was prepared for presentation at the Offshore Technology Conference Asia held in Kuala Lumpur, Malaysia, 22 - 25 March 2016.

Acknowledgments

We would like to thank Petrovietnam (PVN), Petrovietnam Exploration Production Corporation (PVEP), Bien Dong Petroleum Operating Company (Bien Dong POC), and Schlumberger for the support and permission to publish this paper.

References

1. J.Cai, L.Zhen, S.Y.Han, J.YiMing. *LWD sonic data analysis and applicability in South China Sea*. Offshore Technology Conference, Houston, Texas. OTC-25203-MS. http://dx.doi.org/10.4043/25203-MS. 5 - 8 May 2014.

2. B.A.Eaton. *The equation for geopressured prediction from well logs*. Fall Meeting of the Society of Petroleum Engineers of AIME, Dallas, Texas. SPE-5544-MS. http://dx.doi.org/10.2118/5544-MS. 28 September - 1 October 1975.

3. A.Ahmed, R.Hussain, L.Anis, et al. *Real time pore pressure prediction using LWD and borehole seismic data assists in mitigating on an appraisal well offshore Malaysia*. SPE/IADC Drilling Conference and Exhibition, Amsterdam, The Netherlands. SPE-140045-MS. http://dx.doi.org/10.2118/140045-MS. 1 - 3 March 2011.

4. S.S.Shaker. *Predicted vs. Measured pore pressure: Pitfalls and perceptions*. Offshore Technology Conference, Houston, Texas. OTC-14073-MS. http://dx.doi.org/10.4043/14073-MS. 6 - 9 May 2002.

DETERMINATION OF SOURCE AND BREAKTHROUGH MECHANISM OF WATER PRODUCTION IN A NATURALLY FRACTURED BASEMENT RESERVOIR BY ANALYSING WATER PRODUCTION DATA

Le Minh Vu, Tran Thai Son, Vu Viet Hung
Lamson Joint Operating Company
Email: vulm@lsjoc.com.vn

Summary

Excessive production of water in the naturally fractured basement reservoir has been one of the most intriguing problems in production engineering. Water may appear immediately at early production stage or break through after months on stream. Available methods to determine the source of produced water are entirely based on chloride content. Stiff diagram is one of the well-known graphical methods in place to confirm whether it is formation water by various chemical components. With the Stiff diagram, the operators are able to detect formation water at the early days which apparently assists in quantifying the potential of scale deposit, erosion and so on.

Apart from the water sources, it is crucial to understand the water-out mechanism also via graphical approach. The characteristic trend of water-oil-ratio and its derivative with time in log-log plot indicate a variety of slopes reflecting different flowing mechanisms and a vast majority of them are attributed to the coning and channelling dependent on the level of pressure depletion and rock fluid interaction. A thorough understanding of the water source and its break-through mechanism is indispensable to production monitoring and optimising well production performance in the long run.

Key words: *Water analysis, water breakthrough mechanism, excessive water production, production management, fractured basement, graphical methods.*

1. Introduction

Water production is among the problematic issues of the oil and gas industry nowadays. Formation water may appear at the beginning or after a period of production. In the early days, chloride and salinity assists in identifying the origin of water - whether it is drilling mud loss or formation water. In addition, the evaluation of formation water composition provides pertinent information to deal with potential scaling and corrosion from the exposure of formation water to well completion jewelries. During production phase, the produced water has been analysed constantly to monitor well performance and water encroachment so as to come up with a mitigation plan to sustain high production rates.

As mentioned, the determination of formation water from the sample analysis is fundamental along with other theoretical approaches which diagnose production data in the period with and without water production. In this paper, graphical methods are employed to get a close look at the Stiff diagram plotting produced water composition and the water-cut behaviour by a hypothesis developed by K.S.Chan [1]. Those methods have the advantages of being simple, handy and cost effective. However, the downside is the sampling frequency, which apparently increases the sampling cost and lab experiment. The Stiff diagram and Chan's hypothesis have been widely applied in Thang Long and Dong Do fields, Cuu Long basin offshore Vietnam as water production was observed from the early production phase. By diagnostic plots of the chemical indicators and water-cut with time, formation water and coning demeanour were confirmed in few wells which, indeed, supports a revision of production regime to cope with reservoir management policy.

2. Graphical methods for produced water analysis

Most of existing graphical methods are based on comparison of the chemical indicators. These indicators consist of the amount of anionic or cationic necessary to add to or removed from the compound 1 mole.

$$C\ (meq/L) = [g.m^{-3}]\ x\ Change/Mass = [g.m^{-3}]/equal\ wt$$

Where: Change: Chemotherapy;

Mass: Mass mole;

Equivalent wt: Volume equivalent conversion.

The equivalent conversion factor for some common ions is depicted in Table 1.

Table 1. *The equivalent conversion factors [2]*

Ion	Charge	Mass	Equivalent wt	Multiply by (to convert g.m^{-3} to meq/L)
H^+	1	1.0	1	1.0
Na^+	1	23.0	23.0	0.0435
K^+	1	39.0	39.1	0.0256
Ca^{2+}	2	40.1	20.15	0.0499
Mg^{2+}	2	24.3	12.15	0.0823
Fe^{2+}	2	55.9	28.0	0.0347
Zn^{2+}	2	65.4	32.7	0.0306
$(NH_4)^+$(as N)	1	14.0	14.0	0.0714
HCO_3^-	1	61.0	61.0	0.0164
CO_3^{2-}	2	60.0	30.0	0.0333
Cl^-	1	35.5	35.5	0.0282
F^-	1	19.0	19.0	0.0526
SO_4^{2-}	2	96.0	48.0	0.0208
NO_3^- (as N)	1	14.0	14.0	0.0714
H_2PO_4	1	97.0	97.0	0.0103

Stiff diagram

Among the available textbook methodologies in produced water analysis, Stiff diagram is the most popular one in which some key chemical indicators represented for seawater and formation water are plotted altogether as illustrated in Figure 1. In a Stiff diagram, data is plotted as a polygon, with cations to the left and anions to the right. Stiff diagrams are useful for looking at spatial relationships because they can be readily plotted on a map. In this respect, it is also a robust tool to compare between different water sources.

This method is easy to construct graphs of chemical indicators of multiple samples from different sources. When the water is determined, this diagram may point out a change of the chemical indicators from different sources in space and time. However, this method has the disadvantage that there is only one analysis performed on a single diagram.

Similarly, other methodologies being widely used in ground water analysis include Piper, Durov and Schoeller diagram, ion balance diagram, radial plot and chemical properties vs. time plot [2]. Nevertheless, they are simple graphics to track changes of each ion and do not analyse the combination of ions at the same time. Zaporozec summarised the methods for presentation of water analyses which were

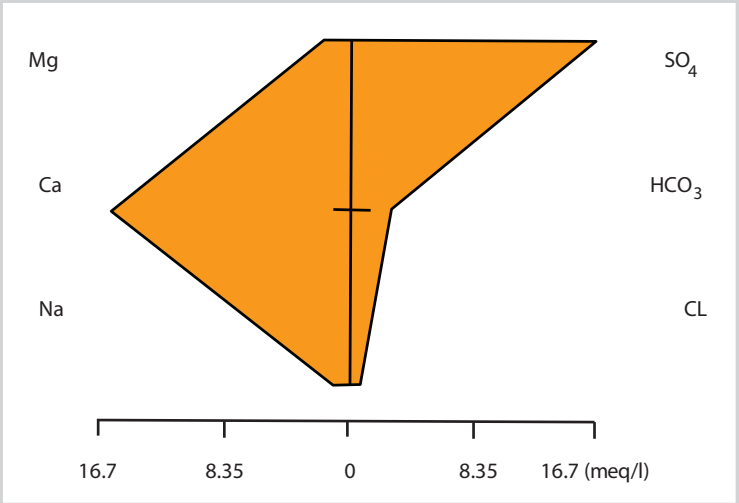

Figure 1. *A typical Stiff diagram [2]*

divided into four major sections: classification, correlation, analytical and illustrative [3].

All the above methods depend primarily on the purpose and the specific field applied. The change in the ion index of formation is complicated because water may penetrate from various sources. In the narrow scope of this research, Stiff diagram is the basis for analysing the water sources and its change with time.

3. Diagnostic plots to determine water breakthrough mechanism

Tracking water movement in the reservoir is a top priority in reservoir management when the wells commence water-out. There are numerous strategies for monitoring water encroachment, such as material balance, graphical analysis of production water and simulation model. An intuitive method introduced by K.S.Chan in

1995 where the WOR (water-oil ratio) and its derivative are drawn on the log-log plot with time. The disparity between the WOR and WOR' suggests potential issues: water channelling or coning. The formula for computing the WOR and its derivative are as follows:

$$WOR = \frac{q_w}{q_o}$$

$$WOR' = \frac{dWOR}{dt} = \frac{WOR_2 - WOR_1}{t_2 - t_1}$$

Chan's hypothesis was based on the examination of actual production data to forecast the water-cut behaviour with time. As mentioned, two typical issues at the excessive water production wells were attributed to the coning and penetration by channel (fractures, and aquifer zones). Figure 2 plots the ideal expression of the WOR-WOR' relationship.

According to Chan, a log-log plot of WOR behaviour for both coning and channelling is divided into three periods. The first period extends from the start of production to water breakthrough where the WOR is constant for both mechanisms. When water production begins, during the second period, WOR behaviour becomes disparate for coning and channelling. In the transition period, the rate of WOR increase after water breakthrough is relatively slow and gradually reached a constant value for the coning mechanism. For channelling, the water production from the breakthrough layers or fracture increases very quickly. The end of this period shows the WOR resumes at about the same rate. After the transition time, Chan's plot describes the WOR increase to be quite rapid for both mechanisms, which begins in the third period.

Figure 2 illustrated WOR time derivatives (WOR') versus time for the different excessive water production mechanisms. Chan mentioned that the WOR' can distinguish between coning and channelling. Coning shows a changing negative slope, as channelling WOR' curves show an almost constant positive slope.

The excessive water production is controlled by the reservoir management or well workover depending on

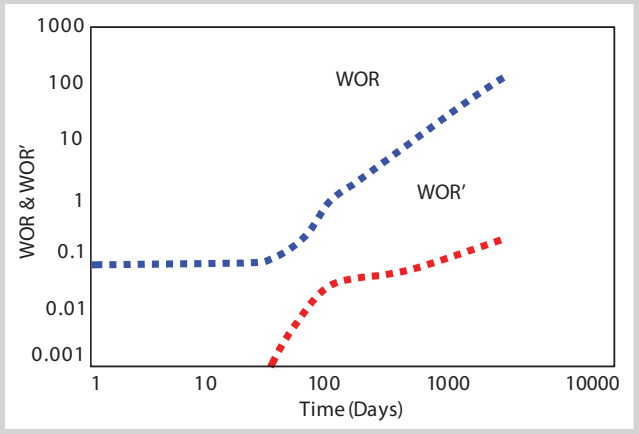

WOR and WOR' multilayer channelling

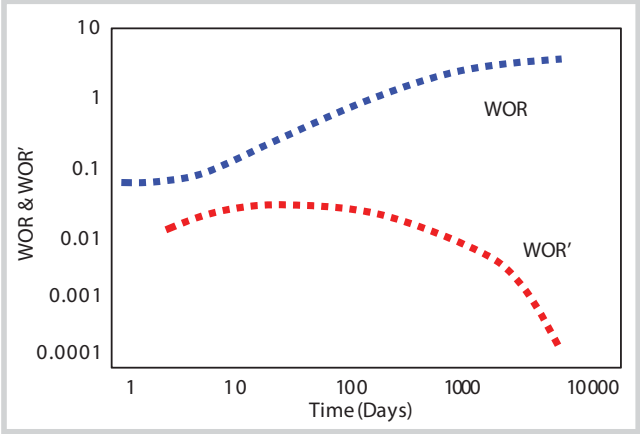

Bottomwater conning WOR and WOR'

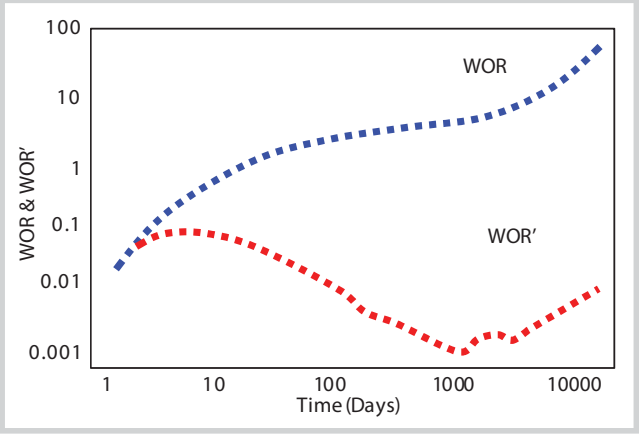

Bottomwater conning with late time channelling behaviour

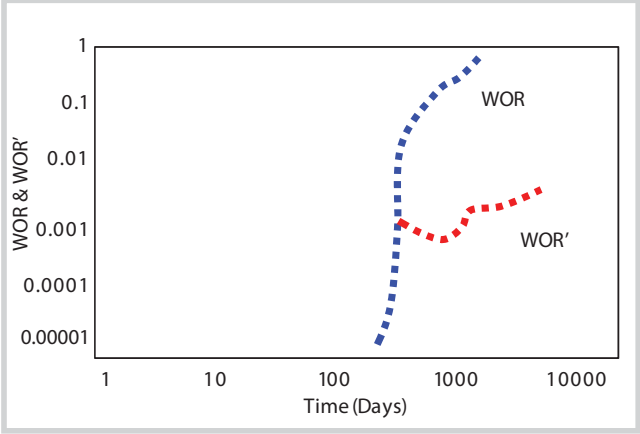

WOR and WOR' thief layer water recycling

Figure 2. *The K.S.Chan ideal plots [1]*

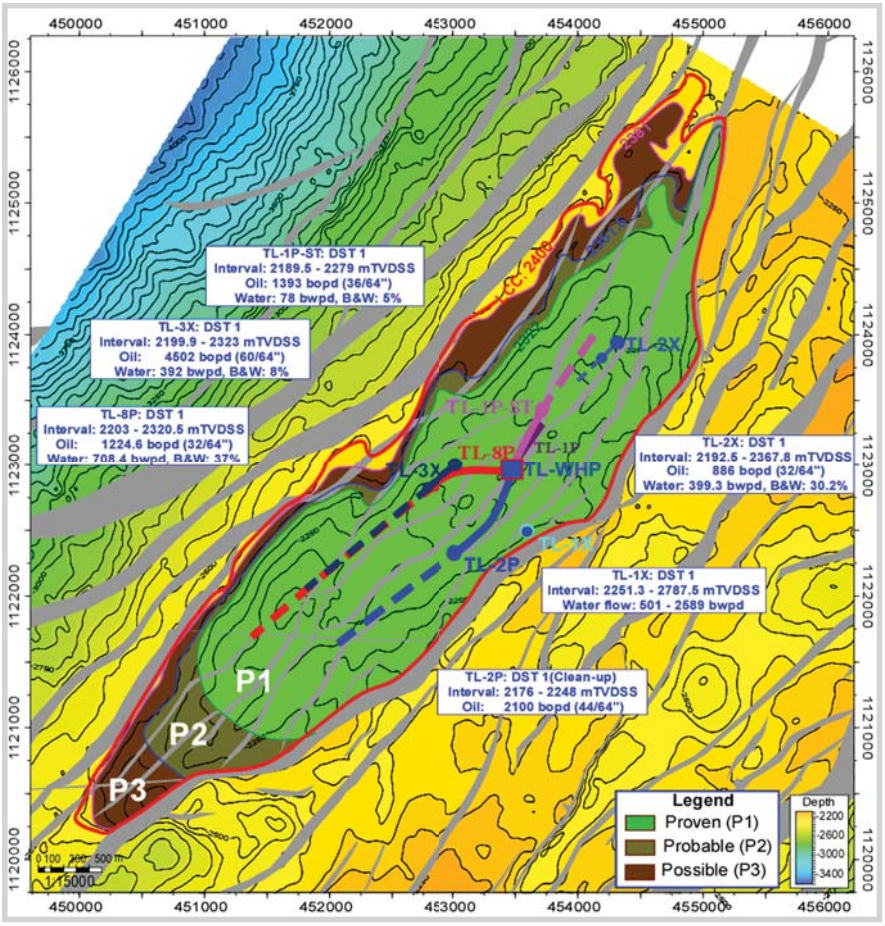

Figure 3. *Top Thang Long fractured basement depth map*

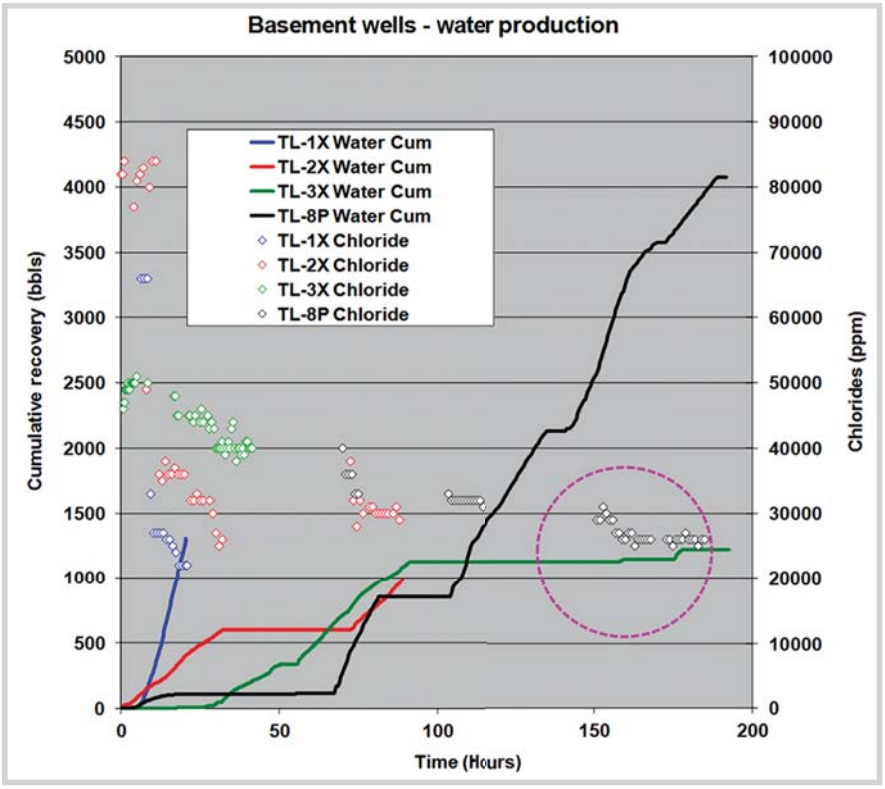

Figure 4. *Water production and chloride content with time in Thang Long fractured basement reservoir producers*

the type of the problem occurring at the well. The prediction of the water-cut tendency is vital to the remedial treatment like water shut-off and changing production conditions. Classification of well problems and water shut-off suggestion are mentioned in [4].

4. Water production behaviour in naturally fractured basement reservoir in Thang Long field

The naturally fractured basement reservoir in Thang Long field was first discovered in 2008 by three wildcat wells. To date, six wells have been drilled into this reservoir in the exploration and development phases as shown in Figure 3. Well testing data from the exploration wells demonstrated the recovered water was identical to the drilling mud loss and there were no signs of formation water. Chloride levels are diminishing steadily but remained above 30000ppm (Figure 4). However, only well TL-8P produced water immediately from the inception. The chloride content was decreasing slowly to around 22000ppm after three months on stream as shown in Figure 4. The question is whether well TL-8P has been producing formation water or drilling mud. After more than a year of production and having no water injection, the chloride content and other chemical components behave consistenly and there is no doubt on its origin.

The results of produced water analysis are shown in Table 2. The sample of LS1.01.41, 01.53, 01.56 and 01.58 are analysed for TL-8P from the beginning. Based on Saline Water Classification, this produced water is a kind of saline water type [5].

Table 2. Water sample analysis of Thang Long fractured basement reservoir producers

Ion	LS1.01.12	LS1.01.58	RD-N-3P (Formation water)	Seawater	TL-8P (13/6/2014)	TL-1P (13/6/2014)	TL-1P (1/7/2014)	TL-8P (18/12/2014)	TL-8P (18/12/2014)	TL-1P (09/5/2015)	TL-8P (09/5/2015)
Sodium Na^+	16052	11226	5649	10180	10352	22101	9020	8314	8408	5732	5643
Potassium K^+	281	128	453	394	173	263	102	154	161	280	179
Calcium Ca^{2+}	4912	4198	2909	495	3690	3814	2534	3422	3512	5320	5200
Magnesium Mg^{2+}	1335	1136	10	3301	168	154	91	142	154	72	96
Chloride Cl-	35678	27944	14914	20411	22609	38697	19986	19216	19382	19525	19170
Bicarbonate (HCO_3)-	439	398	68	264	267	435	267	272	274	250	275
Sulphate $(SO_4)^{2-}$	1478	1342	47	2599	358	974	366	101	104	58	49

Stiff diagram to determine water sources

As soon as water appeared in TL-8P, consistent analysing of samples was indispensable to provide adequate information for plotting the Stiff diagram. The water sample analysis result, then, is double check with the ones of nearby fields for reference.

In Figure 5, the first water samples lay far from the formation curve of nearby fields (in orange - LS.01). Visually, the shape of the envelope of cations and anions has been changing with time. The envelopes gradually shrink and move towards the formation water (the blue and red lines). Water sample analysis dated 18/12/2014 (in orange) was almost approaching the formation water one.

In principle, it is possible to distinguish three fundamental stages in the above Stiff diagram. In the early stage, water production was mostly concluded as drilling mud loss. The shape of the envelope tends to gradually shrink in the second stage depending on the level of water production and the distance to water sources. During the second stage, the envelopes of water production were proximate to formation water and the well may produce entirely formation water. The third stage appeared only when the reservoir had influx from other water sources. The speed of

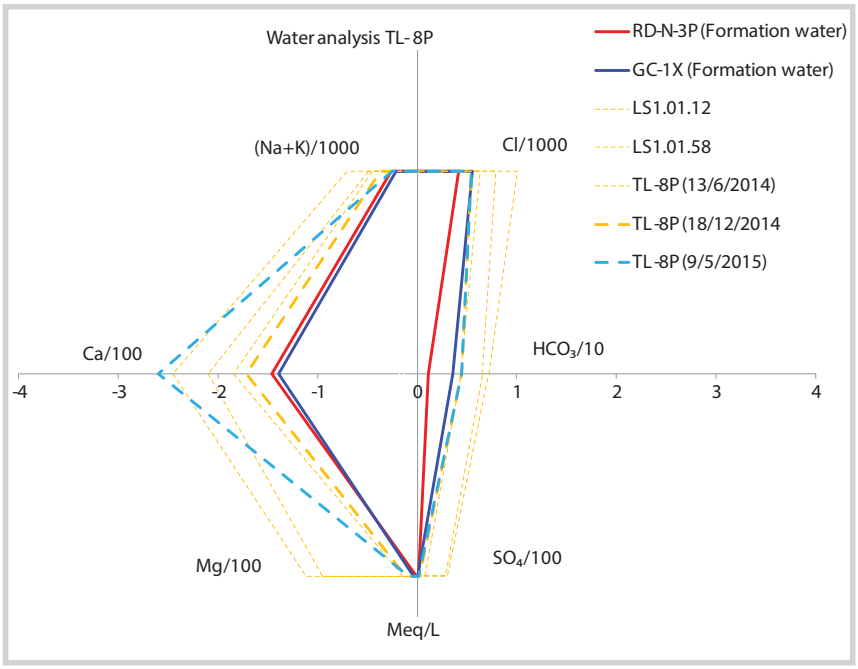

Figure 5. Stiff diagram compares water sample analysis of TL-8P well with time

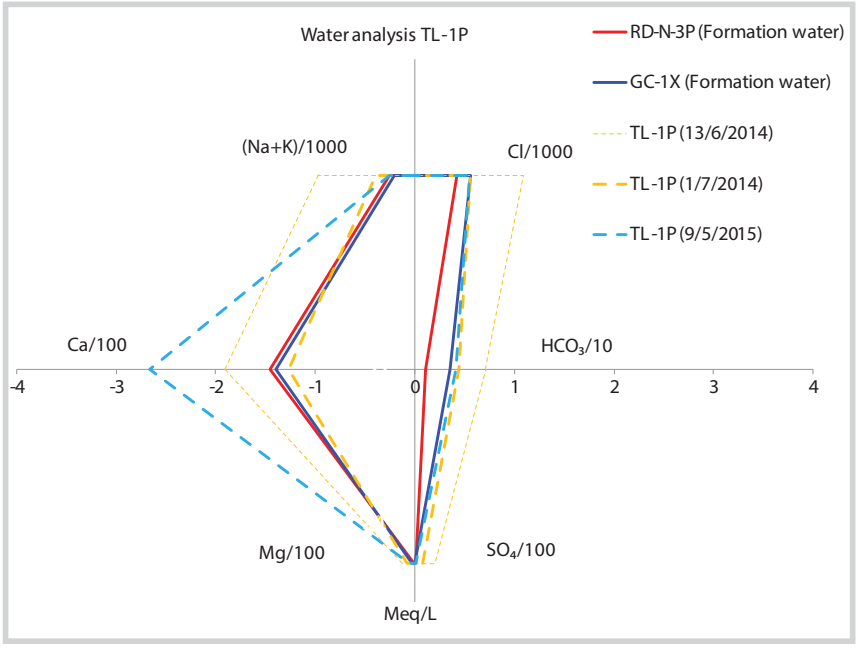

Figure 6. Stiff diagram compares water sample analysis of TL-1P well with time

moving from the second to the third stage depends on the capacity of the external water source. Usually, the indicators change in the third phase is Ca or/and HCO_3.

This technique is similarly applied to the second well TL-1P. The envelope expressed the changes identical to TL-8P well. The envelope of this well, as described in Figure 6, in July 2014 was pretty close to the formation water curve.

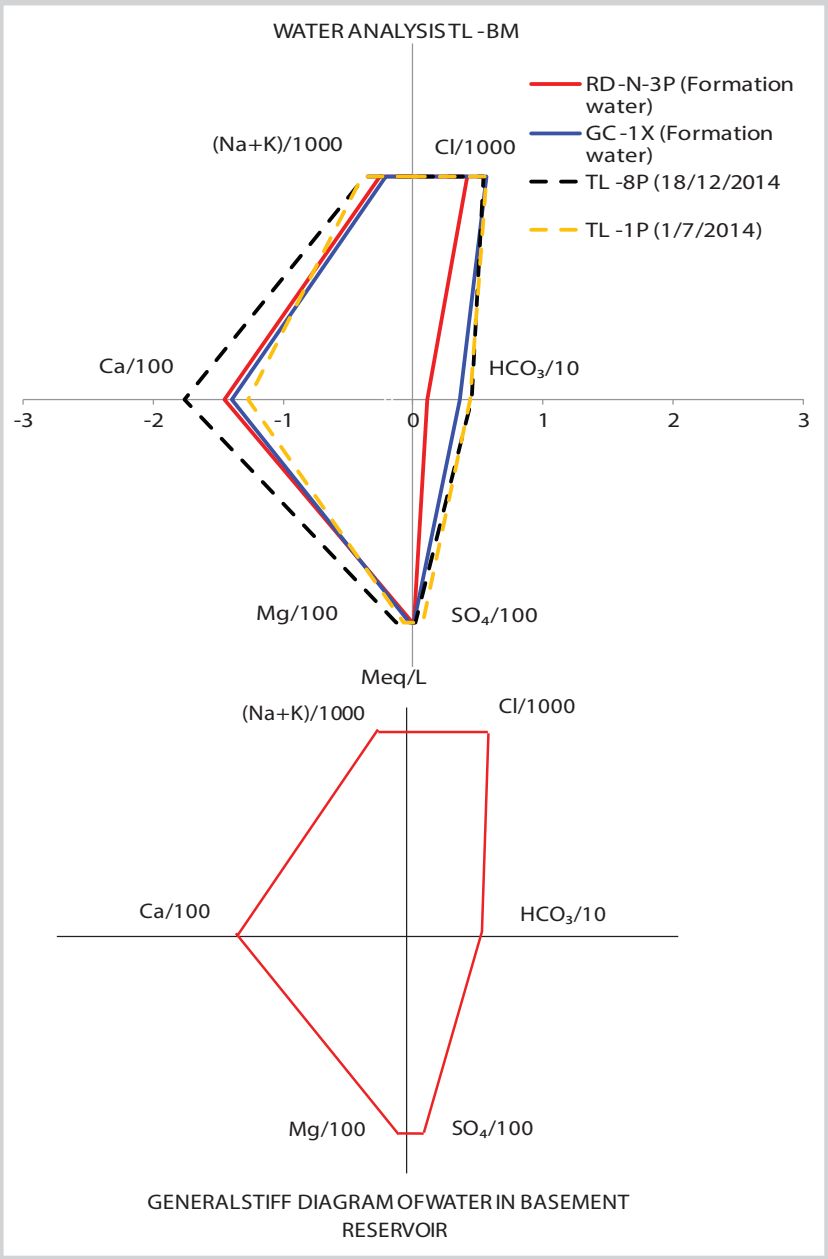

Figure 7. *Baseline of formation water of naturally fractured basement reservoir in Thang Long field*

By statistical methods, a baseline of the formation water for this kind of reservoir is developed and serves as a pragmatic source for analog down the road. The amplitude change in each ion indicator is depicted in Figure 7 and Table 3.

Through the Stiff diagram, water production from this fractured basement reservoir was pinpointed as kinds of formation water. As a result, the well placement of the third production well, TL-2P, was fine-tuned with well trajectory kept in close proximity to the top structure and shunned potential fracture areas which deemed connecting to the water zone. Consequently, the wells produced free water from the beginning and the Stiff diagram proved a good practice in production monitoring and well placement.

5. Determination of water breakthrough mechanism

After confirming the sources of produced water, understanding the breakthrough mechanism is crucial with regard to optimum production regime to level off the water cut. It is the point to bring up Chan's diagnostic plots to analyse production data. The plots in Figures 8 and 9 are designated for wells TL-8P and TL-1P respectively.

The water production in TL-8P and TL-1P appeared from the first days and was presumed to originate from the bottom aquifer. Moreover, the rapid raise

Table 3. *The amplitude changes of ions in the formation water*

Ion	(Na + K)/1000	Ca/100	Mg/100	SO_4/100	HCO_3/10	Cl/1000
Tolerance (meq/L)	-(0.21 - 0.39) / - 0.28	-(1.27 - 4.36) / - 2.68	-(0.01 - 0.12) / - 0.05	(0.004 - 0.076) / 0.002	(0.11 - 1.18) / 0.64	(0.42 - 0.63) / 0.55

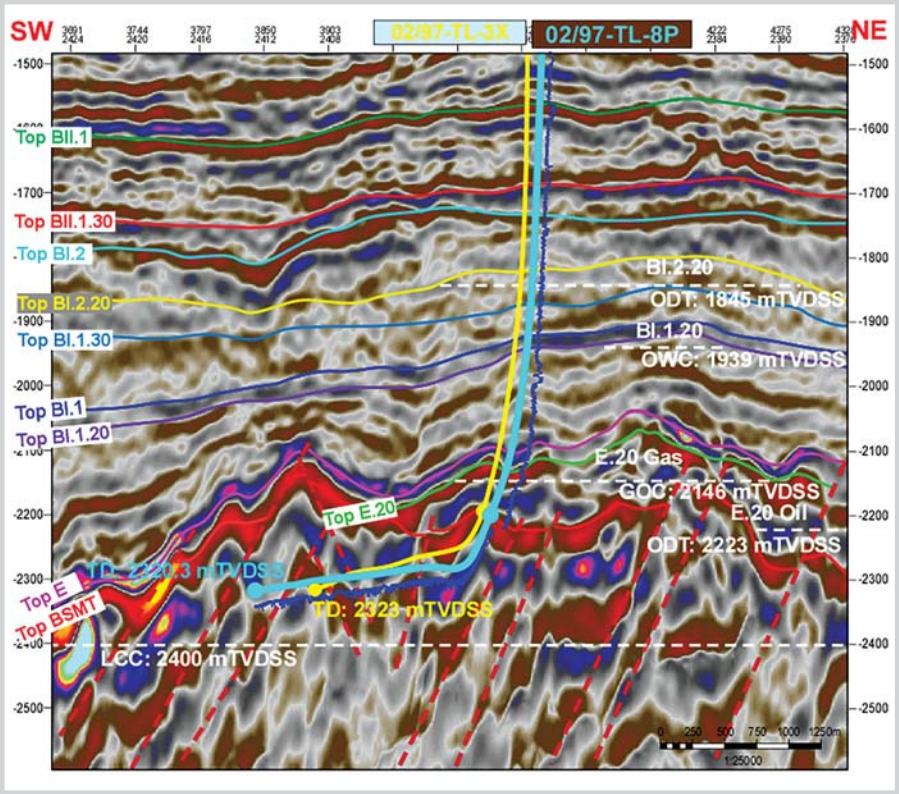

(a)

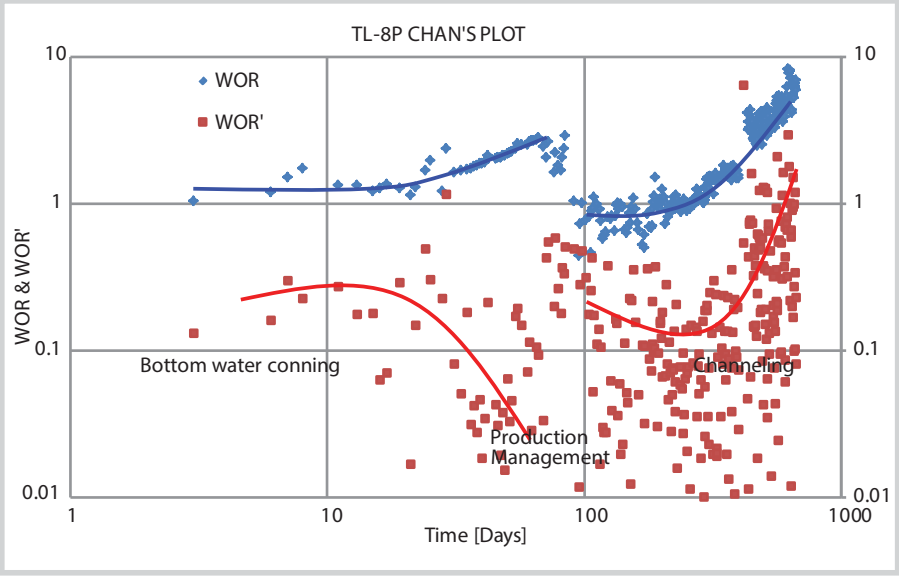

(b)

Figure 8. *Seismic cross section through (a) TL-8P and Chan's diagnostic plot (b)*

of water production could be from high permeability channels (large fractures connected directly to the bottom water zone) as illustrated in the seismic cross section. Oil production was maintained for a while until the coning influence. It can be seen that separate mechanism occurred in both cases where the coning appeared shortly in few months then abruptly switched to channelling.

In the TL-8P case, a step change of data was recorded over 100 days which coincided with the effort to boost production by drastically applying pressure drawdown to productive fractures at the oil zone close to well heel. After a period with severe depletion, water started channelling massively to the well and production curtailment is expected. In contrast, well TL-1P water encroachment was smoothly transitioning from coning to channelling due to low permeability in oil zone and drastic depletion of reservoir energy. Drastic depletion has not made any difference to the well because of low average permeability from the well testing (k ~ 1.7md).

Depending on the mechanism of water production and reservoir properties, an adaptive strategy shall be made to slow down the water-cut development. In the naturally fractured basement reservoir, transition time between coning and channelling are fairly short if producing at excessive rates. Therefore, it is essential to constantly update the Chan's plots to stay tuned with the reservoir performance, thus optimising production.

In a broader view, the more application to the fractured basement wells with longer production history and production rates is paramount to improve the accuracy of the assessment. By far, they are a much simple approach for daily operation monitoring.

6. Conclusions and recommendations

The graphical methods in analysing produced water help determine sources of water production in the naturally fractured basement reservoir in Cuu Long basin. The shift of the envelope in Stiff diagram was exhibited in three main phases:

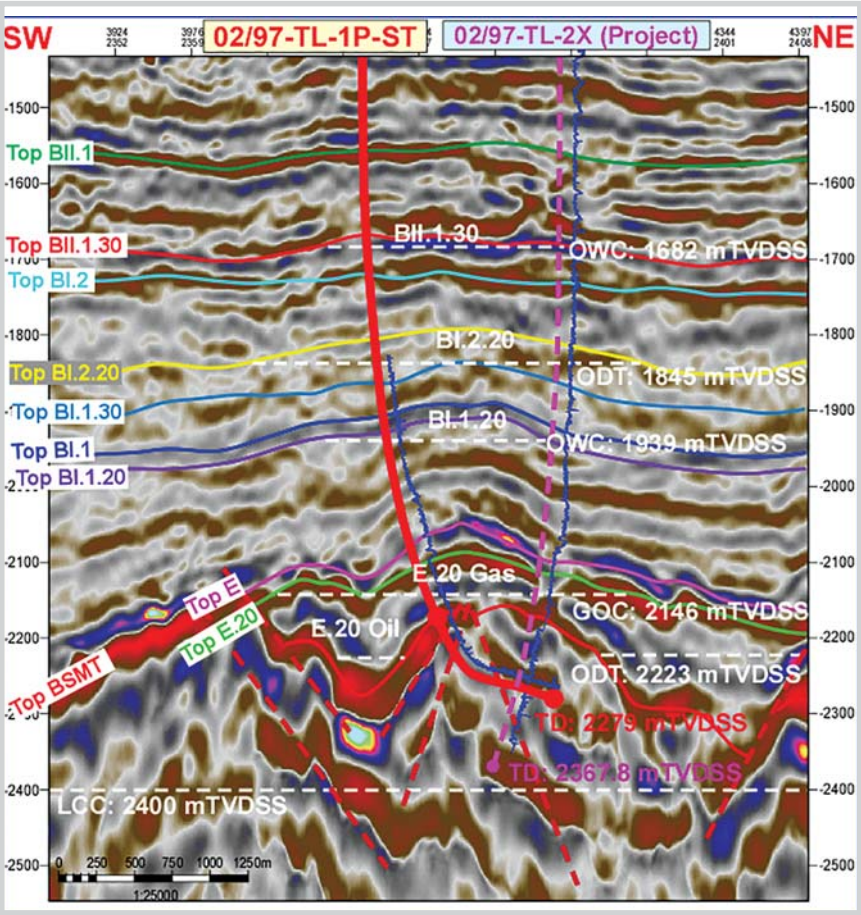

(a)

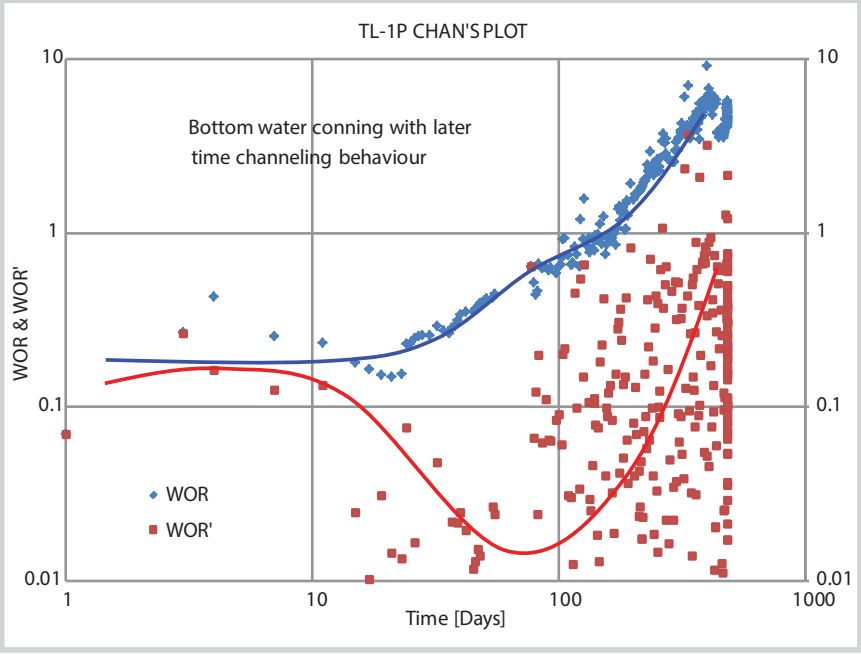

(b)

Figure 9. *Seismic cross section through TL-1P and Chan's diagnostic plot*

phase (1) drilling mud loss, phase (2) formation water and phase (3) additional water influx;

When determining the water-out mechanism, K.S.Chan's diagnostic plots indicate whether it is coning or channelling and the transition time if applicable;

A general trend of water from the naturally fractured basement reservoir in Thang Long field has been developed in a hope to be a source for reference in dynamic Cuu Long basin analysis;

The more applications the better accuracy level of the reservoir performance monitoring by these approach.

References

1. Echufu-Agbo Ogbene Alexis. *Diagnostic plots for analysis of water production and reservoir performance*. Master of Science in Petroleum Engineering. December 2010.

2. Erika Elswick. *Methods for analytical geochemistry*. Geology 214 (Lectures), Indiana University. 2012.

3. Alexander Zaporozec. *Graphical interpretation of water - Quality data*. Department of Geology and Geophysics, University of Wisconsin. 1972; 10(2): p. 32 - 43.

4. Abbas Ali Changalvaie1, Kazem Lovimi, Abbas Khaksar. *Mechanism of excessive water production in an Iranian offshore oilfield*. Petroleum Engineering Department, Islamic Azad University. 2012.

5. *Water sample analysis & evaluation report*. Laboratory of Research & Development Center for Petroleum Processing. December 2014.

INTERNAL PERSPECTIVE – EFFICIENT REACTOR INTERNALS ARE THE SHORTCUT TO EFFICIENT HYDROPROCESSING UNIT PERFORMANCE

Julie Jannerup[1], Emir Zahirović[2], Dan Morton[3]
[1]*Haldor Topsoe Snd Bhd, Kuala Lumpur*
[2]*Haldor Topsoe A/S, Denmark*
[3]*Haldor Topsoe, Inc., USA*
Email: JUJA@topsoe.dk

Summary

Hydroprocessing units are today pushed more and more as environmental legislations are tightening, and margins are reducing. Key factors in achieving high profitability of the hydroprocessing unit are to ensure that the unit has a long cycle length and short turnarounds. Increasing cycle length can of course be done by increasing catalyst activity, but even the highest activity catalysts requires that the distribution of liquid and gas in the reactor is optimal. In two-phase plug flow reactors it is crucial that distribution trays disperse oil and gas on the entire surface area of the reactor, ensuring all catalyst is used and maximum activity is obtained. The distribution trays therefore have major influence on the utilisation of the catalyst, and thus cycle length. Furthermore, cleverly designed reactor internals increase the safety of operators and reduce shutdown time. Access to and through such reactor internals as well as maintenance of the internals is simple and fast.

Taking into account all these facts, it is obvious that the profitability of a hydroprocessing unit is directly dependent on the performances and design of the reactor internals.

Key words: *Safety, optimal performance, increase profitability, increase cycle length, reduce turnaround time, improved mixing, scale catcher, distribution tray, hydroprocessing, refinery, pressure drop.*

1. Introduction

Key factors in maximising profitability in a hydroprocessing unit are utilising the catalyst activity optimally and reducing and shortening shutdowns. Ensuring full utilisation of the catalyst could mean increased feed rates, more severe feeds or simply increased cycle length. All of which will increase profitability.

Optimal catalyst performance would only be obtained with uniform flow distribution, and the assumption that the flow through the catalyst bed is uniform is a part of any model predicting the performance of the catalyst. This means that if the real world conditions are not close to it, the unit performances would not be as expected, consequently the efficiency and profitability of the unit will be decreased.

Quality of catalyst loading is a very important factor, directly affecting flow profile through the catalyst bed and if the catalyst is loaded poorly, it will have negative effects on the catalyst utilisation. But, even the best loaded catalyst cannot neutralise maldistribution caused by underperforming reactor internals.

Historically, the performances of reactor internals were not so critical as today because of tightened product specifications and great variations in feed stock blends as a consequence of market opportunities. New reactor internals are therefore designed to be efficient over a wide range of operating conditions. Collected experiences, together with rapid development of computational software and methods enable developers to optimise reactor internals to perform efficiently in all operating cases, from Start of Run (SOR) to End of Run (EOR).

Design of new reactor internals is adjusted not just to meet the demanding performance requirements, but also to ease installation and maintenance while keeping safety of operators at the highest possible level.

Working in 3D environment and using all latest CAD software enables technology suppliers to customise reactor internals for any existing unit and smoothly replace the old reactor internals technology with new.

The performance of the catalysts in a hydroprocessing reactor is affected by all reactor internals (Figure 1).

There are however three vital internals that govern the performance of the catalyst: Distribution Trays, Quench Mixers and Scale Catchers. These are the backbone of a reactor in terms of process functionality and have the largest impact on catalyst performance and consequently on the profitability of the hydroprocessing unit.

2. Liquid distribution trays

The primary function of the distribution tray is to ensure uniform transfer of liquid and vapour to the bed below and consequently achieve maximal utilisation of the catalyst. A distribution tray must have stable performance over a wide range of operating conditions during the cycle. SOR and EOR conditions are not the same due to different degrees of feed evaporation, hydrogen consumption, temporary and permanent upsets, feed rate changes, gas to liquid ratios and build-up of fouling agents, etc. All are part of a normal reactor cycle and are anticipated in well-designed reactor internals.

At Topsoe, those challenges were solved by the invention of Vapour Lift Tube (VLT) distribution technology.

The Topsoe VLT operates on a "vapour assist" principle where the treat gas drags the liquid up through the riser and through the vertical slots on the side. The slots are partially submerged in the liquid, and the gas flows through the free part of the slot. The velocity of the gas through the free (open) part of the slot will determine the amount of liquid that is pulled up through the riser and thus constantly adjust the liquid on the tray to the same level. This self-adjusting principle of the VLT design ensures the flexibility throughout the cycle, from low to high operating temperatures, as well as a wider range of process conditions (Figure 2).

Due to the high velocities in the risers, dispersed flow regime is established and liquid is discharged to the catalyst below as a mist and this assures uniform wetting of the catalyst.

Industrial example of benefits of reactor internals upgrade.

Existing distribution tray of previous generation was replaced with Topsoe VLT distribution tray in one European hydrotreating unit producing Ultra Low Sulfur Diesel (ULSD). Before the installation of Topsoe VLT tray in 2012, the reactor was suffering from short cycles. This case was perfect for demonstration of the positive impact of Topsoe VLT on the unit performance as the reactor was loaded with the same catalyst type using the same loading method, before and after the revamp. Also process conditions and the product specifications were unchanged.

In Figure 3, the feed density and the product sulfur of the two cycles are showed to be at the same level.

In Figure 4, the Weighted Average Bed Temperatures (WABT) of the two catalyst cycles are shown. The cycle with the new VLT internals was operated at 10°C (18°F) lower WABT than the previous cycle at SOR. This resulted in a cycle length improvement from ~300 days to more than 500 days. The additional cycle length provided the refiner with a very significant profitability increase, thanks to lower catalyst consumption and better on-stream performance. Return On Investment (ROI) for such improvement is high, and the reactor internals therefore have a short payback time.

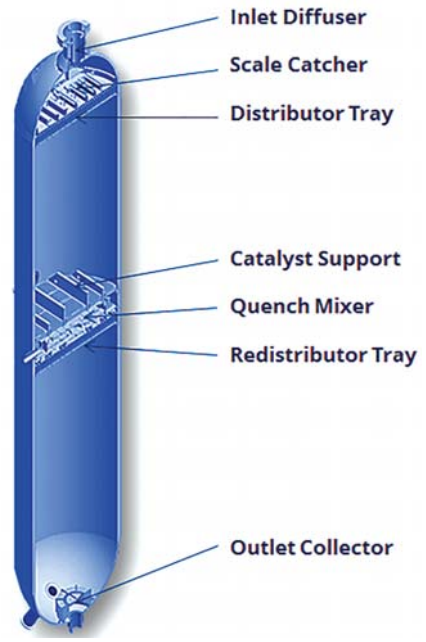

Figure 1. *Cross-section of typical two beds hydroprocessing reactor*

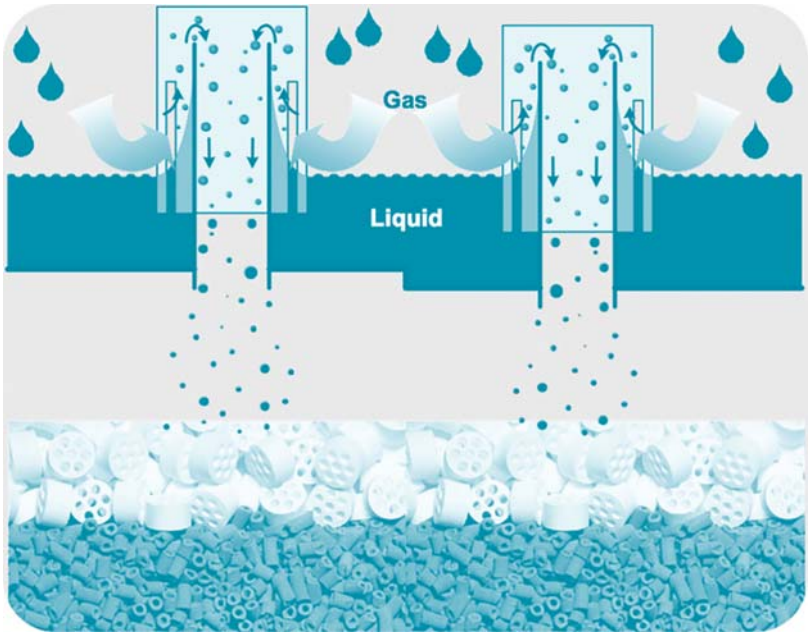

Figure 2. *Topsoe VLT, illustration of low sensitivity on liquid unlevelness on the tray*

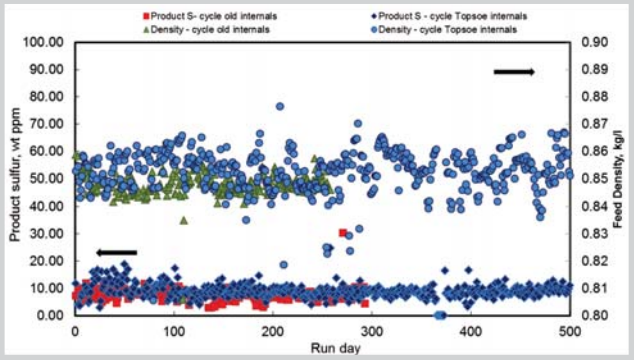

Figure 3. *Case study: revamp of a hydroprocessing reactor with a VLT distribution tray. Product sulfur and density*

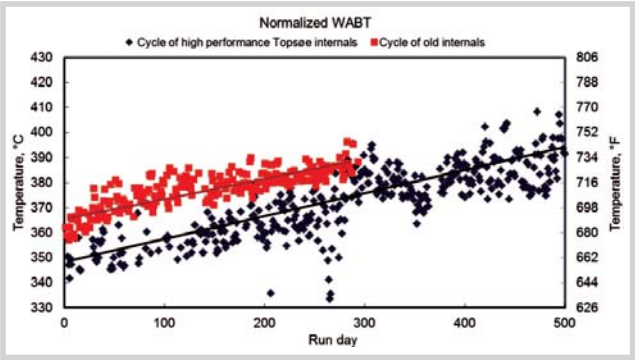

Figure 4. *Case study: revamp of a hydroprocessing reactor with a VLT distribution tray WABT*

3. Quench mixing zone [1]

The importance of the quench section mixer's performances is often overlooked. The main function of the quench section is to control and maintain temperature profile over the reactor by mixing of the cold quench treat gas or liquid with the hot effluents from the bed above. Mixer must also be functioning well to properly mitigate any radial temperature spreads that may develop in the bed above during operation.

The correct design must have four main qualities:

- Mixing;
- Quenching;
- No influence on the distribution tray performance;
- Low height;

Most of the older designs do not achieve all four of these critical elements required to provide optimal performance and economical space usage in the reactor. Topsoe quench mixers utilise these four parameters in the most efficient way. Topsoe Vortex type mixers are achieving all the above stated goals by forcing the hot process stream and cold treat gas into angled openings near the mid-centre of the reactor, where they enter a secondary chamber with enough angular momentum. In this way full mixing is obtained from the two streams, at which point they merge in the centre and exit the mixer onto the distribution tray below. This technique has been proven in over 400 installations to be an ideal mixing chamber.

Another area to look into when the cycle length becomes critically short is the reactor volume available for the catalyst. Quench sections of older design tend to occupy a significant space of the reactor volume, where quench sections with a height in the range of 1,500 - 2,000mm

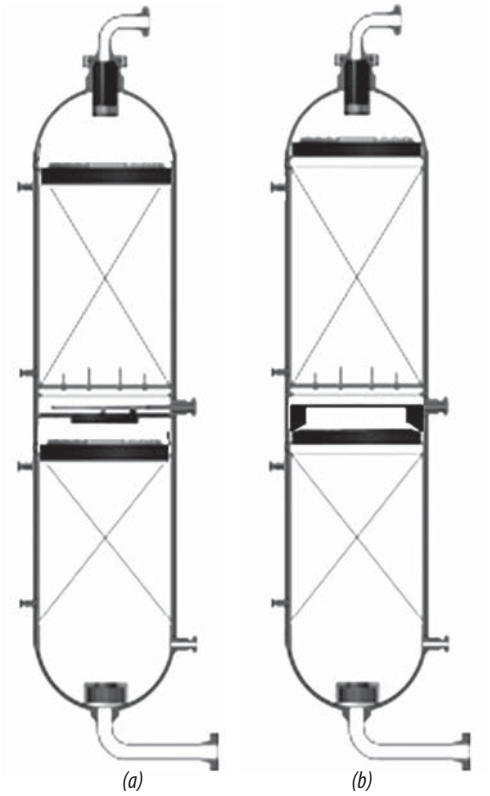

Figure 5. *Old layout (a) and new layout (b). 1.2m of extra loading height equivalent to 16% extra catalyst, increasing cycle length by 7 months*

are quite common. Modern quench sections can be accommodated in a fraction of that height, consequently converting this service space to active reactor volume in which additional catalyst can be loaded. Figure 5 illustrates the significant difference that can be gained by installing new reactor internals. In this case study, the top distribution tray could be lifted up to the tangent line and the quench section could be compressed. This gave an additional height for catalyst of 1.2m, which is equivalent to almost 10m^3 extra catalyst. This was 16% more catalyst than the loading with old internals and would increase the cycle length by 7 months.

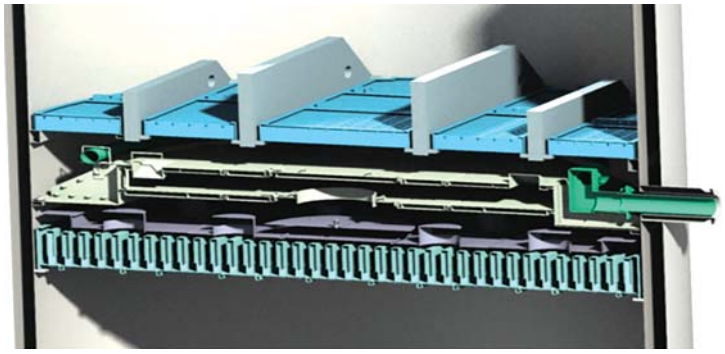

Figure 6. *Compact quench section, traditional*

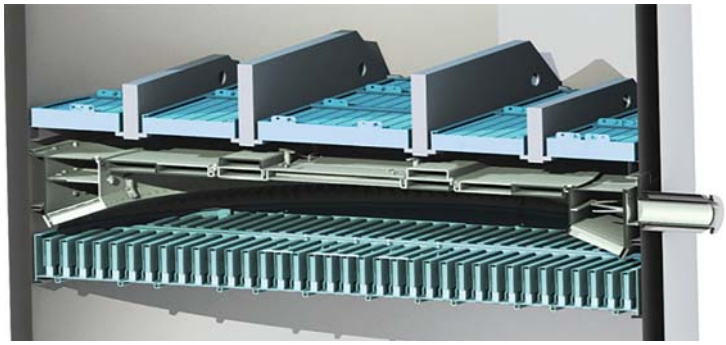

Figure 7. *Compact quench section, based on Torus™*

Figure 8. *Ergonomic and safe inspection of a Torus™ quench section*

Table 1. *Example time savings on a typical 4 bed reactor with better manways*

Manway Access Times			
Conventional Manway		Topsoe Quick Release™ Manway	
Opening	Closing	Opening	Closing
Up to 12hrs+	Up to 24hrs+	10 - 30min	30min max (with gasketing)

Topsoe has recently launched a new innovative mixer design designated as Torus™ mixer, which maintains the same performance as the vortex style mixer, but is designed to use the reactor cross sectional area to its fullest potential. Mixing in its basic forms has always been accomplished by combining and distributing the process streams and treat gas/liquid in the central area of the reactor, where all the mixing vane and outlet distribution components are located. The Torus™ mixer has taken a completely different approach, one that is unique to the industry. By utilising the larger area or volume near the outer walls of the reactor, which is greater than the centre, the mixing zone has more space for performing its job. The existing distribution area is also much larger, allowing for a more relaxed jetting coming out of the mixer exit. Less turbulence at the exit allows for calmer flows down to the distribution tray surface, ensuring less wave action and a lower static pressure differential above the liquid level on the distribution tray below. This ensures a steady uniform liquid level on the VLT distribution tray and provides excellent flow distribution throughout many different process conditions.

Another significant advantage of mixing at the outer walls is that it leaves the centre of the reactor free of obstruction. Therefore access through the manways to the distribution tray below is much improved and can save many hours during a subsequent turn-around for tray access, maintenance and cleaning for years to come. With a traditional mixing chamber the maintenance personnel would need to remove 3 - 5 manways and possibly a quench pipe, from the mixer centre to open it (Figure 6). This can be extremely difficult with compact quench sections, which nowadays may use about 600 - 1,100mm in height. The Torus™ mixer has only one centre manway with the Quick-Release™ system. This is a huge time saver and consequently increases on-stream time of the hydrotreating unit (Figure 7).

As the space is unpopulated, the operators conducting inspections and maintenance may work in an ergonomic and safe position (Figure 8).

The time savings for new manways that are safer, faster and fewer can be immense, especially for multiple bed reactors as shown in Table 1. Just by comparing the normal manway open and closing times, you can save several days per turnaround.

4. Pressure drop management [2]

Inorganic material from the feed such as iron sulfide, carbon, and catalyst fines can critically affect the cycle length of the reactor. A very common approach to managing these types of deposits is through the use of a graded bed system on top of the catalyst bed. The graded bed is typically designed based on the unit's

past experience and can handle the problem to a wide extent. However, there are certain situations where the deposits are so large that the graded bed system will take up too much space in the reactor in order to effectively capture these deposit, thus not leaving enough room for the active main hydrotreating catalyst. Deposits range from coarse construction debris, transported to the reactor as a consequence of insufficient cleaning after maintenance or a revamp, to micron-scale particles generated from corrosion, and polymeric substances growing with time and temperature on some surfaces that act as catalysts or promoters. Corrosion may appear suddenly and be aggravated as a consequence of Total Acid Number (TAN) of the crude. In many gas oil units with large amounts of inorganic contaminates, Haldor Topsoe recommends installing a scale catcher on top of the distribution tray. A scale catcher, by definition, is designed to trap fines, scales, in-organic matter, and rust, etc. in typical hydroprocessing feeds. Doing so will help avoid the plugging of the 1st bed distribution tray and the 1st grading/catalyst bed below. The main goals of a scale catcher design are:

- Pressure Drop Mitigation - installing a device inside the reactor that will trap fines and scales, etc. while not introducing an additional pressure drop into the reactor envelop, either by its addition or as it traps the particles over the life of the cycle;
- Cycle Length Improvement;
- Reduced turnaround times because the scale catcher is easy to clean and the catalyst below is likewise easier to remove;
- Less Capital Cost than additional feed filtration - The scale catcher is designed to fit into the existing reactor above the tangent line. They are not taking up active space inside the first catalyst bed as trash baskets do.

Topsoe has developed a number of scale catchers for many applications. Figure 9 shows the Topsoe two-phase single stage scale catcher. This design has already been proven in over 30 installations, and the results have shown that these can provide significant cycle length

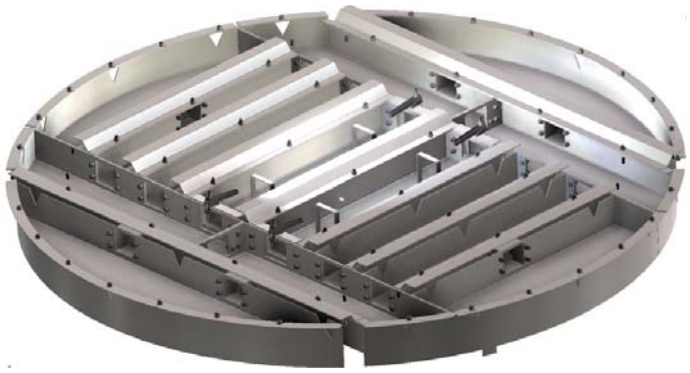

Figure 9. *Two-Phase single stage scale catcher [3]*

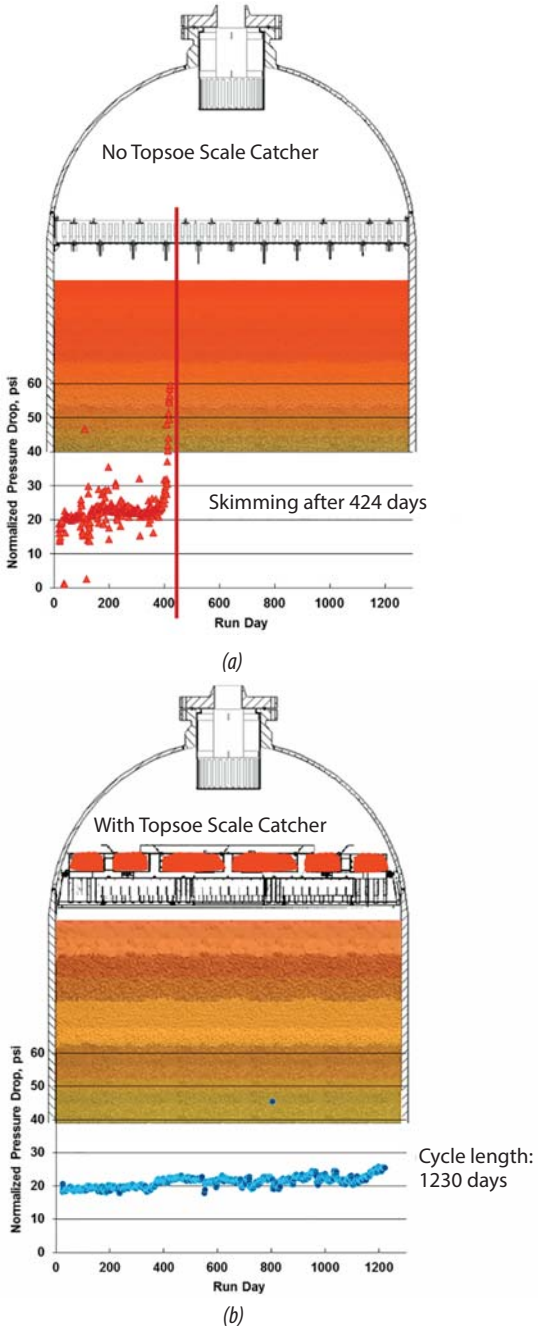

Figure 10. *Case study of a North American hydroprocessing reactor. The reactor was operated with the same grading (non Topsoe) before (a) and after upgrading distribution tray and introducing a scale catcher (b)*

improvements in the right situations. The design is very simple and easy to maintain and clean. An area is used above the existing top distribution tray to allow the liquid feed to have a settling time above the bed, while allowing the process gas stream to bypass the scale catcher entirely. This limits the pressure drop contribution of the scale catcher to a negligible amount, while collecting the liquid in a deep enough chamber so that the turbulence is low enough and retention is long enough to allow the heavier particles to settle to the bottom of the scale catcher.

The collection of more than a cubic metre of sediment is quite common depending on the conditions of the unit. When full capacity of the scale catcher is used the process stream will simply bypass the scale catcher. During the turnaround, the scale catcher can be cleaned very easily compared to a distribution tray, and is completely accessible from the top side for vacuuming out the heavy particles that have settled. Once cleaned, it is ready for the next cycle.

All Topsoe scale catchers are custom-made for each reactor and adjusted for the process conditions and unit type. Scale catchers should definitely be considered if the reactor is experiencing limitations due to pressure drop in the catalyst bed, and if there are visible particulates settling out on the top distribution tray.

Case study of the performance of a scale catcher used in a North American hydroprocessing unit.

The reactor was loaded with Topsoe catalyst and operated great for a little more than a year, but suddenly the pressure drop increased exponentially and the unit had to be shut down for a top bed skimming. This type of pressure drop increase happens when the void fraction of the catalyst bed and grading is reduced to about 22% due to deposit and fouling. (Figure 10, a). After upgrading the existing top tray with a VLT distribution tray and a Topsoe sedimentation scale catcher, the reactor could be operated without interruptions for over 1200 days (Figure 10, b).

It is important to note that scale catchers cannot substitute guard catalyst and grading material but just help full utilisation of those by preventing large particles and scales to enter catalyst bed and prematurely build pressure drop over the unit.

Conclusion

The simplest and most profitable way to maximise the cycle length and profitability of the hydrotreating unit is to equip the hydrotreating reactor with state-of-the-art reactor internals. Such approach will assure maximal utilisation of the catalyst loaded, allowing for higher feed rates, more severe feeds or longer cycle lengths. State-of-the-art internals also increase safety during the operation, by ensuring good mixing and quenching, and during shutdowns, as confined space entry is significantly reduced. Haldor Topsoe has designed scale catchers, distribution trays, quench mixers as well as all reactor internals that will enable the refineries to maintain profitability of their assets even during the most challenging times.

Reference

1. *http://www.topsoe.com/products/quench-mixer.*

2. *http://www.topsoe.com/processes/pressure-drop-control.*

3. *http://www.topsoe.com/products/scale-catcher.*

PRODUCTION OF GREEN GASOLINE AND LIGHT OLEFINS BY CRACKING OF TRIGLYCERIDE-RICH BIOMASS OVER NANO-ZSM-5/SBA-15 ANALOG COMPOSITES WITH VARIABLE Si/Al RATIOS

Vu Xuan Hoan[1], Nguyen Sura[1], Dang Thanh Tung[1], Phan Minh Quoc Binh[1], Nguyen Anh Duc[1]
Michael Hunger[2], Udo Armbruster[3], Andreas Martin[3]
[1]*Vietnam Petroleum Institute*
[2]*The University of Stuttgart*
[3]*Leibniz Institute for Catalysis*
Email: hoanvx.epc@vpi.pvn.vn

Summary

Nano-ZSM-5/SBA-15 analog composites (ZSC) with different Si/Al molar ratios were prepared and their performance was evaluated in catalytic cracking of triglyceride-rich biomass. It was found that the initial Si/Al ratio used in the synthesis mixture significantly affects the physicochemical properties and consequent catalytic performance of ZSC catalysts. Increasing the initial Si/Al ratio raises the content of nano-ZSM-5 phase at the expense of SBA-15 analog phase. The total acidity enhances with the fraction of nano-ZSM-5 phase despite the decreased amount of incorporated aluminum as the Si/Al ratio varies from 10 to 30. However, the total acidity decreases when raising the Si/Al ratio to 50 because the low incorporated aluminium has not been compensated by the increased nano-ZSM-5 phase. The catalytic performance of ZSC catalysts with variable Si/Al ratios was evaluated in the catalytic cracking of waste cooking oil as a real feedstock. The results showed that the sufficient amount of nano-ZSM-5 phase obtained by properly tuning the initial Si/Al ratio is of crucial importance to achieve the superior catalytic performance of ZSC catalysts in catalytic cracking of triglyceride-rich biomass.

Key words: *Nano-ZSM-5, SBA-15 analog, Si/Al ratio, green gasoline, light olefins.*

1. Introduction

The processing of biomass, particularly triglyceride-rich biomass, by catalytic cracking represents a promising alternative for the production of green fuels and chemicals. This strategy allows rapid transition to a more sustainable economy without large capital investments for new reaction equipment by utilising the existing infrastructure of petroleum refineries [1, 2]. However, biomass derived feedstocks are chemically different from petroleum feedstocks; therefore, the development of suitable catalysts is required for efficient conversion of triglyceride-rich biomass.

There is a rich body of literature on catalytic cracking of triglyceride-based feedstocks in which various cracking catalysts have been investigated [1 - 3]. It has shown that the catalyst performance is mainly governed by acidity, pore size and shape. Active alumina, alumina-silica, MCM-41 or SBA-15 type materials usually give a lower gas yield and higher coke formation due to their low acidity and lack of shape selectivity [3, 4]. Compared to these amorphous materials, crystalline zeolites such as ZSM-5, Y or Beta are superior, producing more desirable products, i.e. gasoline and light olefins because they have strong acidity and uniform micropores of molecular dimensions which generate shape selectivity [3 - 6]. Among zeolite-based catalysts, the medium-pore zeolite ZSM-5 stands out as the most effective zeolite type catalyst for conversion of triglycerides to gasoline-range hydrocarbons [5, 6]. Unfortunately, conventional ZSM-5 zeolites generally yield large fractions of undesired gaseous products with low concentrations of C_2-C_4 olefins. Hence, many attempts have been focused on modifications of ZSM-5 zeolites to enhance the selectivity of light olefins. Reducing the amount of acid sites by impregnation with potassium [7] hindered secondary cracking reactions, leading to the increased fractions of liquid products and light olefins, but the decreased fractions of gaseous products. Botas et al. [8] showed that nanocrystalline and hierarchical ZSM-5 catalysts indeed produced more light olefins than conventional ZSM-5 because of their ability to prevent the primary light olefins from further transformation thanks to shortened diffusion path lengths. Recently, we reported a highly selective catalyst, denoted as nano-ZSM-5/SBA-15 analog composite (ZSC) for conversion of triglyceride-rich biomass toward light olefins. The selectivity

to C_2-C_4 olefins is remarkably high (> 90%) regardless of cracking severity and feedstock composition [9].

In this study, we explore the influence of the Si/Al ratio on the catalytic performance of ZSC catalysts in catalytic cracking of triglyceride-rich biomass. It has been reported that the Si/Al ratio is an important factor affecting the physicochemical properties and consequent catalytic performance of ZSM-5 based catalysts in various reactions such as alkane dehydrogenations [10] or cracking of C_4 alkanes [11]. However, the effect of the Si/Al ratio on the performance of ZSM-5 based catalysts in catalytic cracking of triglyceride-rich biomass is scarcely described in the literature.

2. Experimental

2.1. Chemicals

The chemicals used in this study were tetraethyl orthosilicate (TEOS, 99%, Aldrich), tetrapropylammonium hydroxide (TPAOH, 20% in water, Aldrich), aluminum isopropoxide (AIP, 98%, Aldrich), triblock copolymer pluronic P123 (EO20PO70EO20, MW = 5800, Aldrich), hydrochloric acid (HCl, 37%, J.T.Baker) and ammonium hydroxide (NH_4OH, 25%, Acros).

2.2. Synthesis

The preparation of nano-ZSM-5/SBA-15 analogs from ZSM-5 nanoseeds involves a two-step process, being similar to that of the previous work [12]. In the first step, 6.0g of TEOS, 10.0g of TPAOH, 2.0g of distilled H_2O were mixed at room temperature and stirred overnight for complete hydrolysis. Then the amounts of AIP required to obtain the Si/Al molar ratio in the range of 10 - 50 were added and stirred for 24 hours, followed by pre-crystallisation at 90°C for 24 hours in a reflux system to yield the desired precursor solutions.

In the second step, the P123 solution was prepared by dissolving 2.0g of P123 in 75ml of 1.6M HCl at room temperature for 4 hours to get a clear solution. Then, the precursor solution prepared as described above was added dropwise to the P123 solution, followed by aging at 40°C for 24 hours to convert unreacted precursors to ordered mesoporous SBA-15 analogs in strongly acidic media. Before transferring the mixture into a Teflon-lined autoclave for hydrothermal treatment at 200°C for 24 hours, the pH value was adjusted to 3.5 with an aqueous NH_3 solution. The final product was filtered off, washed with distilled water, and dried at 100°C for 12 hours. The as-synthesised material was calcined in air at 550°C for 5 hours with a heating rate of 2K/min to remove the organic template. The calcined solid was transformed into the protonated form by two consecutive exchanges in 0.5M NH_4NO_3 solution at 80°C for 4 hours. The obtained catalysts are denoted as ZSC-SAx, where ZSC represents the nanosized ZSM-5/SBA-15 analog composite; x is the initial Si/Al (SA) molar ratio in the gel mixture.

2.3. Characterisation

SAXS measurements were carried out using a Kratky-type instrument (SAXSess, Anton Paar, Austria) operated at 40kV and 50mA in slit collimation using a two-dimensional CCD detector. X-ray diffraction (XRD) measurements were carried out on a theta/theta diffractometer (X'Pert Pro from Panalytical, Almelo, Netherlands) with CuKα radiation (λ = 0.15418nm; 40kV, 40mA) and an X'Celerator RTMS Detector. Nitrogen physisorption measurements were carried out at -196°C on an ASAP 2010 Micromeritics apparatus. The BET specific surface area was calculated using adsorption data at a relative pressure (p/p_0) of 0.05 - 0.25, and the total pore volume was estimated from the amount adsorbed at a relative pressure of about 0.976. NH_3-TPD experiments were carried out in a quartz tube reactor in the range of 100 - 550°C. The liberated ammonia was continuously detected by a thermal conductivity detector (TCD, Gow-Mac Instrument Co.). The Al and Si contents were determined by ICP-AES (715-ES, Varian) and AAS (Analyst 300, Perkin Elmer), respectively. For this purpose, the samples were digested with a mixture of HCl-HNO_3-HF in a microwave-assisted sample preparation system (Multi wave, Anton Paar/Perkin-Elmer) at 200°C and 60bars. The solid-state NMR investigations were performed with the hydrated material using a Bruker BioSpin Avance III 400WB spectrometer at the resonance frequency of 104.3 MHz for ^{27}Al nuclei. More details of these characterisation methods are described elsewhere [12].

2.4. Catalytic test experiments

The catalytic cracking of waste cooking oil (WCO) was performed on a fully automated Single Receiver Short-Contact-Time Microactivity Test unit (SR-SCT-MAT, Grace Davison). The utilisation of WCO as a potential triglyceride-rich biomass for production of green fuels and chemicals is preferred because it does not compete with food crops and arable land. Details of the experimental setup, testing conditions, feedstock and product analyses are given in the previous work [9].

In a typical run, 1.75g of WCO was fed into the reactor which contained a desired amount of catalyst diluted with glass beads to maintain a constant-volume reaction. The cracking reaction was carried out at ambient pressure, 550°C, the catalyst-to-oil (CTO) mass ratio of 0.4 ($g \cdot g^{-1}$) and a reaction time of 12s. After the reaction, stripping of the catalyst was done by using a nitrogen purge. The gaseous and liquid products were collected in the single receiver cooled to 18°C via an external cooling system. All catalytic test experiments were repeated at least two times to check the reproducibility, and mass balances in all runs were between 95 and 100% of the injected feed.

The products comprised mainly hydrocarbons along with oxygenated compounds (water, CO and CO_2) and coke. The gaseous hydrocarbon fraction was divided into dry gas (hydrogen, methane, ethane, and ethene) and liquefied petroleum gas (LPG, propane, propene, butenes and butanes). The liquid hydrocarbons were lumped in terms of boiling ranges: C_{5+} gasoline (< 221°C), light cycle oil (LCO; 221 - 360°C) and heavy cycle oil (HCO; > 360°C).

The gaseous products were analysed according to the ASTM D1945-3 method using a Refinery Gas Analyser (Agilent 7890A). The liquid organic products were classified according to the boiling ranges: C_{5+} gasoline, LCO and HCO as mentioned above by means of simulated distillation (ASTM D2887) on a Simulated Distillation Gas Chromatograph (Agilent 7890A). Water content was measured by Karl Fischer titration (MKS-520, Kem) and coke amount on the spent catalyst was determined by an elemental analyser (CS600, Leco).

The yield toward different products (Y_i, wt%) is defined as gram of product i per gram of the feed. The standard MAT conversion is defined as 100% - ($Y_{HCO} + Y_{LCO}$). The selectivity to C_2-C_4 olefins (light olefins) is defined as the fraction of C_2-C_4 olefins per total fraction of C_2-C_4 hydrocarbons.

3. Results and discussion

3.1. Physicochemical properties of ZSC catalysts with variable Si/Al ratios

Figure 1 depicts the small angle X-ray scattering (SAXS) patterns of ZSC materials prepared from ZSM-5 precursors with the different initial Si/Al ratios. It can be seen that samples ZSC-SA20 and ZSC-SA30, synthesised from ZSM-5 precursors with the initial Si/Al molar ratios of 20 and 30, respectively, show three well-resolved peaks indexed as (100), (110) and (200) reflections of an ordered 2D hexagonal structure with a p6mm symmetry, which is typical of SBA-15 type materials. Lowering the initial Si/Al ratio to 10 (ZSC-SA10) decreases the mesostructure ordering as confirmed by the only one visible reflection (100). However, when increasing the initial Si/Al ratio to 50, no reflections can be observed in the small angle range, suggesting the absence of an ordered mesostructure in this sample (ZSC-SA50). Wide angle XRD patterns (Figure 2) reveal the presence of a crystalline ZSM-5 phase in samples ZSC-SA30 and ZSC-SA50. Both materials show clear reflections in the 2θ regions of 8 - 10° and 23 - 25°, indicative of crystalline ZSM-5 zeolite. It should be noted that the reflections become sharper and more prominent with the increasing initial Si/Al ratio, suggesting a higher crystallinity degree in ZSC-SA50 compared to ZSC-SA30. For samples ZSC-SA10 and ZSC-SA20, there are no such reflections detected, implying a very low content or absence of a crystalline zeolite phase [12].

It has been reported that increasing the aluminum content of the initial gel mixture resulted in a decrease in the growth rate of ZSM-5 crystals from their precursors [13]. Accordingly, at the highest Si/Al ratio (the lowest aluminum content) the zeolite crystal growth is fast, consuming all precursor species; therefore, the mesoporous framework

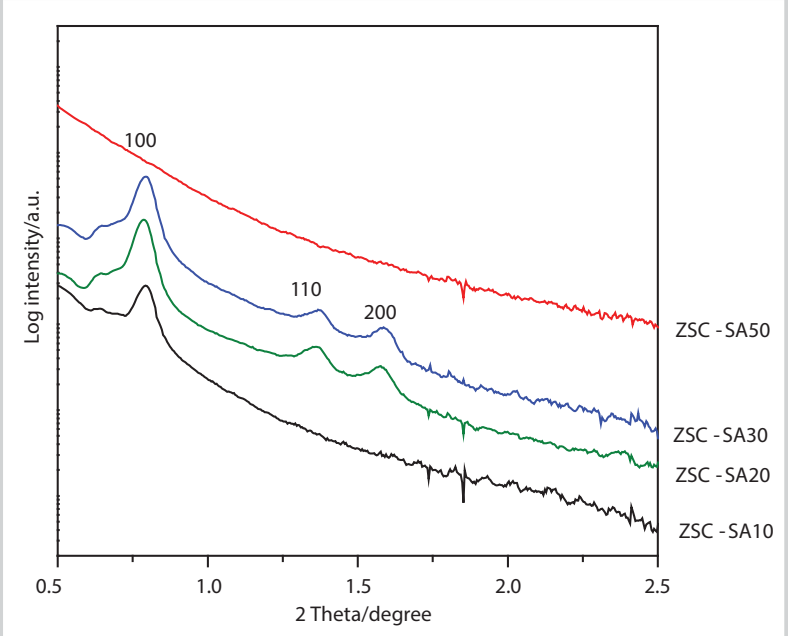

Figure 1. *SAXS patterns of ZSC catalysts with variable Si/Al ratios*

phase cannot be formed in sample ZSC-SA50. In contrast, using the lower initial Si/Al ratio (ZSC-SA10, ZSC-SA-20) produces ZSM-5 precursors which have been hardly consumed in the zeolite formation because of the slow zeolite growth. Consequently, the mesoporous

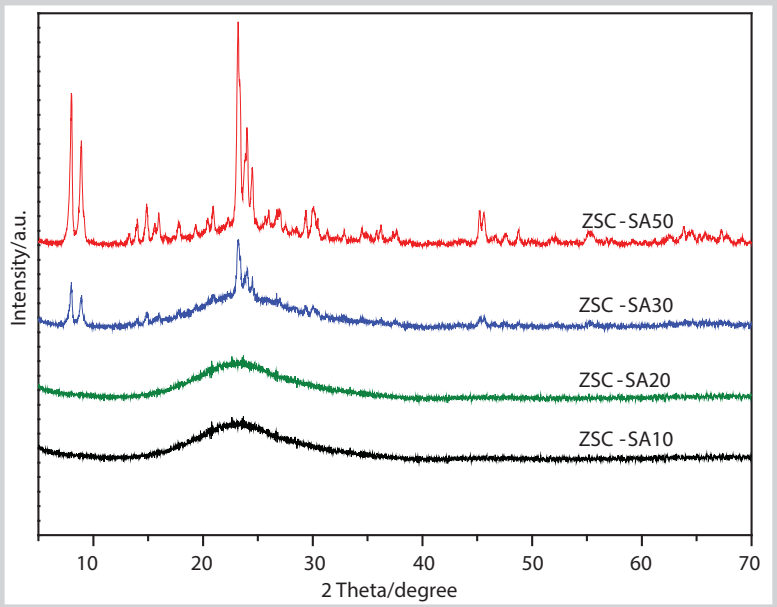

Figure 2. *XRD patterns of ZSC catalysts with variable Si/Al ratios*

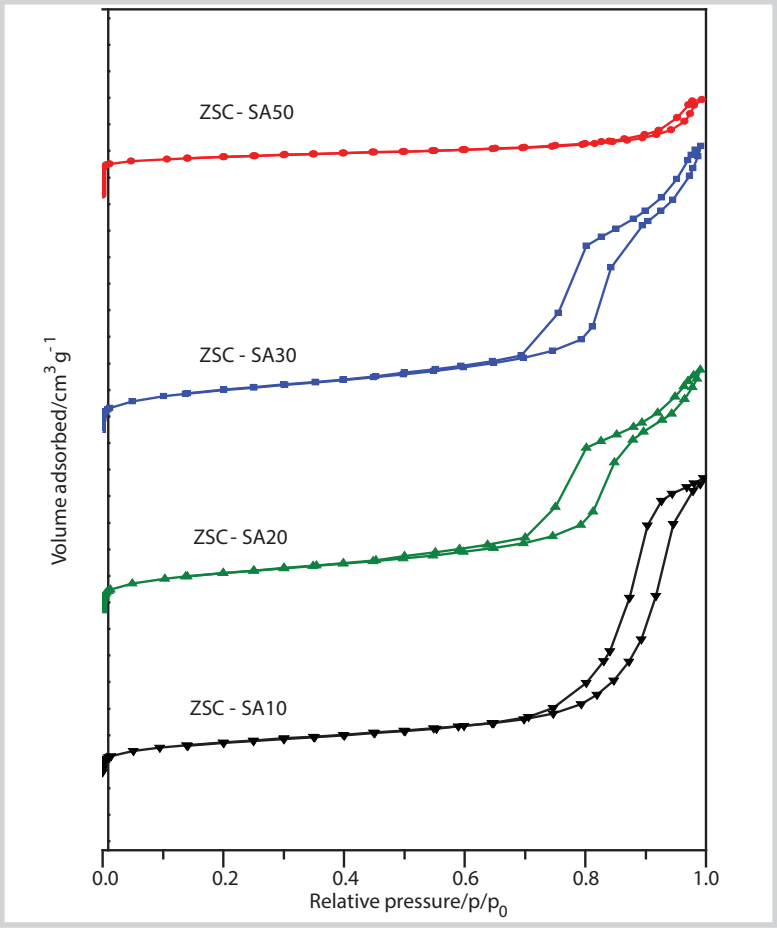

Figure 3. *Nitrogen sorption isotherms of ZSC catalysts with variable Si/Al ratios*

SBA-15 analog phase can be formed from these unreacted precursors in the second synthesis step. Notably, sample ZSC-SA30 contains sufficient amounts of ordered mesoporous SBA-15 analogs (Figure 1) and crystalline ZSM-5 (Figure 2), in order to form detectable amounts of ordered mesoporous phase and microporous zeolite phase.

The interpretation is further supported by the N_2 adsorption/desorption study. From the N_2 adsorption/desorption isotherms (Figure 3), one can see that samples ZSC-SA30, ZSC-SA20 and ZSC-SA10 possess type IV isotherms with a steep capillary condensation step in the relative pressure (p/p_0) range of 0.7 - 0.9, which is characteristic for an ordered mesostructure with a large and uniform pore size. However, the hysteresis loop of the isotherm of ZSC-SA10 is much less regular and shifts to higher relative pressures, suggesting that its pore uniformity is much degraded. It is noteworthy to mention that the isotherm of ZSC-SA30 shows a relatively steep increase of the adsorbed N_2 amount at low relative pressures ($p/p_0 < 0.01$), further confirming the presence of microporous crystalline ZSM-5 phase in this sample. The same phenomenon is observed from the isotherm of ZSC-SA50, but much more pronounced, which clearly evidences its microporous nature. Additionally, a high relative pressure uptake ($p/p_0 > 0.9$) occurs for all samples, suggesting the presence of nanoscale ZSM-5 phase and consequent inter-crystalline pores [12]. The detailed information about the textural properties of ZSC solids is listed in Table 1. The degraded porous structure of ZSC-SA10 is further affirmed by the lowest BET surface area of 210m^2/g compared to that of the other ZSC-SA samples (318 - 361m^2/g).

The local environment of the incorporated aluminum atoms in the representative ZSC samples was investigated by ^{27}Al MAS NMR spectroscopy (Figure 4). The ^{27}Al MAS NMR spectra of the studied samples exhibit two resonances centred at approximately 52ppm and ca. 3ppm which

Table 1. *Physicochemical properties of ZSC catalysts with variable Si/Al ratios*

Sample	Si/Al[a]	d_{100} (nm)	a_0 (nm)	D_p (nm)	S_{BET} (m^2/g)	V_t (cm^3/g)	Total acidity[b] (mmol NH_3/g)
ZSC-SA10	11	11.4	13.1	-	210	0.89	0.24
ZSC-SA20	18	11.2	12.9	9.1	323	0.96	0.30
ZSC-SA30	30	11.2	12.9	7.5	361	0.84	0.34
ZSC-SA50	48	-	-	-	318	0.24	0.27

[a]: In the final product analysed by AAS and ICP-AES; [b]: TPD-NH_3; d_{100}: Basal spacing; a_0: Unit cell parameter ($a_0 = 2 \times d_{100}/3^{1/2}$); D_p: Pore diameter; V_t: Total pore volume; the missing parameters are due to the absence of an ordered mesostructure.

are attributed to tetrahedrally and octahedrally co-ordinated aluminum, respectively. The fraction of octahedral aluminum increases at the expense of the tetrahedral aluminum when increasing the aluminum content in the initial gel mixture. In fact, ZSC-SA10 shows a major fraction of octahedral aluminum whereas ZSC-SA50 is dominated by tetrahedral aluminum. These results can be explained by considering the fact that before calcination, the aluminum atoms introduced by pH adjusting method are exclusively located as tetrahedrally co-ordinated aluminum species. The calcination causes the rearrangement of the aluminum co-ordination environment whose magnitude is strongly influenced by the density of aluminum sites [14, 15]. Thus, the samples with lower density of aluminum sites (ZSC-SA50 and ZSC-SA20) are more stable upon calcination, yielding the dominant fractions of tetrahedral aluminum. In contrast, sample ZSC-SA10 with the highest density of aluminum experiences a substantial conversion of tetrahedral aluminum to octahedral aluminum via condensation reactions between the neighbouring aluminum atoms, which resulted in a major fraction of octahedral aluminum.

The effect of the Si/Al ratio on the acidic properties was studied by temperature-programmed desorption of ammonia (NH_3-TPD). This method provides information on the number and strength of acid sites. The results are shown in Figure 5 and Table 1.

As shown in Figure 5, all samples display a similar TPD profile with two desorption peaks. The dominant peak at ca. 200°C corresponds to weak acid sites and the second broader peak in the range of 300 - 500°C arises from medium and strong acid sites. However, it should be stressed that the second desorption peak of ZSC-SA50 is

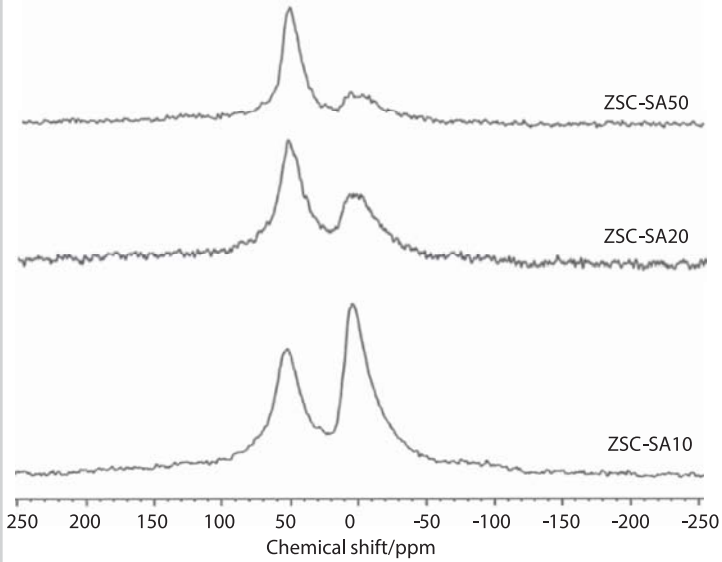

Figure 4. *^{27}Al NMR spectra of ZSC catalysts with variable Si/Al ratios*

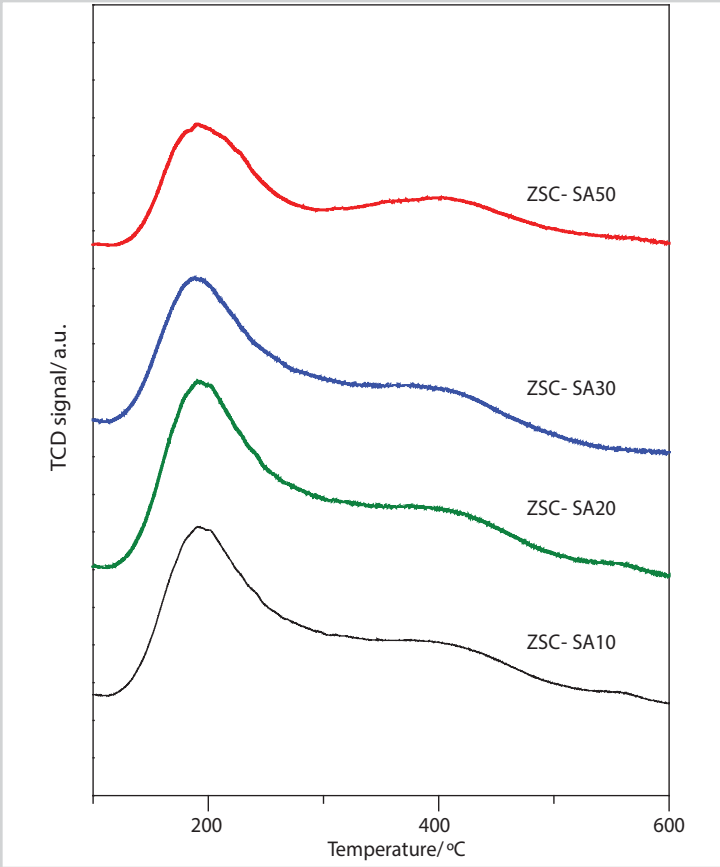

Figure 5. *NH_3-TPD profiles of ZSC catalysts with variable Si/Al ratios*

Table 2. *Catalytic performance of ZSC catalysts with variable Si/Al ratios in the catalytic cracking of waste cooking oil*

Catalysts	ZSC-SA10	ZSC-SA20	ZSC-SA30	ZSC-SA50
Conversion (wt%)	51.3	60.3	70.6	66.4
Product yields (wt%)				
Gas	16.6	21.1	30.7	25.2
Dry gas	2.2	2.4	2.6	1.6
LPG	9.6	13.5	22.1	18.1
Light olefins (C_2-C_4)	9.0	13.2	22.7	18.4
CO/CO_2	4.8	5.1	5.9	5.6
Gasoline	27.6	31.7	32.2	34.0
LCO	30.6	23.3	17.7	19.1
HCO	18.1	16.4	11.7	14.5
Coke	1.9	1.8	1.4	1.3
Water	5.2	5.7	6.3	5.9
Selectivity to C_2-C_4 olefins (%)	80.1	85.3	93.2	94.2

more obvious than that of the other samples, implying its higher fraction of strong acid sites. This might be the fact that ZSC-SA50 contains predominantly nanocrystalline ZSM-5 crystals which have strong Brønsted sites.

The number of acid sites estimated from the peak area in the TPD profiles is listed in Table 1. Although most of aluminum in the initial synthesis mixtures has been successfully incorporated in the final solids, the acid site amount decreases with increasing the incorporated aluminum for the first three samples: ZSC-SA30 > ZSC-SA20 > ZSC-SA10. It is acknowledged that the generation of acid sites from incorporated aluminum is heavily dependent on the crystallinity degree. For amorphous mesoporous SBA-15 type materials, only a partial fraction of grafted aluminum contributes to the formation of acid sites because of the lack of a long-range atomic order [16]. Using zeolite precursors as building blocks to construct a mesostructure has been proved to improve acidity thanks to the retention of zeolite building units in the mesoporous wall [12]. For crystalline zeolites, most of incorporated aluminum in the zeolite framework is tetrahedral aluminum which generates strong acid sites via bridging hydroxyl groups (Si-OH-Al) [17]. Thus, the higher amount of acid sites of ZSC-SA30 compared to that of ZSC-SA20 and ZSC-SA10 can be attributed to its higher content of crystalline ZSM-5 phase as shown by the XRD results (Figure 2) though the two latter samples have greater contents of incorporated aluminum. Similarly, the lowest acidity of ZSC-SA10 might be due to the fact that at such a low Si/Al ratio of 10, the crystallisation process occurs very slowly, resulting in little zeolite building units [13]. In addition, the highest incorporated aluminum content of this sample has caused the formation and aggregation of octahedrally co-ordinated aluminum species as confirmed by the NMR data which reduce the number of acid sites. On the other hand, it should be noted that sample ZSC-SA50 has a higher crystallinity but a lower acid amount than ZSC-SA30. One possible explanation is that ZSC-SA50 has the lowest incorporated aluminum in the framework (the highest Si/Al ratio) which has not been compensated by its highest crystallinity.

3.2. The performance of ZSC catalysts with variable Si/Al ratios in catalytic cracking of triglyceride-rich biomass

Catalytic cracking of triglyceride-rich biomass is often initiated by thermal decomposition of triglyceride molecules into fatty acids by means of free radical mechanism. Then the acid zeolite based catalyst controls the process and converts the formed fatty acid into oxygenated products mainly CO, CO_2 and water, and a mixture of hydrocarbons lumped into gaseous hydrocarbon, gasoline, light cycle (LCO) and heavy cycle oils (HCO) [1, 3, 9]. It is well known that the performance of a catalyst in the cracking of triglyceride-based feedstock is heavily influenced by its physicochemical properties, i.e. acidity and porosity. To understand such effect, in the present work the catalytic cracking of waste cooking oil (WCO) was performed over ZSC catalysts with the different Si/Al ratios under the optimised conditions, i.e. 550°C, a CTO mass ratio of 0.4 ($g \cdot g^{-1}$) and a reaction time of 12s [9]. The catalytic results are summarised in Table 2.

As the Si/Al ratio varies from 10 to 50, the conversion and product distribution over ZSC catalysts experience

significant changes because of their different total acidity and porosity. In fact, the conversion rises steadily from 51.3wt% (ZSC-SA10) to 70.6wt% (ZSC-SA30) as the Si/Al ratio increases from 10 to 30, corresponding to a relative increase of 37.6%. When the Si/Al ratio reaches 50, the conversion decreases to 66.4wt% (ZSC-SA50). In relation with the acid site amount, one can obtain a good correlation with the conversion, emphasising the important role of acid sites in the conversion of intermediate fatty acids to valuable hydrocarbons [7, 9].

Regarding the product distribution, it can be seen from Table 2 that ZSC-SA10 produces the least desirable products, i.e. gasoline (27.6wt%) and light olefins (9.0wt%), but the largest coke (1.9wt%). It sounds reasonable since this sample comprises predominant mesoporous SBA-15 analog phase with the lowest acid site amount. Thus, the large fraction of heavy products, i.e. HCO and LCO (ca. 48wt%) has not been converted to lighter and valuable products. On the other hand, the mesopore channels of SBA-15 analogs can facilitate the formation of polyaromatics involving cyclisation, aromatisation and condensation, leading to the increased formation of coke [9, 18]. A similar product distribution over ZSC-SA20 is obtained, reflecting its predominant SBA-15 analog phase. Furthermore, it should be noted that ZSC-SA20 shows higher yields of gasoline (31.7wt%) and light olefins (13.2wt%) than ZSC-SA10. This is because ZSC-SA20 possesses a greater acid site amount which is more effective than ZSC-SA10 in conversion of intermediate fatty acids to desired products, i.e. gasoline and light olefins.

Compared to the first two samples with the lower Si/Al ratios, ZSC-SA30 exhibits considerably higher yields of gasoline (32.2wt%) and light olefins (22.7wt%), but a lower yield of coke (1.4wt%). The superior catalytic performance of ZSC-SA30 primarily stems from the presence of substantial nano-ZSM-5 phase, which has been proved highly selective toward the formation of gasoline and light olefins [8, 9, 17, 18]. The shape selectivity generated by the medium pore zeolite ZSM-5 (pore mouths diameter of 0.52 - 0.56nm) preferentially directs the cracking process toward the formation of gasoline-range hydrocarbons and light olefins. At the same time, it severely suppresses the formation of polyaromatics because the limited space inside its medium pore channel cannot accommodate these intermediates, thereby reducing the coke fraction [17, 18].

With the predominant ZSM-5 phase, ZSC-SA50 displays a product distribution, which is very similar to that of ZSC-SA30. It is noteworthy that ZSC-SA50 produces more gasoline, but less light olefins than ZSC-SA30. The higher yield of gasoline over the former sample can be explained by the fact that this sample contains a higher content of nano-ZSM-5 phase as evidenced by the XRD results. However, the lower yield of light olefins over ZSC-SA50 can be assigned to its lower conversion. It appears logical since ZSC-SA50 and ZSC-SA30 have comparable selectivities of light olefins (94.2 and 93.2% respectively). Compared to that of ZSC-SA10 (80.1%) and ZSC-SA20 (85.3%), the superior selectivity of light olefins over ZSC-SA30 and ZSC-SA50 stresses the crucial role of substantial nano-ZSM-5 phase in improving the catalytic performance of ZSM-5 based catalysts in catalytic cracking of triglyceride-rich biomass.

4. Conclusions

We have shown that the Si/Al ratio in the initial synthesis mixture greatly influences the physicochemical properties and consequent catalytic performance of ZSC catalysts. Starting from ZSM-5 precursors with the lower Si/Al ratios, the resulting ZSC catalysts are predominated by SBA-15 analog phase (ZSC-SA10 and ZSC-SA20) while the high Si/Al ratio of 50 leads to the predominant nano-ZSM-5 phase (ZSC-SA50). Remarkably, sample ZSC-SA30 comprising the sufficient amount of nano ZSM-5 phase and SBA-15 analog phase detected by XRD and SAXS can be obtained from the ZSM-5 precursors with the initial Si/Al ratio of 30. The total acidity enhances as the Si/Al ratio increases because of the increased nano-ZSM-5 phase except ZSC-SA50. The high Si/Al ratio of 50 has resulted in the low incorporated aluminum, thus the reduced number of acid sites for ZSC-SA50. The catalytic cracking of waste cooking oil over ZSC catalysts with the variable Si/Al ratios evidences that the sufficient amount of nano-ZSM-5 phase obtained by properly adjusting the initial Si/Al ratio is required to achieve the superior catalytic performance of ZSC catalysts. These findings might stimulate future work on rational design of suitable ZSM-5 based catalysts for efficient conversion of triglyceride-rich biomass by petroleum technology to produce green gasoline and light olefins.

References

1. J.A.Melero, J.Iglesias, A.Garcia. *Biomass as renewable feedstock in standard refinery units. Feasibility, opportunities and challenges*. Energy Environmental Science. 2012; 5: p. 7393 - 7420.

2. G.W.Huber, A.Corma. *Synergies between bio- and oil refineries for the production of fuels from biomass*. Angewandte Chemie International Edition. 2007; 46(38): p. 7184 - 7201.

3. K.D.Maher, D.C.Bressler. *Pyrolysis of triglyceride materials for the production of renewable fuels and chemicals*. Bioresource Technology. 2007; 98(12): p. 2351 - 2368.

4. R.O.Idem, S.P.R.Katikaneni, N.N.Bakhshi. *Catalytic conversion of canola oil to fuels and chemicals: roles of catalyst acidity, basicity and shape selectivity on product distribution*. Fuel Processing Technology. 1997; 51(1, 2): p. 101 - 125.

5. D.Chen, N.I.Tracy, D.W.Crunkleton, G.L.Price. *Comparison of canola oil conversion over MFI, BEA, and FAU*. Applied Catalysis A: General. 2010; 384(1, 2): p. 206 - 212.

6. F.A.Twaiq, N.A.M.Zabidi, S.Bhatia. *Catalytic conversion of palm oil to hydrocarbons: performance of various zeolite catalysts*. Industrial Engineering Chemistry Research. 1999; 38(9): p. 3230 - 3237.

7. S.P.R.Katikaneni, J.D.Adjaye, R.O.Idem, N.N.Bakhshi. *Catalytic conversion of canola oil over potassium-impregnated HZSM-5 catalysts: C_2-C_4 olefin production and model reaction studies*. Industrial Engineering Chemistry Research. 1996; 35(10): p. 3332 - 3346.

8. J.A.Botas, D.P.Serrano, A.García, R.Ramos. *Catalytic conversion of rapeseed oil for the production of raw chemicals, fuels and carbon nanotubes over Ni-modified nanocrystalline and hierarchical ZSM-5*. Applied Catalysis B: Environmental. 2014; 145: p. 205 - 215.

9. Vu Xuan Hoan, Nguyen Sura, Dang Thanh Tung, Phan Minh Quoc Binh, Nguyen Anh Duc, U.Armbruster, A.Martin. *Catalytic cracking of triglyceride-rich biomass toward lower olefins over a Nano-ZSM-5/SBA-15 analog composite*. Catalysts. 2015; 5(4): p. 1692 - 1703.

10. Z.Nawaz, T.Xiaoping, F.Wei. *Influence of operating conditions, Si/Al ratio and doping of zinc on Pt-Sn/ZSM-5 catalyst for propane dehydrogenation to propene*. Korean Journal of Chemical Engineering. 2009; 26(6): p. 1528 - 1532.

11. X.Zhu, S.Liu, Y.Song, L.Xu. *Catalytic cracking of C_4 alkenes to propene and ethene: Influences of zeolites pore structures and Si/Al_2 ratios*. Applied Catalysis A: General. 2005; 288(1 - 2): p. 134 - 142.

12. Vu Xuan Hoan, U.Bentrup, M.Hunger, R.Kraehnert, U.Armbruster, A.Martin. *Direct synthesis of nanosized-ZSM-5/SBA-15 analog composites from preformed ZSM-5 precursors for improved catalytic performance as cracking catalyst*. Journal of Materials Science. 2014; 49(16): p. 5676 - 5689.

13. C.H.Cheng, G.Juttu, S.F.Mitchell, D.F.Shantz. *Synthesis, characterization and growth rates of aluminum- and Ge, Al-substituted silicalite-1 materials grown from clear solutions*. Journal Of Physical Chemistry B. 2006; 110(45): p. 22488 - 22495.

14. Q.Li, Z.Wu, B.Tu, S.S.Park, C.S.Ha, D.Zhao. *Highly hydrothermal stability of ordered mesoporous aluminosilicates Al-SBA-15 with high Si/Al ratio*. Microporous And Mesoporous Materials. 2010; 135(1 - 3): p. 95 - 104.

15. A.Ungureanu, B.Dragoi, V.Hulea, T.Cacciaguerra, D.Meloni, V.Solinas, E.Dumitriu. *Effect of aluminium incorporation by the "pH-adjusting" method on the structural, acidic and catalytic properties of mesoporous SBA-15*. Microporous and Mesoporous Material. 2012; 163: p. 51 - 64.

16. Z.Luan, J.A.Fournier. *In situ FTIR spectroscopic investigation of active sites and adsorbate interactions in mesoporous aluminosilicate SBA-15 molecular sieves*. Microporous and Mesoporous Material. 2005; 79(1 - 3): p. 235 - 240.

17. M.Stöcker. *Gas phase catalysis by zeolites*. Microporous and Mesoporous Material. 2005; 82(3): p. 257 - 292.

18. Vu Xuan Hoan, M.Schneider, U.Bentrup, Dang Thanh Tung, Phan Minh Quoc Binh, Nguyen Anh Duc, U.Armbruster, A.Martin. *Hierarchical ZSM-5 materials for an enhanced formation of gasoline-range hydrocarbons and light olefins in catalytic cracking of triglyceride-rich biomass*. Industrial and Engineering Chemistry Research. 2015; 54(6): p. 1773 - 1782.

CONVERSION OF RUBBER SEED OIL TO BIO-LUBRICANT USING SUPER ACID CATALYST

Dam Thi Thanh Hai[1], Tran Tan Viet[2], Do Chiem Tai[1], Tong Thi Thom[1]
[1]*Petrovietnam University*
[2]*Ho Chi Minh City University of Technology*
Email: haidtt@pvu.edu.vn

Summary

Non-edible vegetable oils can be potential alternatives to mineral oils for lubricant base stocks owing to their inherent properties such as high viscosity, high boiling range and biodegradability. In this research, rubber seed oil fatty acid methyl ester (RSOFAME) polymer was derived by polymerisation reaction from RSOFAME to be used as a bio-lubricant base stock. During the reaction, the super-acid HBF4 was used as a homogeneous catalyst. The reaction efficiency strongly depended on the reaction time (1 - 6 hours), reaction temperature (120 - 220°C) and the mass ratio of oil: catalyst (0 - 6wt%). The resulting products were confirmed by GC-MS, FTIR spectroscopy and also analysed for viscosity. The polymerisation product has a higher viscosity than FAME and RSO (96.98cSt, 5.32cSt and 37.0cSt respectively) but lower iodine value (gI_2/100g) than FAME and RSO (81.2, 132 and 134 respectively). In addition, the properties of the polymerisation product are better than refined mineral oil properties such as high flash point temperature (255°C), and high viscosity index (131.4). The best viscosity value of RSOFAME polymer was 96.98cSt and 12.97cSt at 40°C and 100°C respectively when the conditions of the polymerisation reaction were 200°C, a reaction time of 2 hours, and the oil: catalyst mass ratio of 6wt%.

Key words: *Bio-lubricant, rubber seed oil, polymerisation reaction.*

1. Introduction

The rising demand for mineral-based lubricants continuously adds to the petroleum energy supply tension and their concurrent harmful effects on the environment have led to increasing interests in the development of bio-lubricants from renewable resources.

Plant-based oils are an important part of developing new strategies, policies, and subsidies that aid in reducing the dependence on mineral oil and other non-renewable sources. These oils are promising candidates as base fluid for eco-friendly lubricants and able to replace the mineral-oil-based lubricants because of their unique chemical structures, structurally similar to the long-chained hydrocarbons in mineral oils, and their excellent lubricity, viscosity-temperature characteristics, non-toxicity, renewability and biodegradability. In addition, the development of a lubricant from non-edible vegetable oil feedstock is advantageous as it can overcome the economic, environmental and food versus fuel issues associated with edible vegetable oils [1, 2].

However, these lubricants are limited by low oxidative stability, filter clogging tendency and poor thermal stability. In general, it has been widely understood that the internal 1, 2 disubstituted unconjugated double bonds and the hydrogen atoms on the β-carbon atom of the alcohol fragment in ester molecule lead to poor oxidative and thermal stability [3, 4]. Consequently, vegetable oil has to be chemically modified by transesterification [5] or polymerisation [6] to eliminate vulnerable sites for oxidation and to interrupt the formation of crystals at low temperature. Goodrum and Geller [7] found that castor methyl ester and Lesquerella oil methyl ester also enhanced lubricity to acceptable levels at concentrations below 1%. It is believed that the high concentration of the unique fatty acid methyl ester methyl ricinolate could be responsible for the lubricity enhancing properties of castor oil methyl ester. As a general observation, cationic polymerisation of fatty acids or of fatty acid methyl esters, by using the BF_3 as a catalyst, was described in the literature [8]. The cationic oligomerisation of fatty acids to dimeric and trimeric acids catalysed by acidic clays at higher temperatures (230 - 240°C) is discovered [9].

Cationic polymerisation of natural oils or methyl ester of vegetable oil such as soybean, Jatropha, and palm oil has improved the oil stability for bio-lubricant base stock [10, 11]. However, the cationic polymerisation of rubber seed oil (RSO) has not reported discover. The biggest disadvantage of RSO is very high concentration of free fatty acid (FFA), therefore the oil remains unsuitable for many applications. On the other hand, the presence of high FFA is not a limiting factor in the case of bio-lubricants prepared from

fatty acid methyl ester (FAME). Taking this as an advantage, the present study concentrated on the use of unsaturated FAME rich rubber seed oil (82%, unsaturation) for lubricant base stock preparation [12 - 14].

2. Methods and materials

2.1. Materials

RSO is pressed from the seeds in Binh Phuoc province, Vietnam in December 2014. The oil has a dark yellow colour and no impurities, and is used as a feedstock directly for reaction. Oil samples were analysed to determine the composition of fatty acids by gas chromatography GC-MS analysis and the results were showed on Table 1.

This methanol (grade: chromasolv), tetrafluoroboric acid (HBF_4), acid sulfuric (H_2SO_4) 98% potassium hydroxide powder (ACS reagent, ≥ 85%, pellets) and calcium hydroxide powder (ACS reagent, ≥ 95.0%) were purchased from Sigma-Aldrich and were used directly without further purification.

2.2. Preparation of FAME from RSO

This was due to the fact that RSO oil had a high free fatty acid value; hence, a modified two-step process of Hanny and Shizuko was used to produce FAME from RSO. This method included acid esterification followed by base transesterification [15].

In the first step, RSO was esterified with methanol to lower the fatty acid content catalysed by H_2SO_4. In the second step, the product of the first step was used for the base transesterification. The calculated amount of KOH (catalyst) and methanol was added for each reaction for the temperature and reaction time specified. The residual methanol in the crude FAME was removed by a rotary evaporator and then twice subjected to hot water (80°C) washing to remove residual glycerol and soap. The washed FAME was then dried and purified and FAME was obtained.

2.3. Polymerisation of FAME

The polymerisation was performed under different operating conditions, including various mass percentage value of tetrafluoroboric acid (HBF_4) from 0 to 6%wt, at reaction temperatures from 130°C to 220°C, and five reaction times from 0 to 6 hours.

Table 1. *Composition of fatty acids in RSO*

Fatty acid	Formula	Composition (wt. %)
Palmitic acid ($C_{16:0}$)	$C_{16}H_{32}O_2$	10.102
Stearic acid ($C_{18:0}$)	$C_{18}H_{36}O_2$	10.704
Oleic acid ($C_{18:1}$)	$C_{18}H_{34}O_2$	25.605
11-Octadecenoic acid, (Z) ($C_{18:1}$)	$C_{18}H_{34}O_2$	1.436
Linoleic acid ($C_{18:2}$)	$C_{18}H_{32}O_2$	37.054
Linolenic acid ($C_{18:3}$)	$C_{18}H_{30}O_2$	15.099

The synthesis of polymer from FAME was carried out in a three-necked flask. Firstly, FAME was introduced and then the catalyst was loaded with various percentage values. The reaction was conducted under protective atmosphere of nitrogen and using a glass condenser with circulating cooling water, which was connected with the second neck of the flask. The flask was heated by an electric heater with magnetic stirrer. A magnetic stirrer of 2.0cm radius was used to stir the reaction mixture. After the reaction was completed, the mixture was chilled to 60°C and calcium hydroxide powder was added to the mixture to neutralise the catalyst. The mixture was stirred for a period of 20 minutes at 60°C in a heater. Then, the oil was separated by vacuum filtration at 60°C. All experiments were repeated three times, and the value reported in this paper was the average value.

2.4. GC-MS analysis

Oil samples were analysed to determine the composition of fatty acids by gas chromatography GC-MS analysis with DB-1 column and the FAME produced were analysed on HP-5 column with MSD 5973 equipment (Hewlett Packard) operating in EI mode at 209eV and 1µl of each sample was injected into the column. The carrier gas used was helium at a constant flow rate of 1.4ml/min. The components were identified based on their retention time of peak.

2.5. FT-IR analysis

The identification of functional groups present was carried out through Fourier Transform Infrared Resonance (FT-IR). FT-IR analysis was done by placing the sample on sodium chloride plate (sample holder) to form a thin layer of sample. The second NaCl plate was taken and mounted on the first NaCl plate. The plate was then placed on the sample holder ready for FTIR analysis. The range of wave number used was 4000cm^{-1} to 500cm^{-1}.

2.6. Rheological property

The kinematic viscosity of the RSO-biolubricant was determined according to ASTM D 445 (ASTM Standards, 1995), which is an important characteristic of any lubricating oil, which measures the resistance of a fluid to flow under gravity at a definite temperature.

A Cannon-Fenske Opaque (Reverse-Flow) viscometer with viscometer number Y604 and a size of 150 was selected and used throughout this study. The capability of a lubricant to show good viscosity is determined by its viscosity index. Lubricants with a high viscosity index tend to display less change in viscosity with temperature and this property is desirable for most lubricants. The viscosity index was obtained by referring to ASTM D 2270 after finding the kinematic viscosities at 40°C and 100°C.

2.7. Physical characterisation

Standard ASTM (American Society for Testing and Materials) methods were followed to study the physical and chemical properties which included the iodine value, acid value, water content, and density. All the analysis was carried out in triplicate and an average was taken.

3. Results and discussion

The present study explored the potential of the unsaturated non-edible RSO for the development of a biodegradable lubricant base stock. Table 2 shows the results of the physicochemical characterisation of RSO compared with FAME from RSO. The colour of rubber seed oil was light brown after clarification and it remained liquid at room temperature. The density of RSO and FAME was found to be 0.915g/cm^3 and 0.886g/cm^3 respectively which implies that both oils are less dense than water and that there is no heavy element present in the oil. The physicochemical characters seem to be similar to that of common vegetable oils and hence validate the claim that RSO can be exploited as a base stock for developing an environment friendly lubricant. Iodine number gives an idea about the degree of unsaturation of the oil and its oxidation stability. The iodine value of 134gI_2/100g indicates that RSO is a semi drying oil. The acid value of RSO is 42.7, extremely higher than that of FAME, which indicates high levels of free fatty acids which might be a limiting factor in its use as a biolubricant directly. It is true that RSO has higher free fatty acids compared with some other vegetable oils. But there are several approaches which can be adopted to deacidify RSO such as chemical re-esterification, physical refining or conventional alkali de-acidification [2]. In this research, transesterification by two steps method reduced acid value from 42.7 (RSO) to 0.4 (FAME).

Table 2. *Physicochemical characterisation of RSO and FAME*

Oil type	RSO	FAME
Colour	Light brown	Light yellow
Density (g/cm^3)	0.915	0.886
Acid value (mg KOH/g)	42.7	0.4
Iodine value (gI_2/100g)	134	132
Water content mass %	0.223	0.01
Viscosity at 40°C (cSt)	37	5.32

The characteristic formation of the oil strongly depends on fatty acid composition. According to the GC-MS result, RSO consists of five types major fatty acids and the percentage composition of them was in the following order: linoleic acid, oleic acid, linolenic acid, stearic acid, palmitic acid (37.054%, 25.605%, 15.099%, 10.704% and 10.102% respectively). Similar trends were observed by M.Mahbub et al. when conducting quantitative analysis of RSO. The high percentage of unsaturated fatty acid in RSO (more than 80%) provides compelling evidence of the liquid form of oil at room temperature.

3.1. Effect of temperature on the synthesis of biolubricant

Temperature is the major focus of parameter in this present study because it strongly affects the rate of reaction. Polymerisation is a temperature dependent reaction, where higher temperatures enable more energy delivery to overcome the minimum activation energy required in the reaction in order to result in more successful particle collisions. Thus, the product yield can be improved. The effect of temperature on the conversion of FAME to biolubricant was carried out in the batch reactor via polymerisation of FAME with tetrafluoroboric acid as the catalyst. The reaction temperatures investigated were ranging from 130°C to 220°C. Some literatures and published research work of optimum parameters for palm based biolubricant production have also been referred prior to carry out this study [11]. Therefore, in this temperature study, the molar ratio, the amount of catalyst used as well as the oscillation settings remain constant throughout the experiments. The effect of temperature on viscosity of the reaction during cationic polymerisation of FAME is presented in Figure 1. According to Ionescu et al., the increase of viscosity is a direct measure of the efficiency of the polymerisation process and the linoleic acid polymerises more rapidly to high molecular weight polymers. As can be seen, the viscosity of the reaction product was almost increased 2 times when the reaction temperature changed from 130°C to 200°C, which is consistent with the results obtained in previous studies. In addition, the conjugated double bonds in hydrocarbon chain are significantly reactive in cationic polymerisation reaction condition with superacids [16]. As expected, the reaction product has higher viscosity than FAME as a result of cationic polymerisation involving double bonds which

are consumed during the reaction. The reaction temperature is higher than 200°C, resulting in solid polymers, therefore, the liquid product is less in amount and less in viscosity values.

3.2. Effect of reaction time on the synthesis of biolubricant

Beside the temperature, the reaction time plays an important role in cationic polymerisation reaction on the conversion efficiency in biolubricant production with superacid catalyst. The increase of viscosity during the cationic polymerisation of FAME is small in the first 1 - 2 hours of reaction but very strong after 3 - 6 hours. Figure 2 shows the viscosity increase during the polymerisation of FAME with tetrafluoroboric acid (3% mass), at 200°C. The increase of viscosity proved the increase of high molecular weight species with time.

3.3. Effect of the percentage of catalyst on the synthesis of biolubricant

A tetraflouroboric acid (HBF_4) which is the most common superacid was used in the present study because HBF_4 is one of the cheapest superacids available commercially. It is known from the literature that superacids in pure form or as a solution in organic nonprotic solvents are catalytically active for oil polymerisation because water in solution destroys the carbocations, which is important species of cationic polymerisation. In addition, the polymerisation reaction of fatty acid derivatives with only one internal double bond does not occur even though superacid has been used.

Figure 3 shows the effect of tetrafluoroboric acid concentration on viscosity after 3 hours of reaction. In this figure, the viscosity of biolubricant product of reaction with 0% mass of catalyst is small (8cSt compared with 5.32cSt of reactant), which implies that thermal polymerisation occurs in this case but the reaction rate is too slow.

When the percentage of catalyst increases from 0 to 6wt%, the viscosity of product increases rapidly. However, the concentration of superacid was more than 6wt%, the rate of reaction was very difficult to control and generated solid polymerisation product.

Figure 4 illustrates the decrease of iodine value, which is a direct measure of the double bond content, with time, during the cationic polymerisation of FAME. In addition, iodine number gives an idea about the degree of unsaturation of the oil and its oxidation stability. The iodine value was reduced from 134 (RSO) to 81.2 (polymerisation product), which implied that a huge number of double bone content in RSO was reacted under superacid condition.

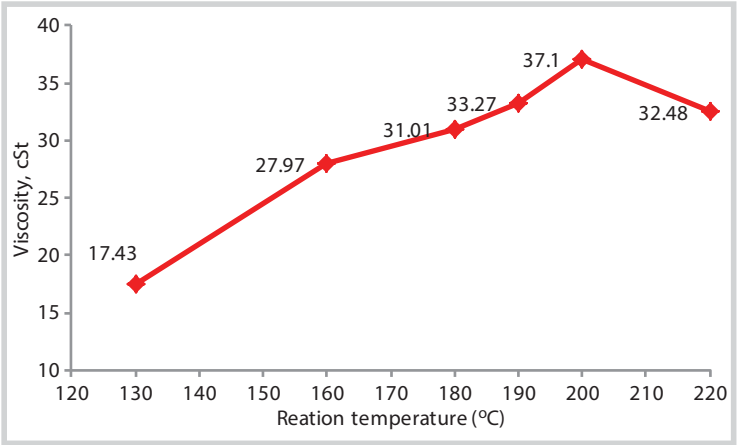

Figure 1. *Effect of reaction temperature on the product's viscosity (reaction time: 3 hours, 3% mass of catalyst)*

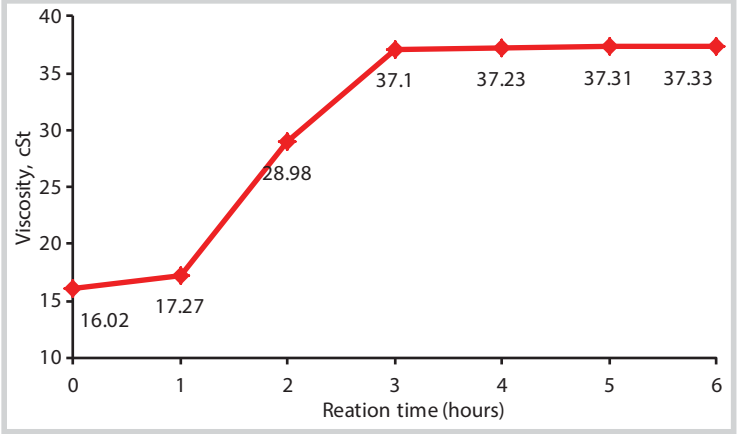

Figure 2. *Effect of reaction time on the product's viscosity (reaction temperature: 200°C, 3% mass of catalyst)*

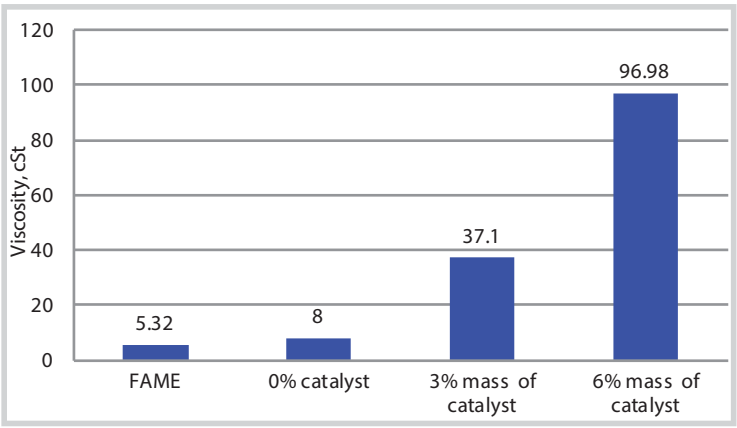

Figure 3. *Effect of percentage of catalyst on the product's viscosity (reaction temperature: 200°C, reaction time: 3 hours)*

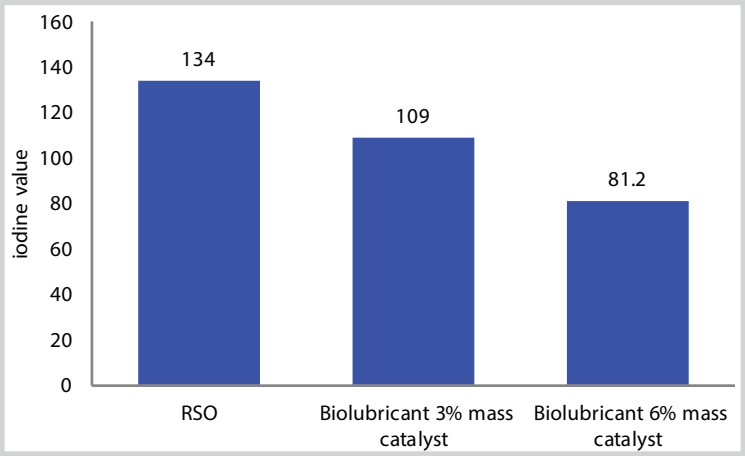

Figure 4. *Iodine value of RSO and various biolubricant products*

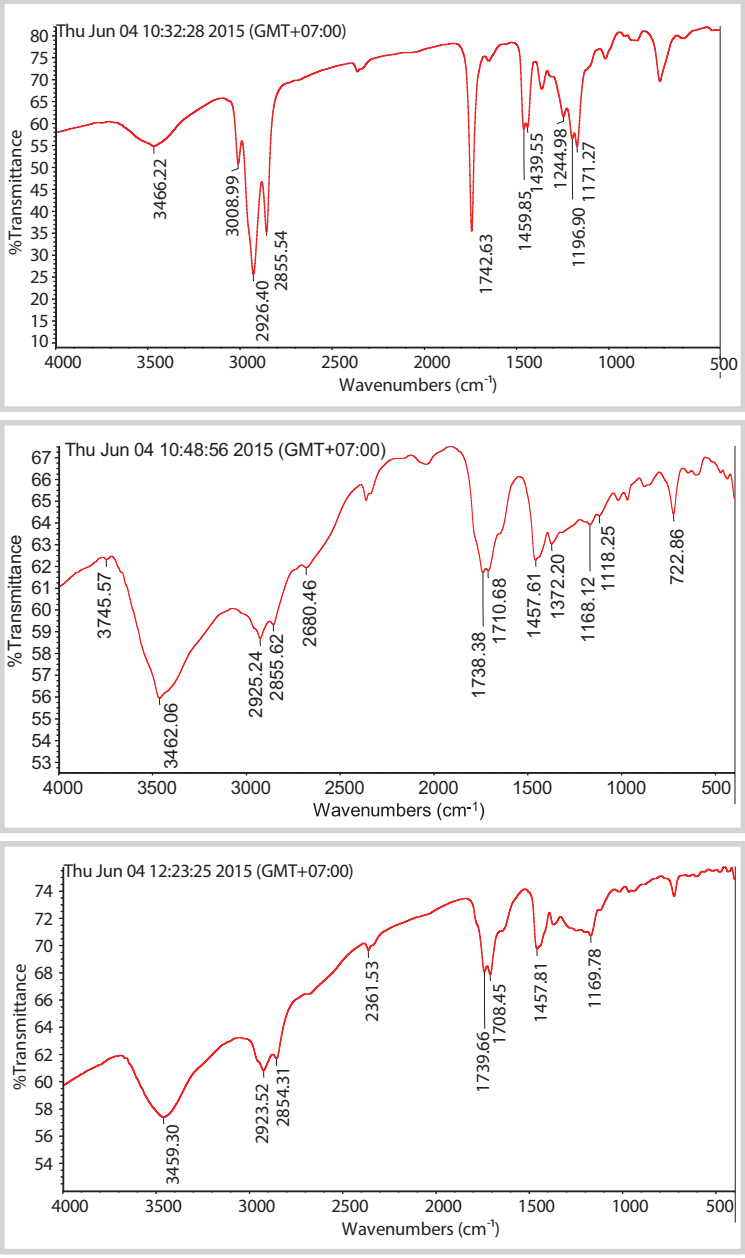

Figure 5. *FT-IR spectra of initial RSO, FAME and polymerised FAME*

Moreover, the formation of polymer was confirmed by the disappearance of C=C groups following FTIR analysis.

Figures 5 shows the FT-IR spectra of initial RSO, FAME and polymerised FAME after 6 hours of reaction, respectively. The spectrum from the FTIR analysis displays several absorption peaks of C-C=C symmetric stretch double bonds at 1675 - 1600cm^{-1}, of various C-H from CH_2 groups, CH groups and CH_3 groups (2925cm^{-1}, 2854cm^{-1}, 1163 - 1463cm^{-1}). Functional groups representing C = O (1737, 1738cm^{-1}) and the C-O bands of esters (1117 - 1118cm^{-1}) are clearly visible in the spectra.

The important peaks observed in the FTIR spectrum of polymerised FAME is the absorption characteristic of "cis" double bonds at 790cm^{-1}. On the other hand, the FTIR spectra of FAME, the absorption bands from the "cis" double bonds were lower intensity. This result suggests that the rearrangement of some initial "trans" double bonds of FAME to "cis" double bonds occurs under the polymerisation reaction conditions.

The polymerisation of FAME with superacid has increased the oil stability. Table 3 shows the lubricant characterisation of the polymerisation product in comparison with FAME. Based on this table, the flash point of polymerisation product is high at 255°C compared to the flash point of FAME which was at 140°C.

The polymerisation of FAME with superacid has increased the oil stability. Table 3 shows the lubricant characterisation of the polymerisation product in comparison with FAME. Based on this table, the flash point of polymerisation product is high at 255°C compared to the flash point of FAME or normal lubricating oil which is at 140°C and 210°C, respectively. The high value of flash point and the less amount of double bond content in the polymerisation product suggest that the oil thermal stability has been increased.

In addition, the lubricant characterisation of polymerisation product was compared with the properties of FAME and RSO. As shown in Tables 2 and 3, the value of viscosity followed the order polymerisation product > RSO > FAME at 40°C (96.98cSt, 37cSt and 5.32cSt respectively). The

Table 3. *Lubricant characterisation of the polymerisation product and FAME*

Oil type	FAME	Polymerisation product
Density (g/cm^3)	0.886	0.929
Viscosity at 40°C (cSt)	5.32	96.98
Viscosity at 100°C (cSt)	0.03	12.97
Flash point, °C	140	255
Iodine value (gI_2/100g)	132	81.2
Viscosity index	-	131.4

evidence points to the possibility that in many cases, increase in viscosity can contribute to certain types of the slight branching and mass increases in the ester structure.

Based on the viscosity at 40°C and 100°C, the viscosity index of polymerisation product was determined and compared with the viscosity index of refined mineral oil and synthetic oil in the market. Generally, their viscosity index is around 100 and 150 and the result implied that the polymerisation product has high viscosity index. High viscosity index indicates little changes in oil viscosity with temperature therefore it forms better protective layer or film surrounding the metal surfaces [2].

4. Conclusion

By chemically modifying plant oil through polymerisation reaction of FAME of RSO with super acid HBF_4 catalyst, the characteristics of products such as viscosity, flash point, and oil thermal stability can be improved. The effect of temperature reaction, reaction time, the percentage of superacid catalyst on the synthesis of biolubricant was studied and the best reaction conditions were 200°C, reaction time 2 hours, and oil: catalyst mass ratio of 6wt%. Our results provide compelling evidence that the oil stability has increased and reduced the amount of double bond content in the synthetic ester structure by the polymerisation of FAME. The polymerisation synthetic ester with high lubricant characteristics such as viscosity, viscosity index, and flash point allowed it to be utilised as biolubricant base stock.

Acknowledgment

The authors acknowledge financial support from Petrovietnam University under grant number GV1521.

References

1. P.Nagendramma, S.Kaul. *Development of ecofriendly/biodegradable lubricants: An overview*. Renewable Sustainable Energy Reviews. 2012; 16(1): p. 764 - 774.

2. S.J.Randles. *Chapter 3: Esters in Synthetics, mineral oils, and bio-based lubricants: chemistry and technology* (L.R.Rudnick, editor). Boca Raton: CRC Press Inc. 2006.

3. P.Hamblin. *Oxidative stabilisation of synthetic fluids and vegetable oils*. Journal of Synthetic Lubrication. 1999; 16: p. 157 - 181.

4. P.S.Lathi, B.Mattiasson. *Green approach for the preparation of biodegradable lubricant base stock from epoxidized vegetable oil*. Applied Catalysis B: Environmental. 2007; 69(3, 4): p. 207 - 212.

5. V.V.Bokade, G.D.Yadav. *Synthesis of bio-diesel and bio-lubricant by transesterification of vegetable oil with lower and higher alcohols over heteropolyacids supported by clay (K-10)*. Process Safety and Environmental Protection. 2007; 85(5): p. 372 - 377.

6. M.Ionescu, S.ZPetrović. *Polymerization of biological oils with superacids*. Patent US 7501479 B2. 2009.

7. J.W.Goodrum, D.P.Geller. *Influence of fatty acid methyl esters from hydroxylated vegetable oils on diesel fuel lubricity*. Bioresource Technology. 2005; 96(7): p. 851 - 855.

8. S.W.Turner, C.W.Blewett. *Process for production of polybasic acid esters with recovery of boron trifluoride*. Patent US4973743 A. 1990.

9. S.Z.Erhan, M.O.Bugby. *Polymerization of vegetable oils and their uses in printing Inks*. Journal of the American Oil Chemists' Society. 1994; 71(11): p. 1223 - 1226.

10. K.S.Hayes. *Polymerization of unsaturated fatty acids*. Patent US3632822. 1972.

11. L.R.Rudnick. *Synthetics, mineral oils, and bio-based lubricants: chemistry and technology*. Boca Raton: CRC Press Inc. 2013.

12. M.Mahbub, F.Kaniz. *Rubber seed oil as a potential source for biodiesel production in Bangladesh*. Fuel. 2011; 90(10): p. 2981 - 2986.

13. A.S.Ramadhas, S.Jayaraj, C.Muraleedharan. *Biodiesel production from high FFA rubber seed oil*. Fuel. 2005; 84(4): p. 335 - 340.

14. A.Junaid, Y.Suzana. *Study of fuel properties of rubber seed oil based biodiesel*. Energy Conversion Management. 2014; 78: p. 266 - 275.

15. J.B.Hanny, H.Shizuko. *Biodiesel production from crude Jatropha curcas L.seed oil with a high content of free fatty acids*. Bioresource. Technology. 2008; 99(6): p. 1716 - 1721.

16. W.C.Ault, J.C.Cowan, J.P.Kass, J.E.Jackson. *Polymerization of drying oils*. Industrial Engineering Chemistry. 1942; 34(9): p. 1120 - 1123.

WIND POWER DEVELOPMENT IN VIETNAM: SOLUTIONS TO REDUCE GENERATION COST

Le Viet Trung[1], Le Ngoc Anh[1], Nguyen Thanh Luan[1], Nguyen Tien Vinh[2], Tran Khanh Viet Dzung[2]
[1]*Vietnam Petroleum Institute*
[2]*Vietnam Oil and Gas Group*
Email: trunglv@vpi.pvn.vn

Summary

Vietnam is estimated to have an advantageous position to develop wind energy. However, the current status of Vietnam's wind energy industry has yet met such great expectation, due to the uncompetitiveness of the cost of wind power generation. There have been few solutions to this problem, while the government's policies have not been supportive enough. This paper will present the lessons from the countries around the world and also from the wind power projects that have been developed in Vietnam in order to propose practical solutions for reducing generation cost of wind energy. The paper also uses these solutions to examine the factors that influence the generation costs of a wind power project in Vietnam (Hoa Thang Wind Power Project). The research finds that the generation cost varies from 7.01 to 9.14¢/kWh, depending on different measures (compared with 12.26¢/kWh in the reference case). However, beside optimistic scenarios which are hard to happen in the near future, wind generation costs in other cases are all higher than 7.8¢/kWh - the tariff set by the Government for wind power. If the Government does not increase the tariff, wind power projects in Vietnam will face huge challenges in attracting commercial investors.

Key words: *Wind energy, wind power project in Vietnam, generation cost.*

1. Introduction

Vietnam has favourable natural conditions to develop wind power. Besides the World Bank's estimate of nearly 512,000MW [1], another report [2] also calculates the theoretical wind energy potential of Vietnam at 80m height to be up to 430,000MW. The areas which have an average wind speed of at least 6m/s exceed 2,676km^2 and the respective capacity can be installed is estimated at approximately 26,760MW. Although nearly 50 wind power projects have been registered to be constructed in Vietnam with a total capacity of almost 5,000MW, only 3 projects have been built and put into operation (Tuy Phong project, Phu Quy project and Bac Lieu project) by 2014. One of the main reasons for the slow development of those projects is their high production cost which makes it difficult for them to compete with the traditional power plants. There are suggestions that the current electricity purchase price of 7.8¢/kWh according to the Government's regulations for wind projects is not really cost-effective for investors.

Meanwhile, the global statistical data shows that in the 1980 - 2003 period, wind power production cost of the world was reduced by 3 times; from 15¢/kWh to only 5¢/kWh, thanks to a series of cost reduction solutions applied. Therefore, while waiting for the Government to issue new regulations on electricity purchase price that is more attractive for investors, it is necessary to conduct researches to actively reduce the production cost of wind power. This article will focus on analysing the experience of the world and some lessons learned from the wind power projects which have been implemented in the country in order to propose a number of solutions for reducing the costs of wind power in Vietnam.

2. Overview of wind power generation cost

2.1. Global wind power market

The technical potential of wind energy in the world has been assessed at nearly 94 - 95TW (with the regions having an average wind speed of 5m/s at height of 10m above ground level) and concentrates in North America (11TW), EU and Russia (73.5TW), while the rest of the world just has limited potential (10.4TW) [3].

The share of renewable energy is 22.1% of total world energy consumption by the end of 2013, showing a strong growth in comparison with 8% in 2011 and 19% in 2012. In particular, wind power accounts for 2.9% of total world energy consumption [4].

The installed capacity share of wind power is approximately 57% of the total power capacity of renewable energy in 2013. The average growth of wind power capacity during the period 2005 - 2014 reached 23%. By the end of 2014, the total capacity of wind power is 369.6 GW and the new installed capacity is about 37GW. The share of wind power market has shifted from the Eurozone to Asia during the period 2001 - 2014; while the market share of Europe has decreased by nearly half from 71% in 2001 to 36.25% in 2014, that in Asia has increased almost 5 times from 8% in 2001 to 38% in 2014 [3, 5, 6].

Europe had an annual growth rate of new installations of 9.8% in the period from 2000 to 2014 and its total installed capacity was approximately 134GW (8,045GW offshore wind power) by 2014, concentrating mainly in the EU-28 with 96.1%. Asia has 6 years in a row leading the world in new installed capacity, which reached 141.96GW in 2014, mainly in China and India (accounting for 96.6%). North America has a total capacity of 78.1GW by 2014, with growth rates of about 30%/year over the period from 2001 to 2012, then decreased significantly in 2013 and 2014. The United States is leading the region with 84.3% of the capacity. The share of the remaining areas is only about 4.2% of the total wind power capacity in the world [6].

Although the wind energy industry has seen great development in the past decades, the turbines are still supplied by a limited number of manufacturers. Among the top 10 wind turbine manufacturers in the world, there are 5 from Europe (Vestas - 13.2%, Enercon - 10.1%, Siemens - 8%, Gamesa - 4.6% and Nordex - 3.4%) and 3 from China (Goldwind - 10.3%, United Power - 3.9%, Ming Yang - 3.7%), and the others are GE from US (4.9%) and Sulzon Group from India (6.3%) [7].

2.2. Wind power generation cost

For wind power, levelised cost of energy (LCOE) is often used to examine the cost of producing a kWh or MWh of electricity from wind. LCOE of a wind power project is proportional to the investment cost, capital cost, operating and maintenance cost (O&M) and inversely proportional to the power factor/performance (based on wind speed and turbines), turbine life-time. LCOE is calculated using the following formula:

$$LCOE = \frac{R_E \times C_0 + \sum_{t=1}^{T} \frac{(1-Tax) \times VC_t - Tax \times (I_t + Dep_t)}{(1+d)^t}}{\sum_{t=1}^{T} \frac{Q_t(1-Tax)}{(1+d)^t}}$$

Where:

LCOE is levelised cost of energy (cent/kWh);

R_E is percentage of equity (%);

C_o is total fixed cost (cent);

Tax is corporate income tax (%);

VC_t is variable cost in year t (cent);

I_t is cost of borrowing in year t (cent);

Dep_t is depreciation in year t (cent);

Q_t is production in year t (kWh);

d is discount rate (%).

According to data collected from the 2014 projects of IRENA [8] and IEA [9], the investment cost for onshore projects ranged from USD 1.28 million to USD 2.29 million/MW (USD 2.7 million - USD 5.07 million/MW for offshore projects). Operation and maintenance (O&M) cost is about USD 12 - USD 32/MWh (USD 21 - USD 28/MWh for offshore projects). LCOE of onshore wind power is in the range of 6¢/kWh to 12¢/kWh depending on the cost of investment and operation, longevity and wind energy turbines. For offshore wind power, LCOE is higher than that for onshore since the costs of installation, operation and maintenance are higher and in the range of 10¢/kWh to 21¢/kWh. The main factors affecting the cost of wind power are as follows:

2.2.1. Fixed costs

Fixed costs are the total cost of initial investment before the plant goes into operation. Fixed costs of wind power projects include the cost of the wind turbine, the cost of building infrastructure, grid connection cost and other fixed costs. Fixed costs account for 64 - 84% of the total cost of the project life [5, 10].

Turbine prices fell continuously during the period 1980 - 2000 due to improved technologies and the expansion of production from pilot projects to commercial scale. The price downs to the lowest around USD 700/kW in 2002 [5]. However, the turbine price in the next period increased due to the soaring in demand and the limitations of the supply chain of wind power equipment [10]. Price turbine orders increased from USD 1,130/kW in 2004 to USD 1,730/kW in 2009. By 2014, turbine prices fell by 30 - 35% compared with

the peak in 2009 when the producers scaled up to meet the new demands from the US and China. In addition, the base metal prices also fell, contributing to pulling turbine prices down to around USD 931 - USD 1,174/kW in the US and USD 676/kW in China in 2014 [8].

Construction costs include the cost of building the foundation, internal roads, as well as the cost to build a system of lines, sub-stations, and other ancillary works. The foundation of onshore wind projects is mainly made of concrete, so most of its costs depend only on the price of construction materials such as cement, steel, sand, and stone, etc., and cost of transporting these materials to the construction site. The average construction cost for onshore wind power projects is 4 - 10% of the total fixed costs, and for offshore wind projects is 15 - 25% [8].

Grid connection cost depends on the distance and type of grid (high or low voltage) that the wind farm will connect to, so this cost will vary between projects in different countries. The average cost of grid connection in Spain in 2006 was EUR 115.24/kW and increased to EUR 131.18/kW in 2008 [10]. IRENA [8] used average data for the countries and estimated that the average cost of connection for onshore wind projects ranges from 9 - 14% of the total fixed cost, and for offshore wind projects from 15 - 30%.

2.2.2. Variable costs

One of the most advantages of wind power as well as other forms of renewable energy is zero fuel costs. Thus the variable cost of wind power accounted for only 10 - 20% of the total cost compared to 40 - 60% in gas-fired power projects. Data from Germany from 1997 - 2001 showed that O&M costs ranged from 0.39 - 0.52¢/kWh (for projects under 2 years) to about 0.78 - 0.91¢/kWh for onshore projects. On average, O&M accounts for 26% of the variable cost of the projects in Germany. However, the variable cost of wind power has also changed a lot over time and varies widely between countries and regions as well as between locations around the world. For example, data from the US showed that O&M expenses decreased from 2.4¢/kWh for projects in 2013 to 1¢/kWh for projects since 2014 [8, 10, 11].

2.2.3. Production output

While fixed costs and variable costs decide the total cost of the project, wind power production output is the most important part of the decision on the cost per unit of energy produced. This is also a factor explaining the difference of the cost of wind power among countries and projects. Wind power output depends on the project location, farm design and the nominal capacity of the turbine. Data about the number of maximum operating hours among the different regions not only demonstrates the potential of wind, but also reflects the nominal capacity of turbine used. The number of maximum operating hours of North America is considered the world's largest, ranging from 2,628 to 3,942 hours (corresponding to the power factor of 30 - 45%), Europe 2,190 - 3,066 hours (corresponding to the power factor of 25 - 35%), China and Korea 1,752 - 2,628 (corresponding to the power factor of 20 - 30%). The average level for an onshore project is usually from 1,700 - 3,000 hours/year (Spain: 2,342 hours, Denmark: 2,300 hours, and England: 2,600 hours) [5, 8, 10].

2.3. Lessons learned from reducing costs of wind power

2.3.1. Technical improvements

- Turbine technology improvement

Improvements in technology such as design, materials used, operating procedures and logistics, enable the development of larger size turbines with lower costs. The average capacity of turbines in the United States increased from 0.7MW to 1.5MW in 5 years from 1999 to 2005, then stabilised at 1.5 - 2MW and currently up to 7MW. In addition, the height of tower increases from 55m in 1999 to more than 80m, the rotor diameter is also raised from 50m to more than 90m during this period. Similarly, in Germany wind power projects are also using more and more large-scale turbines. The capacity of the new turbines installed continuously increased from less than 0.5MW in the period from 1990 to 1992 up to 2 - 3MW turbines since 2006. Turbines bigger than 3MW also began to appear in 2003 and accounted for nearly 20% of newly installed turbines in 2011. Meanwhile in China, the biggest change in turbine technology is the average capacity, which has been continuously increased over the years, from 850kW in 2005 to more than 1.5MW in 2011. Larger capacity turbines will significantly reduce the number of towers, the area of used land and the costs of infrastructure construction such as road construction, tower foundation, or the cost of cables, leading to reduction of initially fixed costs [12 - 15].

With the characteristics of Vietnam's wind energy, the interviews with experts show that the suitable model for

turbine can be the 1.5MW. This is also the popular model for many manufacturers, and therefore easy to purchase, repair and replace. However, when selecting the turbine, it is also important to consider the simulation and detailed information based on project inputs. In general, the selection of 2MW turbine for Phu Quy project, 1.5MW turbine for Tuy Phong project and 1.6MW turbine for Bac Lieu project has proved suitable for the wind conditions of each project. It should also be noted that equipment selection must take into account all other factors such as climate and geographical condition, transportation, O&M costs, etc.

- Localisation

For countries like the US and China, localisation of wind turbine manufacture also significantly reduces the cost. The proportion of imported equipment in the total investment of wind power projects in the US fell considerably, from more than 64% in 2005 - 2006 to around 33% in 2011 [13]. The greater domestic production capacity helps to reduce costs of transportation of imported equipment from Europe. In addition, local firms can also provide better warranty service, maintenance and replacement of equipment, which help to save time and costs in the operation of wind farms.

The fast growth rate of installed capacity helped the rapid development in wind power equipment manufacture industry in China. So far, China has basically been producing parts of the wind turbine. When the wind power projects have to ensure the provisions of the localisation rate of 70%, foreign firms opened production facilities in China. Policies supporting local businesses allow local firms to rapidly scale up, utilise local resources and increase their market share in the wind power equipment market. Using the domestically manufactured devices is the most important economic solution for wind power projects in China to reduce costs. Among the benefits are lower turbine price, cheaper shipping cost, and avoidance of import taxes. Particularly, the price of domestically manufactured turbines is estimated to be 20 - 30% lower than that of imported turbines [16 - 19].

At present, Vietnam does not have enough capacity and funding for localisation of key equipment (turbines and propellers). Therefore, the only way is to choose equipment supply that has reasonable cost. Wind turbines can be divided into two groups based on their country of origin: from countries outside the G7 (China) and from G7 (Table 1). Accordingly, if using Chinese equipment, the price will be cheaper. However, the quality is lower (Table 1). Currently, there is a number of domestic enterprises in Vietnam that have sufficient capacity to produce towers such as UBI Tower, Vina Halla, and CS Wind, etc. The price is about USD 200,000/MW and may continue to fall after negotiations. However, using local towers is only really economically effective in case the investment size is large enough.

- Project location

Investors prefer looking for locations with good wind potential, and placement of wind farms that make the best use of the advantages of terrain and geology. The place which has the best wind resources in the US may have a power factor of over 40% [13]. In China, wind farms are concentrated in three regions in the North, namely Xinjiang, Gansu and Inner Mongolia, where the potential of wind resources is high. However, these areas are quite far from areas having large demand for electricity such as Liaoning, Shanghai and Guangdong in the eastern coast. Hence, the requirements for transmission lines are really big. A new direction in China today is to invest in the South, where the wind speed is low but the area is near the power consumers. The solution is to use the height tower and large blade turbine (up to 108m). Greater costs due to the use of this turbine will be offset by lower costs of investment in the power line and all production will be consumed.

The wind farm location also has a great impact on the effectiveness of the project and wind power generation cost in Vietnam. Tuy Phong project is one of the most successful projects, since it has one of the best locations

Table 1. *Comparison of wind turbines*

	Turbines from G7 countries	**Turbines from China**
Manufacturers	Vestas (Denmark), Enercon, Siemens, Repower (Germany), Gamesa (Spain), etc.	Sinovel, Dongfang, Sany, Goldwind
Characteristics	Tested for quality, reliability. High performance	Quality is lower. Operating time that has proven is short
Price	USD 1,100 - 1,400/MW	USD 900 - 1,000/MW
Time to supply	More than 6 months	4 - 6 months

with great wind energy potential, favourable terrain characteristics, proximity to the grid (1.5km) as well as to other key transportation infrastructures such as ports, and a far distance from the community. On the other hand, Phu Quy project was set up on the island with the purpose of supplying power for the local communities amid difficulties in connecting to the national grid. The project also faces challenges in equipment transportation, construction, and unfavourable weather conditions. Meanwhile, Bac Lieu project was selected to site at a coastal area. Despite great wind potential, the unique terrain characteristics make the project construction cost go up sharply and exceed the initial estimates.

2.3.2. Economic and management factors

- Economy of scale

Besides the use of larger size turbines, wind power projects in the world are also growing in scale to take advantage of the economy of scale. Increasing in size combined with increasing in turbine capacity can reduce the area of used land and the cost of renting. In addition, Lewis & Wiser [20] estimated the turbine price can be reduced about 5 - 10% when purchased in bulk. Qiu & Anadon [21] estimated production cost can be reduced from 6 - 8.9% if the project size is doubled.

Selecting the scale of investment is a solution to the rational use of resources, avoid unnecessary costs and thereby reduce costs incurred for wind power projects. However, the choice of scale depends on many factors. From the practical experiences in Vietnam, the experts (from REVN, Bac Lieu and Phu Quy projects) have estimated that for an onshore project in Vietnam, investors should give priority to large-scale projects and the lowest threshold to be considered for investment is 30MW.

- Learning experience

Another factor that can help the wind power company to increase efficiency and reduce costs is learning through the production process (learning-by-doing and learning-by-searching). Expanding production brings experience in production management and organisation, and therefore reduce the cost of manpower and time. Cost is reduced when manufacturers learn from each other, and the cost can be cut from 1.1 - 5.06% depending on the size of the manufacturer [21]. The lessons from some implemented projects in Vietnam (Phu Quy, Tuy Phong and Bac Lieu projects) show that good management of wind power projects may help save 15 - 20% of investment cost. The process of good governance for a wind power project needs to co-ordinate the work contemporaneously, to select the suitable and qualified contractors and ensure the progress of construction and installation of turbines, etc.

- Government policies

In the US, common policy applied to wind power projects is the Renewable Portfolio Standard - RPS. In California, the company was forced to increase its power generation from renewable energy by 1%/year and this had to reach 20% in 2010, with adjustments later in 2010 to 25% for the period 2011 - 2013 [5]. The Production Tax Credit (PTC) policy has the greatest impact on the development of wind power in the US in the 2000s. PTC began in 1992 under the provisions of the Energy Policy Act and has been extended six times. PTC reduces the corporate income tax component, thereby reduces the cost of wind power in the United States a lot. In addition, a revenue-based PTC thus promotes wind power plants to maximise annual production [5]. Modified Accelerated Cost Recovery System (MACRS) allows devices such as turbines, electrical systems, and transmission devices to enjoy 200% accelerated depreciation over 5 years. With the rules, tax and accounting methods in the United States, accelerated depreciation helps reduce and optimise the taxation part of the first year, increase taxes to pay part of the project the following year, thus reducing total taxes and thereby reducing production costs.

In Germany, the Renewable Energy Act (EEG), which came into force in 2000 and was amended in 2004, 2008, and 2012, is the most important policy to support the development of wind power in Germany. Accordingly, wind power projects in the first 5 years will receive higher premium tariff, which was about 11.93¢/kWh from 2012. Actual production after 5 years will be measured and if it is lower than the reference site, the time to enjoy high prices will be extended. Then lower basic tariff will be applied for the remaining years. Furthermore, projects which started before 2015 and meet the requirements of the System Service Regulation will receive a bonus of 0.63¢/kWh, while the repowering wind farm projects will receive 0.65¢/kWh [22].

In China, the development policy for renewable energies started in the period 1986 - 1993, but after 2003 it saw incredible growth of the market with the introduction of national wind power procurement programme. With this programme, the government chooses the locations

Table 2. *Incentives for the development of wind power market in Vietnam*

	Scope	Content
1	Power buyer	- EVN or authorised body is responsible to buy electricity - Legal responsibility under power purchase contract
2	Incentives	- Waiver of import tax - Waiver or reduction of corporate income tax (10% in the first 15 years, able to extend to 30 years; tax waiver in the first 4 years, 50% reduction in the next 9 years) - Waiver or reduction of land fee
3	Tariff (for grid-connected)	- Tariff at connection hub is VND 1,614/kWh (7.8US¢/kWh, excluding VAT) - Tariff adjusted according to exchange rate of VND/USD. The government subsidise VND 207/kWh (1US¢/kWh) from the environment protection fund

which have good wind potential and organises bidding to select investors with the lowest prices. The Renewable Energy Law in 2005 continued to concretise the priority development of renewable energy in a number of key measures. The first is mandatory that electricity producers must have a minimum of 3% of electricity generated from renewable energy (other than hydropower) before 2010, and then this level will be raised to 8% in 2020. The Chinese government also requires the transmission company to provide connectivity line and buy all electricity production from renewable energy. Feed-in-tariff is also applied to four different areas, ranging from 7.7¢/kWh in regions with high wind energy potential as Inner Mongolia and up to 9.2¢/kWh for areas with less potential for wind power development [19, 21, 23].

The tax incentives for imported equipment in China also reduce the cost of imports and the turbine domestic products. Specifically, since 2004 the import tax on turbines was reduced by 8% and that on equipment was reduced to 3% if they were used for domestic projects. Besides, in 2008 China adopted a policy of tax refund for turbines and related components with a capacity over 2.5MW in order to encourage technology transfer. For the domestic industry, the domestic wind power equipment only bear 50% of VAT. Corporate income tax for the wind power projects is also exempted for two years, and then exempted 50% for the next 3 years [16, 19, 24]. Also in 2008, to encourage the production of large turbines, each local firms (at least 51% stake) will receive USD 88,000/MW for the first 50 turbines with a capacity of 1MW [24]. This policy has helped firms such as Sinovel to catch up with major international brands such as Vestas and Enercon in the production of large-scale turbines.

To promote the development of wind power market in Vietnam, the role of the Government is very important. The energy prices in Vietnam are not very high, there are many incentives and preferential treatment offered by the Vietnamese Government to the wind power industry. Decision 37 dated 29/6/2011 offers incentives and preferential treatment in terms of funding, tax and fee to wind energy projects as shown in Table 2.

Under Decision 37, Electricity of Vietnam (EVN) has the responsibility for buying the whole electricity output from wind power projects with the electricity buying price at the point of electricity receipt being VND 1,614/kWh (excluding VAT, equivalent to 7.8US¢/kWh). This current subsidised tariff is too low in comparison with that in other ASEAN countries (19US¢/kWh in Thailand and 21.8US¢/kWh in the Philippines). The low power purchasing price is also a big barrier to wind energy projects.

3. Cost reduction of wind energy in Vietnam

3.1. Overview of wind power development in Vietnam

Up to date, only 3 projects are already operating[1] and around 42 wind power projects of 3,900MW are being implemented at various stages. The average size of projects is 95MW of capacity, with projects from 50 - 100MW being the most popular. About a third of the projects are developed by foreign investors. According to the Vietnamese Power Master Plan VII, Vietnam has set a target for wind power development at 1,000MW by 2020 that accounts for 0.7% in the power mix in 2020, and 6,200MW by 2030.

Wind power projects are approved by the Government in co-ordination with related Ministries, Departments and

[1] *In 2011, Tuy Phong project in Binh Thuan province was completed for phase 1 with a capacity of 30MW to be grid-connected by Vietnam Renewable Energy Joint Stock Company (REVN). In 2012, the wind-diesel system developed by Petrovietnam with a capacity of 6MW for Phu Quy island also in Binh Thuan province started operation. In 2013, Bac Lieu near-shore project completed its phase 1 with a capacity of 16MW. Phase 2 and Phase 3 of the project are also being implemented with the total capacity of 500MW to be achieved around 2016.*

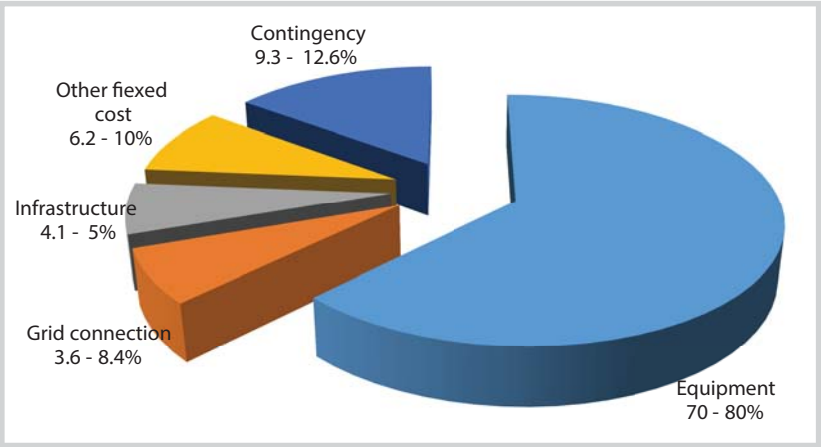

Figure 1. *Fixed cost components for wind projects in Vietnam*

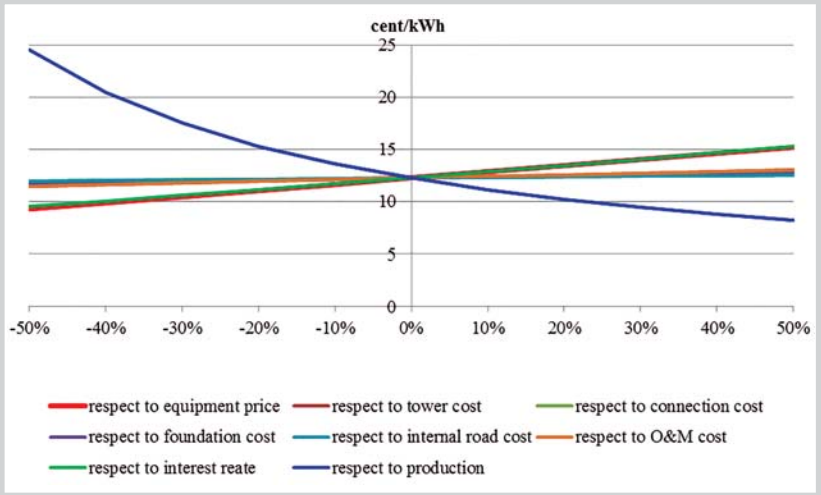

Figure 2. *Sensitivity analysis for factors affecting generation costs*

Agencies. Decision 37/2011/QD-TTg dated 29/6/2011 on the financial mechanism to support grid-connected wind power projects is the key legal document detailing the incentives. Besides, Circular 96/2012/TT-BTC dated 8/6/2012 provides more details for the developers and authorities in implementing and starting the operation of wind power projects. In particular, EVN will purchase electricity from wind power projects at the price of VND 1,614/kWh - equivalent to 7.8US¢/kWh, with the exchange rate to be adjusted to the rate set by the Government. Apart from being relatively low compared to the development cost of wind power, the actual procedures to receive the Government's support can be lengthy.

The cost for wind generation in Vietnam is decided by 3 major components: fixed cost, variable costs and electricity production. Fixed cost includes equipment, which varies from USD 1.5 to 1.7 million per MW and accounts for 70 - 80% of the total fixed cost. Other fixed cost items are grid connection, which ranges from USD 78,000 - 160,000/MW depending on the project's specific features; infrastructure costs which can be around 4 - 5% of the total fixed cost; and other items including contingency - about 9 to 12% of the total fixed cost (Figure 2). Variable costs in Vietnam comprise of O&M costs, which are around 2% of the fixed cost, equivalent to 0.8 - 1.21US¢/kWh. However, these figures can increase sharply due to both the climate characteristics in Vietnam and the expertise of local operators. Variable costs also include interest payments - which vary significantly from project to project, and corporate income tax, which is waived for the first 4 years with profit, and 50% of the standard rate (10%) for the next 9 years. For electricity production, the capacity factor in Vietnam is estimated to be from 34.2 - 37.5% (full load hour from 3,000 - 3,285 hours/year according to the FS of projects). But the figure again can change according to project location, for example Phu Quy project can achieve maximum capacity factor of 47.9% and 4,204 full load hours. All these cost estimates however only become more reliable when more and more projects are put into operation for a considerable period.

3.2. The cost of wind projects in Vietnam

3.2.1. Generation cost of wind energy

This section will deal with generation cost for onshore wind projects. The project selected for cost calculation is Hoa Thang wind power project invested by Petrovietnam. In terms of cost per kWh, estimate has been made for the reference scenario (base case), based on a number of assumptions as follows:

- The project is expected to be built on an area of about 734 hectares in Hoa Thang commune, Binh Thuan Province. The project uses equipment of Vestas manufacturer (Denmark), with a capacity of 49.5MW. The plant is connected to the national power system with 110kV voltage level. The distance to 110kV line is 5.5km from the 110kV transformer substation to the nearest transit of EVN;

- Annual energy output of each turbine is 3,715MWh, the wind farms

generate an output of 122,598.1GWh/year for 33 turbines, which is equivalent to full load hours of 2,477 (25% capacity factor);

- Total investment in the entire project (before taxes, not including interest) is USD 118 million (as estimated by the investor) and power project investment of about USD 2.39 million/MW. In which, the cost of equipment accounts for 64.4% of total fixed costs;

- O&M costs are assumed to be 2% of the total cost of equipment investment and construction, equivalent to 1.51¢/kWh;

- The lifetime of the turbine is set at 20 years;

- The debt/equity ratio is assumed to be 80% and 20% respectively, with interest rate of 8%/year, repayment period of 10 years and a grace period of 2 years. The discount rate is 10%.

Based on these assumptions, the generation cost of wind power production (LCOE) of Hoa Thang project is calculated at 12.26¢/kWh. 0 shows the impact caused by a 10% change of a number of key variables on wind power generation cost for Hoa Thang project, as compared with the base case. It can be seen that the generation cost of the project is mostly influenced by power output (for each 10% increase in output the price will reduce by nearly 10%), equipment cost and interest cost. The remaining factors such as the cost of wind towers, grid connection cost, O&M, etc. also affect the cost of wind power production but with lower level of impact.

3.2.2. Cost reduction senarios

The aim of this section is to propose a choice of measures that can contribute to reducing generation costs of wind energy in Vietnam. In general, the measures should concentrate on the variables or factors that most influence the cost of a wind energy investment. According to the solutions and sensitivity analysis mentioned above, these are as follows.

- Capacity factor or the output;

- Capital cost, which in turn driven by using equipment (Turbine, blade, sub-components etc.) from G7 or non-G7 equipment (China);

- O&M costs;

- Access to cheap capital finance.

According to the solutions proposed above, the reference scenario and cost reduction scenarios are summarised in Table 3. The difference of these scenarios is the selection of key equipment (turbines and its sub-components) from the manufacturer of the G7 countries or outside the G7 countries (China). For each option of the source device, there are two scenarios which are feasible scenario (likely scenario) and optimistic scenario (the most favourable conditions possible). According to the four proposed scenarios, the generation cost can be significantly reduced from 12.26¢/kWh to less than 9.14¢/kWh. However, except the optimistic scenarios (Scenario 2 and 4) which are difficult to prevail in the near future,

Table 3. *Scenarios to reduce wind power generation cost in comparison with base case*

Criteria		Reference case	G7 equipment		Non-G7 equipment (China)	
			Feasible (Scenario 1)	***Optimistic (Scenario 2)***	***Feasible (Scenario 3)***	***Optimistic (Scenario 4)***
1	Equipment	G7 equipment	G7 equipment		Non-G7 equipment[b]	
2	Price discounts[a]	No discount	Discount 5%	Discount 10%	Discount 5%	Discount 10%
3	Wind tower	Imported tower	Vietnam-manufactured tower			
4	Grid connection to 110kV	Self-invested	Self-invested	EVN invested (saving VND 29.56 billion)	Self-invested	EVN invested (saving VND 29,56 billion)
5	Internal road costs	As in FS	Saving 50% cost due to reduction of internal roads			
6	O&M costs[b]	2% of equipment	2% of equipment	2% of equipment	5% of equipment	5% of equipment
7	Interest rate	8%/pa	5%/pa	3%/pa	5%/pa	3%/pa
8	Output (million kWh/year)[c]	122.59	122.59	128.73 (Reference case + 5%)	122.59	128.73 (Reference case + 5%)
9	Contingency (% of capex)[d]	13.4%	13.4%	10%	13.4%	10%
	Generation cost (cent/kWh)	12.26	9.14	7.01	8.99	7.14

[a] Price discount for buying equipment can be up to 2%, 5% or 10%, depending on negotiation; [b] O&M cost for G7 and non-G7 equipment are 2%/pa and 5%/pa of Capex.
[c] Output can be raised by 5% with above-mentioned technical solutions; [d] Contingency cost is 10% by Vietnamese laws for projects less than 1 year, 13.4% for projects above 2 years. If project management is well applied, the project can be finished within 1 year.

other scenarios can reduce the generation cost to a certain degree, but still the final figure is higher than 7.8¢/kWh, the level that the Government sets for EVN to buy power from wind power projects. Therefore, it is possible to reduce the cost of wind power in Vietnam by some extent, but it is not an easy task to get to the level as low as set out by the Government.

Besides, the results show that if the favourable conditions in 2 optimistic scenarios do happen, using the equipment from China for Hoa Thang project will not be as efficient as using those from G7 (as compared between Scenario 2 and 4). The reason is O&M cost for non-G7 turbines is about 5% of Capex cost, significantly higher than the 2% level of G7 wind turbines. This makes the lower Capex from non-G7 manufacturers not a huge advantage after taking into account considerable variable costs over the years.

4. Conclusions and Implications

This paper aims to analyse the generation costs and solutions to reduce this cost for wind power production in Vietnam and other countries. The results show that capex costs, full load hours, and financial costs are three main factors that have the most impacts on generation costs. Lessons to make wind energy more competitive in other countries as well as from projects developed in Vietnam reveal three main solutions. First is the technical solutions. These include improvements in location selection process, wind measurement, project design and appraisal, turbine's rated capacity, turbine manufacturers and related O&M issues. Second is the economic-financial and management solutions. These include solutions to access credit, improve project management, minimise construction delays and related cost escalation. Third is the policy solutions. These include the measures taken by the Government to support local wind industries, as well as solutions to support directly wind projects in terms of electricity price, taxes and other incentives.

These solutions have been analysed and applied for a case study in Vietnam (Hoa Thang project). The results show that the generation cost varies from 7.01¢/kWh to 9.14¢/kWh, depending on different measures (compared with 12.26¢/kWh in the reference case). However, beside the optimistic scenarios which are hard to happen in the near future, wind generation costs in other cases are all higher than 7.8¢/kWh - the tariff set by the Government for wind power. Therefore, with such low level for renewable, wind projects in Vietnam will face huge challenges to attract commercial investors.

In order to develop wind energy in Vietnam, the Government should have a long-term plan for localisation of the equipment as well as attracting more foreign manufacturers to the country. Besides, the financial costs of a wind project can be sharply reduced if the project can access the assistance from the Government in terms of official guarantee, including ODA funding or special interest rates from state-owned banks. Also, the Government can consider to raise the power price to ensure the minimum margin for wind investors. In practice, the wind energy investors in Vietnam still keep complaining about very low purchasing price while the current cost of electricity generated from wind power plants is still quite high due to large technical investment. Discussion with various experts and stakeholders in Vietnam as well as our research results reveal that a power price around 10 - 12¢/kWh might be needed to make the wind energy projects become more financially feasible. If the price of wind energy (Feed in Tariff) is not increased to region levels, it will be very difficult to attract foreign investors.

References

1. Năng lượng Việt Nam. *Tiềm năng năng lượng gió của Việt Nam*. http://nangluongvietnam.vn/news/vn/dien-hat-nhan-nang-luong-tai-tao/tiem-nang-nang-luong-gio-cua-viet-nam.html. 2012.

2. AWS Truepower. *Wind resource Atlas of Vietnam*. AWS Truepower report. 2011.

3. WWEA. *World wind resource assessment report*. WWEA technical paper series. 2014.

4. REN21. *Renewables 2014 global status report*. 2014.

5. IRENA. *Renewable power generation costs in 2012: An overview*. IRENA report. 2012.

6. GWEC. *Global wind report 2014 - Annual market update*. Global Wind Energy Council. 2015.

7. Kevin Smead. *Top 10 wind turbine suppliers*. Energy Digital. November 2014: p. 40 - 47.

8. IRENA. *Renewable power generation costs in 2014: An overview*. IRENA report. 2015.

9. IEA Wind Task 26: *The past and future cost of wind energy*. NREL. 2012.

10. M.I.Blanco. *The economics of wind energy.* Renewable and Sustainable Energy Reviews. 2009; 13: p. 1372 - 1382.

11. S.Krohn et al. *The economics of wind energy*. The European Wind Energy Association (EWEA). 2009.

12. EWEA. *The economics of wind energy*. European Wind Energy Association. 2009.

13. R.Wiser & M.Bolinger. *2011 wind technologies market report*. U.S. Department of Energy (U.S. DOE). 2012.

14. J.Martino. *Advancements in windturbine technology: Improving efficiency and reducing costs*. http://www.renewableenergyworld.com/articles/2014/04/advancements-in-wind-turbine-technology-improving-efficiency-and-reducing-cost.html. 2014.

15. J.Timmer. *The technical advances that could make wind power viable everywhere*. http://arstechnica.com/science/2015/06/making-wind-power-work-even-in-low-wind-locations/. 2015.

16. J.Han et al. *Onshore wind power development in China: Challenges behind a successful story*. Energy policy. 2009; 37 (8): p. 2941 - 2951.

17. Yadav. *Chinese wind tuabin manufacturers eyeing global markets - challenges and opportunities*. Chinese Wind Power 2011. 2011.

18. Z.Zhao et al. *A critical review of factors affecting the wind power generation industry in China*. Renewable and Sustainable Energy Reviews. 2013; 19: p. 499 - 508.

19. Z.Liu et al. *The economics of wind power in China and policy implication*. Energies. 2015; 8: p. 1529 - 1546.

20. J.I.Lewis, R.H.Wiser. *Fostering a renewable energy technology industry: An international comparison of wind industry policy support mechanisms.* Energy Policy. 2007; 35: p. 1844 - 1857.

21. Y.Qiu & L.D. Anadon. *The price of wind power in China during its expansion: Technology adoption, learning-by-doing, economies of scale, and manufacturing localization*. Energy Economics. 2012; 34 (3): p. 772 - 785.

22. Fraunhofer Institute for wind energy and energy system technology (IWES). *Wind energy report Germany 2011*. Last assessed: http://windmonitor.iwes.fraunhofer.de/bilder/upload/Windreport_2011_engl.pdf. 2012.

23. Q.Wang. *Effective policies for renewable energy - the example of China's wind power - lessons for China's photovoltaic power.* Renewable and sustainable energy reviews. 2010; 14 (2): p. 702 - 712.

24. Qiang Wang et al. *Cost analysis and pricing policy of wind power in China*. Journal of Energy Engineering. 2011; 137 (3): p. 138 - 150.

PV GAS strives to exceed the production plan

Mr. Nguyen Vu Truong Son, Petrovietnam President and CEO, worked with Petrovietnam Gas Joint Stock Corporation (PV GAS). Photo: PV GAS

On 28 June 2016, Mr. Nguyen Vu Truong Son, President and CEO of the Vietnam Oil and Gas Group (Petrovietnam), worked with Petrovietnam Gas Joint Stock Corporation (PV GAS) on the preliminary results of PV GAS' production and business.

In the first 6 months of 2016, PV GAS has safely operated gas projects and ensured the maximum supply possible to gas consumers, contributing to the assurance of national energy and food security. The Corporation expects to overfulfil its production target by 6 - 27%. In particular, the gas supply to customers from Cuu Long basin is expected to reach nearly 800 million m^3, which will highly exceed the planned target of the first half of 2016 (approximately 136%), equivalent to an increase of more than 30% over the same period of 2015, and contribute to increasing PV GAS' total revenue and profit.

In the last 6 months of the year, PV GAS will continue to ensure gas project operation, gas assignment and moderation to supply maximum gas and gas products to customers with the highest efficiency. At the same time, the Corporation will carefully review the preparation works and carry out the maintenance and repair of Nam Con Son, Bach Ho, and PM3 - Ca Mau systems with good quality during gas interruption phases, which are scheduled in August and September 2016, thus ensuring safety and minimising gas supply downtime.

Ho Cam

PTSC to hit estimated revenue of VND 8,900 billion

On 27 June 2016, Mr. Nguyen Vu Truong Son, President and CEO of the Vietnam Oil and Gas Group (Petrovietnam), worked with Petrovietnam Technical Services Corporation (PTSC). According to PTSC General Director Phan Thanh Tung, the sustained low oil price and the downward pressure on service prices have greatly affected the Corporation's production and business results. In the first half of 2016, PTSC expects to hit estimated revenues of VND 8,900 billion (equal to 101% of the plan) and total profit before tax of VND 700 billion (equal to 146% of the plan).

Mr. Nguyen Vu Truong Son, Petrovietnam President and CEO, worked with Petrovietnam Technical Services Corporation. Photo: PTSC

In the second half of the year, PTSC will continue to safely and efficiently manage and operate the fleet of specialised service vessels, and the FSO/FPSO. The Corporation will continue to ensure efficient implementation, the quality and progress of the projects, including Su Tu Trang, Daman, Long Phu 1 Thermal Power Plant, the packages of Nghi Son project, NPK, NH_3, and GPP Ca Mau projects, thereby confirming its reputation and capacity to provide oil and gas engineering services and other services for industrial projects.

Petrovietnam President and CEO Nguyen Vu Truong Son requested PTSC to maximise cost savings, continue to promote investment in human resource development, and improve the Corporation's competitiveness.

Hong Minh

Petrovietnam Chairman has a working meeting with Tokyo Gas

On 26 May 2016, on the sidelines of Vietnam-Japan High-level Economic Policy Dialogue in Nagoya, Mr. Nguyen Quoc Khanh, Chairman of Vietnam Oil and Gas Group (Petrovietnam), had a working session with Mr. Michiaki Hirose, President of Tokyo Gas.

The Tokyo Gas leader expressed the desire to extensively co-operate with Petrovietnam in general and Petrovietnam Gas Joint Stock Corporation (PV GAS) in particular, especially in the development of the LNG value chain in Vietnam. The two parties emphasised the importance of the co-operation and establishment of LNG trading company in Vietnam, the plan for investment in the construction and operation of Thi Vai LNG terminal project as well as the expansion and management of LNG warehouse infrastructure, and the development of Vietnam LNG market in the future.

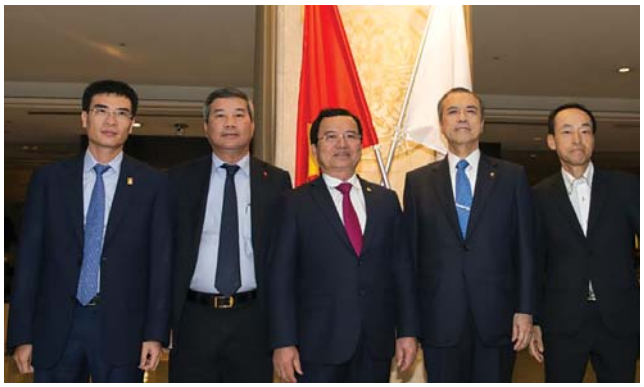

Petrovietnam and Tokyo Gas leaders at the Vietnam - Japan High-level Economic Policy Dialogue in Nagoya. Photo: PVN

Also at the conference, the Petrovietnam leader had a meeting with Mr. Hidetoshi Ohashi, Vice President of JX NOEX, a long-term partner of Petrovietnam.

Huong Giang

Petrovietnam leader works with BSR

Petrovietnam leaders checked the production and operation at Dung Quat Refinery. Photo: BSR

On 9 June 2016, the delegation of the Vietnam Oil and Gas Group (Petrovietnam) worked with Binh Son Refining and Petrochemical Company Limited (BSR) on production and business results of the first 6 months of 2016.

In the first half of the year, BSR has produced over 3.407 million tons of products, which is equal to 117% of the plan, earned a total revenue of more than VND 33.5 trillion, and contributed to the State Budget an estimated amount of VND 6.11 trillion. From the beginning of 2016, Dung Quat Refinery has been operating continuously, safely and stably with an average capacity of 103 - 105% of its design capacity, and ensuring the product quality.

Dr. Le Manh Hung, Vice President of Petrovietnam, appreciated the production and business results of BSR in recent years. He asked BSR to continue to strengthen governance and enhance competitiveness, promote research and development, assess risks of technology and equipment, and optimise production. At the same time, BSR continues to implement the plan to expand and upgrade Dung Quat Refinery and other investment projects according to schedule.

Tran Minh

PVFCCo AWARDED "TOP 50 BEST LISTED COMPANIES IN VIETNAM" PRIZE FOR THE 4TH SUCCESSIVE TIME

PVFCCo (stock code DPM) is the producer and trader of Phu My fertilisers. Photo: PVFCCo

Petrovietnam Fertilizer and Chemicals Company (PVFCCo) announced that it has continued to be honoured in the top 50 best listed companies in Vietnam stock market in 2016 by Forbes Vietnam. This is the 4th time Forbes Vietnam publicly releases the list and PVFCCo is the only member in the fertiliser industry to be honoured by the award for 4 successive years.

The ranking list recognises that PVFCCo still achieves outstanding growth in spite of the challenging year 2015, and is considered to be the most capable enterprise in the domestic fertiliser industry thanks to its effective business with turnover in 2015 reaching VND 10,047 billion, profit after tax of VND 1,488 billion, dividend payout ratio of 40%, with potential growth in the fields of fertiliser and chemical. DPM stock is evaluated to be in an attractive stock group for investors.

Bui Ha

PVEP Song Hong becomes operator of An Chau Scheme phase II

On 9 June 2016, the Petrovietnam Exploration Production Corporation (PVEP) and PVEP Song Hong signed a contract to authorise the latter to operate the scheme of An Chau phase II.

The An Chau trough lies in the northeast, spreading over the provinces of Lang Son, Bac Giang and Quang Ninh, with an area of 10,000km^2. PVEP Song Hong has accomplished the An Chau Scheme phase I with a large workload of clarifying the geological structure and petroleum geology system in this region. On that basis, the Vietnam Oil and Gas Group and PVEP decided to assign PVEP Song Hong to continue to study and implement the An Chau Scheme phase II, and authorise PVEP Song Hong to operate the petroleum contracts of 5 blocks.

Dr. Ngo Huu Hai, PVEP President and CEO, and Mr. Ha Van Tuan, General Manager of PVEP Song Hong, signed the contract. Photo: PVEP

PVEP President and CEO Ngo Huu Hai emphasised that this scheme is of important significance to the Vietnam Oil and Gas Group in general and PVEP in particular in the exploration of new oil and gas sources, and at the same time will help PVEP Song Hong improve the quality of their project management and scientific research activities in the field of petroleum prospecting and exploration.

Manh Hoa

PVC-MS commences the construction of Tho Trang 3 platform

The construction of Tho Trang 3 platform. Photo: PVC-MS

On 1 June 2016, the Petroleum Equipment Assembly and Metal Structure Joint Stock Company (PVC-MS) held a launching ceremony at Vietsovpetro port for the fabrication of Tho Trang 3 platform. This project will be implemented by PVC-MS as the construction contractor and Vietsovpetro Joint Venture as the investor.

Tho Trang 3 platform is part of Tho Trang field development project, which is located at Block 09-01 in the southern continental shelf, about 145km south east of Vung Tau city. PVC-MS is required to carry out the project with very urgent progress. It is expected that the company will complete the jacket onshore on 31 August 2016 and the topside in February 2017 in order to hand over to Vietsovpetro for offshore installation.

Hong Minh

PVC-MS COMPLETED THE LIVING QUARTER MODULE OF SU TU TRANG LIVING QUARTER PROJECT

Su Tu Trang Living Quarter has a total weight of 4,500 tons. Photo: PVC-MS

Petroleum Equipment Assembly and Metal Structure Joint Stock Company (PVC-MS) announced it has successfully completed the Living Quarter Module, which is part of Su Tu Trang living quarter project.

Su Tu Trang Living Quarter has a total weight of 4,500 tons. PVC-MS is the EPC contractor executing 3 main components: jacket, topside and living quarter module.

Currently, the company is rushing to complete the jacket, the topside and the helipad. PVC-MS will then hand over the jacket in July and the topside in August 2016 for offshore installation.

Pham Minh

PVEP strengthens co-operation with PTTEP

On 2 June 2016, the delegation of the Petrovietnam Exploration Production Corporation (PVEP) had a meeting with Mr. Somporn Vongvuthipornchai, President and CEO of Thailand's PTT Exploration and Production Public Company Ltd (PTTEP) in Bangkok, Thailand.

PVEP's leaders at PTTEP's head office. Photo: PVEP

The leaders from both parties highly appreciated the results of co-operation in recent years, especially the projects in Vietnam (Block 16-1, Block 09-2, Blocks B, 48/95 and 52/97) and Algeria (Blocks 433a and 416b). The two parties also discussed measures for managing and directing production and business activities in the context of low oil prices.

Concerning the orientation for co-operation in the coming period, PVEP and PTTEP agreed to strengthen and promote co-operation in areas of mutual interest, including the overlapping areas between the three countries Vietnam, Malaysia and Thailand, and third countries such as Iran, Algeria, and Thailand. The two parties also shared their objectives and strategic plans in the short and medium term with respect to finance, investment orientation, and organisation and administration.

Nguyen Hoa

Phu My Fertilizer Plant reaches the production landmark of 9 million tons

Phu My Fertilizer Plant. Photo: PVFCCo

Petrovietnam Fertilizer and Chemicals Corporation (PVFCCo) announced that at 11 pm on 6 May 2016, Phu My Fertilizer Plant reached the output of 9 million tons, marking another significant milestone in the process of establishment and development of PVFCCo as well as the domestic fertiliser industry.

In addition, PVFCCo is focusing on the domestic consumption market with its plan to supply 365,500 tons of various Phu My fertilisers in the second quarter of 2016. Specifically, PVFCCo plans to supply 260,000 tons of Phu My urea, 51,000 tons of Phu My NPK, 41,000 tons of Phu My kali, and 13,500 tons of Phu My DAP, meeting roughly 40% of urea fertiliser demand for the Summer-Fall crop.

Phu My Fertiliser products supplied by PVFCCo are of high quality, meeting international standards, being tested and certified by the Quality Assurance and Testing Centre 3 (QUATEST 3) and the Analysis and Testing Centre 2 - Vinacontrol. Besides, since 2015, Phu My fertiliser products have been certified by the Ministry of Agriculture, Forestry and Fisheries of Japan for meeting quality standards after the strict testing process at Japanese quality testing agencies.

Thuy Anh

Two contracts signed for Song Hau 1 Thermal Power Plant

On 1 June 2016, in Hanoi, Petrovietnam Construction Joint Stock Company (PVC) signed contracts with subcontractors for the construction of 2 items under the Song Hau 1 Thermal Power Plant project with total value of nearly VND 470 billion. Specifically, PVC has signed the contracts for the "Construction of the steel structure for turbine house of Unit 2 and the steel structure for the desulfurisation system" package with the Petroleum Equipment Assembly and Metal Structure JSC (PVC-MS) and the "Construction of the steel structure bunker" package with the Petroleum Pipeline and Tank Construction JSC (PVC-PT).

PVC signed the contract with PVC-MS. Photo: PVC

Song Hau 1 Thermal Power Plant belongs to Song Hau Electricity Centre and is located in Chau Thanh district, Hau Giang province. The plant has a total capacity of 1,200MW consisting of 2 machine units (2 x 600MW). Its investor is the Vietnam Oil and Gas Group (Petrovietnam). Lilama Corporation is the EPC main contractor while Doosan Corporation is the contractor supplying main equipment for the plant.

This is one of the national key projects under the Electricity Master Plan VII which was approved by the Prime Minister and allowed to apply the special mechanism to invest in the construction of urgent power projects pursuant to the Prime Minister's Decision No. 2414/QD-TTg dated 11 December 2013. According to the signed schedule, Song Hau 1 Thermal Power Plant will be completed and have its machine units on stream in 2019.

Once on stream, the plant will supply to the national grid approximately 7.8 billion kWh per year, thus contributing to ensuring the national energy security and economic development in the Mekong Delta in general and Hau Giang province in particular.

Minh Anh

Techcombank, PVI step up co-operation

Mr. Bui Van Thuan, President & CEO of PVI, and Mr. Ho Hung Anh, Chairman of Techcombank, signed a comprehensive co-operation agreement. Photo: PVI

On 2 June 2016, PVI Holdings and Vietnam Technological and Commercial Joint Stock Bank (Techcombank) signed a comprehensive co-operation agreement. Accordingly, Techcombank will provide financial solutions such as cash flow management, foreign exchange, and bond investors, etc., for PVI, its subsidiaries and associated companies to help PVI save operational costs and human resources, and especially maximise the efficiency of cash flow.

At the same time, PVI will design and provide quality insurance programmes for Techcombank's staff and clients with preferential fees, terms and conditions exclusively for a strategic partner of PVI.

Ha Thu


Source: jordan-engineering.co.uk

OIL AND GAS GLOBAL MARKET

Brief oil and gas activity news

Thailand's Banpu PCL has acquired a 29.4% stake in Chaffee Corners joint exploration agreement (Marcellus gas field) for USD 112 million. It is the first instance of a Thai company taking a stake in the US shale gas industry. The deal provides Banpu with a net interest equivalent 156bcfd of gas. The agreement targets the net output of 21MMcfd this year. The field lies in northeast Pennsylvania about 200 miles from New York city and is currently owned by Talisman Energy Inc., which was purchased by Repsol SA for USD 13 billion, a deal that was finalised in May 2015.

ONGC (India's state-owned Oil & Natural Gas Corp.) is seeking approval for 17 shale oil and gas exploration wells along the east and west coasts of India. The operator wants to invest USD 105 million in exploring the countrie's unconventional resource potential. If approved, this project would be the largest push for shale exploration in India but not the first. GAIL Ltd. spudded its first of eight exploratory wells in the Cambay basin in western India. Drilling began on 27 March 2016, and target depth of 2,500m was expected to be reached by mid-May. The US Energy Information Agency (EIA) estimates India has 98tcf of technically recoverable shale gas reserves.

Moroccan national oil firm ***ONHYM*** commenced drilling on its Tenerara Lakbir permit targeting Triassic sandstones at a total depth of 2,640m. ONHYM's partners include Oil and Gas Investment Funds (OGIF) and Sound Energy Morocco (SEM). In 2015 SEM acquired 37.5% interest on Phase I. SEM will assume operatorship of the license and take 55% working interest in Phase II of the project. OGIF will retain 20% and ONHYM 25%. Schlumberger will provide service, equipment, and personnel to SEM in exchange for a share of future production.

ExxonMobil Corp. has started production at its Point Thomson project on Alaska's North Slope (ANS) near the Arctic National Wildlife Refuge (ANWR). At full-rate the central pad facilities are designed to produce as much as 10,000 barrels per day (bpd) of gas-condensate and 200MMcfd of recycled gas. Point Thomson reservoir holds an estimated 8tcf of gas and associated condensate, representing 25% of the known gas on the ANS. ExxonMobil and the working-interest owners have invested USD 4 billion in the development of Point Thomson production facilities through 2015.

CNOOC Ltd. (China) started oil production from Panyu 11-5 field in the Pearl River Mouth basin. A single well is producing 3,270bpd at the water depth of 110m. The company expects peak production of 3,900bpd later this year. CNOOC said it is using facilities of Panyu5-1 and that three horizontal wells have been drilled.

Indonesia has approved the Amanah Timur No.1 (AT1) appraisal well, and ACL International Ltd.'s subsidiary Renco Elang Energy Ltd. said the well will spud before 30/11/2016. Renco is drilling AT1 to test the Paya Bili prospect at TD of 700m and to evaluate reservoir

productivity in a pre-1940 oil field as well as deeper untested sandstones.

The prospect lies within the North Sumatra basin and is one of the most productive hydrocarbon provinces in Indonesia with more than 80 known oil and gas fields. The operator estimates combined P50 unrisked resources at 442bcf of gas and 47 million barrels (MMbbl) of oil and condensate. The probability of success with identified leads range from 11% to 48%.

Carlyle Group's Black Sea Oil & Gas SRL has awarded GC Rieber Shipping a 45-day contract for seismic work offshore Romania in the Black Sea. Black Sea Oil & Gas has interest in three blocks here, which cover 5,000km^2 within the underexplored Romanian continental shelf. According to company's website, first production is expected before 2020.

Ocean Rig UDW Inc.'s recently announced acquisition of a deepwater drillship at less than 10% of its newbuild cost provides yet another signal of the dim market outlook for offshore drillers. The drillship named Cerrado was sold at auction for USD 65 million, and it has no pending contract and will be renamed the Ocean Rig Paros upon delivery to Ocean Rig. Ocean Rig expects it could generate positive cash flow and earn an attractive return on capital, subject to any additional upgrade costs with an anticipated day rate in the low USD 200,000 if awarded a multi-year tender.

Refining firms ***Indian Oil Corp. Ltd. (IOC), Bharat Petroleum Corp Ltd. (BPC) and Hindustan Petroleum Corp. Ltd. (HPC)*** are advancing a previously announced plan to jointly invest in construction of a grassroots 60 million-ton/year integrated refining and petrochemical complex in India's Maharashtra state.

IOC, BPC, and HPC have enlisted fellow partner Engineers India Ltd. (EIL) to carry out a detailed feasibility study for the complex. The project partners plan to make decisions regarding equity structure and financing for the project once site selection and the detailed feasibility study have been completed. Implementation for the proposed project likely would be 7 years following acquisition of a land site. To be built in two phases, the complex would produce gasoline, diesel, LPG, and jet fuel, as well as other feedstock for India's petrochemical industry.

Chevron USA Inc. has entered a deal for the sale of its 54,000 barrels per day (bpd) Kapolei, Hawaii, refinery and other associated Hawaiian downstream assets to Island

Energy Services LLC, a subsidiary of One Rock Capital Partners LP, New York.

As part of the agreement, Island Energy Services will purchase the refinery as well as certain distribution and retail assets located in Hawaii. Chevron's sale of the Hawaii refinery and related downstream assets comes as part of the company's strategy to optimise its portfolio by divesting noncore holdings, including its interest in Caltex Australia Ltd. and New Zealand Refining Co. downstream operations.

Similarly to Chevron strategy, Husky Energy Inc., Calgary, is to sell 65% interest in certain midstream assets in the Lloydminster region of Alberta (Canada) and Saskatchewan to Cheung Kong Infrastructure Holdings

Tweneboa, Enyenra and Ntomme (TEN) Field project offshore Ghana. Source: www.ghanaiantimes.com

Ltd. and Power Assets Holdings Ltd. (PAH). Husky will receive CAD 1.7 billion of gross cash proceeds and will remain operator with 35% interest in the assets.

Russia's Rosneft and PT Pertamina of Indonesia have signed a framework agreement to co-operate on development of a grassroots refining and petrochemical complex to be built at Tuban, in East Java, Indonesia. As part of the agreement, Rosneft and Pertamina will perform a bankable feasibility study to finance the project as well as establish a joint venture for its implementation. The companies also have agreed to execute studies to investigate the following: prospects for joint projects in the area of crude and oil products supplies, logistics, and infrastructure; potential for Pertamina to enter in Rosneft's upstream projects in Russia as an equity holder; and partnership in international joint projects for refining.

Cambodian Petrochemical Co. Ltd. (CPC) has let a contract to China National Petroleum Corp. (CNPC) subsidiary Northeast Refining & Chemical Engineering Co. to build the first phase of a proposed 5 million-ton/year refinery in Cambodia's southwestern province of Preah Sihanouk, along the Gulf of Thailand. As part of the USD 620 million Phase 1 contract, CNPC Northeast Refining & Chemical Engineering will provide engineering, procurement, and construction on the project. Construction on phase 1 of the refinery, which will have a capacity of 2 million tpy, is scheduled to begin this October and be completed by year-end 2018. In the years following

commissioning of Phase 1, CPC plans to invest in additional expansions of the refinery that will increase its overall crude processing capacity to 5 million tpy, according to the government of Cambodia. CPC's total capital investment in the grassroots refinery will be about USD 3 billion, the company said.

Saudi Aramco has entered agreements aimed to make Aramco an industrial conglomerate in a programme of sweeping economic reform called Saudi Vision 2030. The objective of the joint development agreement between Aramco with National Shipping Co. of Saudi Arabia, Lamprell of Dubai, and Hyundai Heavy Industries is to build a maritime yard in eastern Saudi Arabia to provide engineering, manufacturing and repair services for offshore rigs, commercial vessels, and offshore support vessels. Joint investment would be more than USD 400 million.

Southern African petroleum activities

Maersk, the Danish oil conglomerate, has bought into licenses covering 100,000km^2, including eight oil discoveries in the Lokichar basin of the Turkana region in northern Kenya. Four of the blocks are operated by Tullow Oil PLC and the remaining by Africa Oil.

Maersk is to pay Africa Oil USD 350 million to cover 50% of the past costs incurred before April 2016. From that date, Maersk will also carry up to USD 75 million of the company's share of development costs, with this latter amount expected also to be payable on closing. Upon confirmation of resources it will also pay USD 15 million of the company's share of exploration expenditures.

At the point of the final investment decision, Maersk will also carry up to USD 405 million of Africa Oil's share of the costs of developing the Lokichar project, the actual amount depending upon certain reserve growth thresholds being met and upon the timing of first oil. The transaction is expected to escape capital gain tax, which had been a major concern for Africa Oil, and is still subject to Kenyan government and regulatory approvals. A dozen companies had expressed interest in the licences and several offers were made. The Kenyan government was very receptive to Maersk as a partner particularly as the company is not only highly interested in the possible participation in a future pipeline but is also interested in participating in port facilities and a terminal to export Kenya's crude to the global markets.

Gabon officially launched a new 2016 offshore bid round, offering five deep fields as the country aims to reverse a slow downward trend in production. Announcing the bid round at an African Oil Week in Cape Town, the country's Petroleum and Hydrocarbons Minister Etienne Dieudonne Ngoubou said the ministry expected to finalise the bidding by mid-2016.

Gabon held its 10th licensing round for production-sharing contracts in October 2013. Bid for 18 blocks were made, of which 13 where successful, although this was reduced to nine deepwater blocks and ultra-deepwater blocks in July 2014.

In September 2014, Gabon's new hydrocarbons law was published. The law has been a cause of concern for a number of companies, many of whom are questioning the state's control in production-sharing contracts.

It enables the state to take up to a 20% stake, paid at market value, in the share capital of companies requiring or holding an exclusive use. Further, it establishes a mandatory state participation of 20% without payment in all new production-sharing contracts. In addition, the Gabon Oil Company has the option to acquire a 15% stake at the market price. The law also reinforces local content quotas, requiring 9% of workers to be Gabonese.

French major Total's announcement in 2013 that it had found hydrocarbons in Gabon's ultra-deepwater pre-salt layer raised interest. In July 2014, Eni said it had struck gas and condensate in offshore D4 block. The company estimates that the discovery may be significant with potential in place estimated at 500 million barrels of oil equivalent (boe). In October 2014, Royal Dutch Shell announced a frontier discovery offshore Gabon in a pre-salt reservoir with Block BC10. This raised hopes that offshore West Africa may contain deepwater reserves on a scale comparable to those found offshore Brazil.

Tullow Oil Company said its operated Tweneboa-Enyenra-Ntomme (TEN) development in Ghana will rapidly increase its West African production when the project comes on stream in mid-2016. Its capital budget will go from USD 1.9 billion down to USD 1.2 billion so the outlay is going down by USD 700 million and the production is going up by 50%. The project's total estimated cost is almost USD 5 billion and the output will be over 100,000bpd.

Ghana could be the first country in sub-Saharan Africa to play host to a floating storage and regasification unit

(FSRU), having contracted Golar LNG to provide one for West African Gas Ltd. (WAGL) for an LNG import facility at the port of Tema on the coast of Ghana West Africa with a planned start up in Q2 2016. Several FSRUs will be deployed in Sub-Saharan Africa as countries in the region seek to take advantage of forecast ample global LNG supply to meet growing domestic energy demand and provide an alternative to their often-unreliable existing energy supply. FSRUs have also been proposed for Benin, Ivory Coast, Namibia, South Africa, Mozambique and Kenya among other nations.

Russia Rosneft and ExxonMobil have won the rights to explore three blocks in ***Mozambique's*** latest licensing round. The US and Russian partners were awarded blocks A5-B in the Angoche basin as well as Z5-C and Z5-D in the Zambezi basin. Talks will begin with the government of Mozambique and the Institute of National Petroleum of Mozambique (INP) on the detailed terms of participation. Once completed ExxonMobil will become the operator, Rosneft announced in a statement.

South Africa's Sasol was also awarded block PT5-C adjacent to the Pande and Temane fields with partner, Mozambique's state-owned ENH. Italy's Eni was awarded block A5-A in the Angoche basin with partners Sasol and Norway's Statoil. Delonex Energy in partnership with India Oil Corporation was awarded block P5-A in the Palmeira basin. The fifth licensing round offered 15 blocks in 11 offshore and onshore areas, which will represent an investment of USD 711 million over the next four years. Bids were received from a number of companies for eight of the 15 areas on offer. INP said it would launch a new tender in October 2016. A string of significant gas discoveries in the Rovuma basin in the north-east has substantially increased the prospectivity in the country and exploration activity has picked up. Current estimates from two of five exploration blocks in Cabo Delgado province where Mozambique meets Tanzania indicate that the country holds well over 100 trillion cubic feet of gas.

Crude-oil prices

With exception of light fluctuations and short duration in February, April and May, crude-oil prices from mid-January to mid-June 2016 have continuously risen and could rise further in the rest time of this year. There is a real risk of this opinion in the present social-economic contexts, but there are some unforeseen supply disruptions in recent time, plus the security deterioration in many regions of the world which have consolidated this forecast. Following Gadfly information written on Bloomberg, EIA saw disruptions removing more than 3.6 million barrels per day (mbpd) of potential supply in May; US output declines due to the collapsing of the fracking wells as oil prices are not high enough to compensate the production costs; in Nigeria oil production has slumped under the weight of attacks on oil infrastructure, which provokes a slow-down of output to 1.45mbpd in May from 2.0mbpd in January 2016; in Libya the output fell to 250,000 barrels per day (bpd) on average in May due to the political chaos, the lowest since February 2015, and there is little chance for recovering soon.

In India, in the first quarter of 2016, liquid fuels demand grew by 400,000bpd, accounting for about 30% of the total global increase. That level is more remarkable given that India's oil demand grew at an average of 120,000bpd every year for the past decade. Similarly to China situation in 2002 when the demand of this country for oil and other commodities started to skyrocket at the acceleration of the industrialisation and economic transformation process, India is now at a structural inflection point for oil growth, with several factors responsible for the surge in demand: GDP is rising at a 7.6% annual rate; the government programme to expand the nation's highway system; and a shift towards building out manufacturing capacity to make up a larger share of the Indian economy. In this social background, India needs more oil, gasoline demand is up 14.5 %, diesel 7.5% and crude oil imports have jumped by 12% so far this year from 2015 levels, and more domestic refinery capacity is needed. Several analysts admit that India is simultaneously contributing to oil demand in today's oil market, putting a floor beneath prices, and will also be the largest driver of oil demand over the long term.

A monthly report from OPEC released on 13 June 2016 showed that the group kept forecasts for global oil supply and demand unchanged. But OPEC has also joined a growing tide of forecasters that are now calling for a less substantial decline to US production going forward, following the recent rise in prices.

After the oil futures prices settled on 13 June 2016, EIA reported that oil production from seven major US shale plays is expected to fall by 118,000bpd to 4.72mbpd in July from June, extending the overall decline over the past several months. In electronic trading shortly after the data

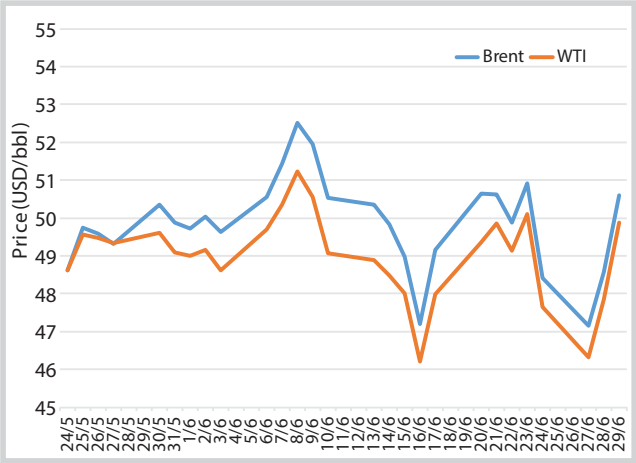

Source: www.oilcrudeprice.com

were released, WTI oil was at USD 48.84/bbl, near the day's settlement. Back on Nymex, prices for July gasoline lost 2.3 cents, or 1.5% to USD 1.536 a gallon, while July heating oil fell less than half a cent to USD 1.515/gallon. July natural gas ended at USD 2.585/MMBtu, up 2.9 cents, or 1.1%.

Gas markets

Worldwide natural gas consumption in 2016 is characterised by moderate growth after having stagnated in the past years. The inability of natural gas demand to keep pace with an accelerated supply growth lead to an imbalance in the global gas market and to a price weakness which is expected to continue in the short and medium term, amid a sluggish economic environment. Gas market in the present day are impacted by many events that include the decline in prices for all fossil fuels, the slowdown of the world economic growth combined with a booming expansion of renewable energy capacity, the fast decline of energy intensity and gas-pricing reform of user countries. Demand growth remains concentrated in a small number of countries with the North American market, under the impetus of the US and the Middle East providing the largest contribution, followed by Europe. In the US, record low gas prices alongside environmental policy initiatives are encouraging coal-to-gas switching. Strong growth is also recorded in the Middle East, under the impulsion of Iran and the UAE. In Europe, the recovery of gas demand depends on weather conditions in the winter months of the year.

Conversely, gas consumption growth comes to a halt in Asia with strong declines recorded in Japan, and South Korea and a marked slowdown in China. In North America, despite gas prices are depressed, production grows up strongly, where gas supply continues to be boosted by unconventional gas. Production also increases significantly in Asian and in Oceania countries. Reversely, it stagnates in Latin America and dwindles in Europe.

Overall, regional gas prices tend to converge except for North American prices which remain significantly lower than in the rest of the world.

New LNG supplies are coming online just as demand growth in some major markets are weakening, leading to major shifts in global natural gas trade patterns over the next 5 years, the IEA said in its 2016 Medium-Term Gas Market Report. The combined factors of cheaper coal and continued strong renewable growth were blocking gas from expanding more rapidly in the power sector. The slowdown in Asia gas demand has intensified, prompting a rare decline in the region's LNG imports. As imports from two world's top LNG buyers, Japan and South Korea, are set to decline, the rebalancing of global market will depend on the rate of expansion in China, India, and other countries in developing Asia.

While gas demand is projected to remain weak, global LNG exports will increase substantially due to global liquefaction capacity, which will increase by 45% between 2015 and 2021, mostly from the US, Qatar and Australia. Spot LNG prices will remain under pressure due to oversupply in the market horizon.

A particular trait of gas markets in the present time is the role of NGLs (natural gas liquids) in creating the current surplus of light and sweet liquids production (Tables 1 and 2) which has begun to shift pricing, trade, marketing and supply-demand balances for light-heavy versus sweet-sour crudes and in products. A "light-ends space" is emerging, not only in the US and the Atlantic basin but also globally, as markets attempt to adjust to this surge in light, low sulphur hydrocarbon supply.

Tran Ngoc Toan

Table 1. *Global LPG supply*

Unit: Thousand bpd

	2014	2015	2016	2017	2018	2019	2020	2021
NORTH AMERICA	2,143	2,225	2,268	2,401	2,516	2,609	2,677	2,738
US	1,626	1,700	1,730	1,840	1,935	2,010	2,070	2,120
Canada	315	325	336	358	367	377	379	382
Mexico	202	200	202	203	214	222	228	236
EAST OF SUEZ	3,831	3,886	3,985	4,108	4,235	4,320	4,394	4,466
MIDEAST GULF	1,921	1,998	2,067	2,132	2,208	2,278	2,336	2,411
Iran	226	250	285	315	350	380	410	440
Iraq	43	48	54	60	68	84	94	104
Kuwait	110	136	138	140	142	146	150	154
Oman	9	10	12	12	15	15	17	18
Qatar	380	410	410	413	425	430	430	435
Saudi Arabia	867	860	884	905	918	924	922	930
UAE	261	270	272	274	276	285	295	308
Yemen	25	14	12	13	14	14	18	22
ASIA PACIFIC	1,910	1,888	1,918	1,976	2,027	2,042	2,058	2,055
Australia	89	73	80	96	128	140	140	142
Bangladesh	1	1	1	1	1	1	1	1
Brunei	1	6	5	7	8	9	9	9
China	850	795	808	832	839	845	842	840
India	317	326	330	333	335	336	352	352
Indonesia	61	83	84	84	84	87	87	87
Japan	139	134	129	128	129	126	123	119
Malaysia	102	113	117	122	124	124	128	129
Myanmar	1	2	2	2	3	3	3	4
New Zealand	6	6	6	6	6	5	5	5
Pakistan	10	11	13	13	13	13	12	11
Papua New Guinea	2	3	5	5	5	5	5	5
Philippines	9	9	8	8	8	5	5	5
Singapore	30	28	27	29	32	33	33	34
South Korea	67	72	76	81	84	84	86	86
Taiwan	41	42	42	44	46	46	47	48
Thailand	146	148	151	149	147	147	145	145
Timor-Leste	19	17	16	14	12	10	9	7
Vietnam	19	19	18	22	23	23	26	26
EUROPE	1,230	1,201	1,235	1,285	1,331	1,399	1,442	1,481
Azerbaijan	8	9	13	16	16	16	18	18
France	47	40	38	35	34	39	42	44
Germany	80	83	83	82	80	78	77	75
Italy	52	57	63	75	76	74	73	72
Kazakhstan	15	15	16	18	20	20	22	23
Netherlands	52	45	45	44	44	44	43	43
Norway	241	252	265	268	270	276	282	288
Russia	573	540	552	589	638	699	736	773
Spain	51	52	54	54	53	53	53	53
UIP	111	108	106	104	100	100	96	92
AFRICA	482	490	496	520	533	555	594	607
Algeria	283	286	286	290	294	298	304	310
Angola	21	23	26	30	34	36	42	44
Egypt	55	53	55	59	61	68	74	78
Equatorial Guinea	21	21	21	21	23	30	38	38
Libya	29	35	35	42	42	42	49	49
Mozambique	2	2	2	3	3	3	4	4
Nigeria	57	61	62	65	66	68	69	70
South Africa	14	9	9	10	10	10	14	14
SOUTH AMERICA	421	438	458	482	509	528	542	560
Argentina	87	91	96	102	110	118	128	134
Brazil	179	186	190	196	206	208	212	218
Colombia	21	21	22	22	25	25	25	27
Peru	45	49	51	54	54	54	54	53
Trinidad	22	21	21	26	32	33	33	32
Venezuela	67	70	78	82	82	90	90	96
TOTAL	**8,107**	**8,240**	**8,442**	**8,796**	**9,124**	**9,411**	**9,649**	**9,852**

Sources: Oil & Gas Journal 6/6/2016

Table 2. *Global NGL supply*

Unit: Thousand bpd

	2014	2015	2016	2017	2018	2019	2020	2021
NORTH AMERICA	4,362	4,623	4,934	5,404	5,702	5,979	6,138	6,294
US	3,220	3,430	3,670	4,030	4,245	4,460	4,575	4,665
Canada	756	806	847	924	968	1,011	1,039	1,077
Mexico	386	387	417	450	489	508	524	552
EAST OP SUEZ	7,816	8,066	8,391	8,706	9,077	9,404	9,677	9,898
MIDEAST GULF	4,896	5,163	5,430	5,609	5,817	6,086	6,285	6,461
Iran	749	804	937	1,039	1,155	1,227	1,301	1,384
Iraq	63	68	77	92	123	172	202	227
Kuwait	154	180	182	183	185	189	220	238
Oman	10	14	20	20	27	45	75	76
Qatar	1,260	1,337	1,364	1,372	1,378	1,389	1,378	1,383
Saudi Arabia	1,875	1,945	2,001	2,033	2,078	2,166	2,189	2,214
UAE	760	801	837	857	857	884	902	917
Yemen[1]	25	14	12	13	14	14	18	22
ASIA PACIFIC	2,920	2,903	2,961	3,097	3,260	3,318	3,392	3,437
Australia	233	234	252	325	435	450	464	473
Bangladesh	10	13	14	19	19	18	18	17
Brunei	20	25	26	30	33	35	39	44
China	1,045	992	1,024	1,079	1,107	1,132	1,145	1,151
India	363	372	376	379	401	424	448	448
Indonesia	202	212	199	191	192	200	216	234
Japan	139	134	129	128	129	126	123	119
Malaysia	238	250	272	289	292	292	292	290
Myanmar	28	31	37	37	38	38	37	38
New Zealand	25	28	28	27	25	24	23	22
Pakistan	25	26	28	28	29	29	28	27
Papua New Guinea	3	4	6	7	9	9	17	29
Philippines	23	22	21	21	21	18	17	17
Singapore	30	28	27	29	32	33	33	34
South Korea	67	72	76	81	84	84	86	86
Taiwan	41	42	42	44	46	46	47	48
Thailand	294	300	300	287	279	278	275	275
Timor-Leste	73	57	46	34	28	22	19	15
Vietnam	61	61	58	62	61	60	65	70
EUROPE	2,661	2,701	2,814	2,912	3,018	3,190	3,322	3,433
Azerbaijan	8	9	13	16	16	16	18	18
France	48	41	39	36	35	40	43	45
Germany	80	83	83	82	80	78	77	75
Italy	52	57	63	75	76	74	73	72
Kazakhstan	266	270	303	313	338	375	432	448
Netherlands	77	67	67	65	64	63	62	62
Norway	328	342	352	357	357	366	382	396
Russia	1,628	1,660	1,722	1,799	1,888	2,014	2,076	2,163
Spain	51	52	54	54	53	53	53	53
UK	123	120	118	115	111	111	106	101
AFRICA	1,083	1,056	1,076	1,210	1,301	1,391	1,485	1,561
Algeria	675	679	689	713	737	788	824	865
Angola	25	23	38	51	58	60	76	88
Equatorial Guinea	136	126	130	174	186	187	187	182
Libya	121	100	90	128	147	178	214	241
Mozambique	6	6	7	8	8	8	9	9
Nigeria	95	102	103	116	141	146	147	148
South Africa	25	20	19	20	24	24	28	28
SOUTH AMERICA	819	876	927	995	1,075	1,138	1,182	1,223
Argentina	165	185	199	226	257	292	326	360
Brazil	212	220	228	237	249	255	261	267
Colombia	55	61	64	62	61	59	57	57
Peru	111	127	137	150	158	164	166	165
Trinidad	49	47	47	61	86	88	88	86
Venezuela	227	236	252	259	264	280	284	288
TOTAL	**16,741**	**17,322**	**18,142**	**19,227**	**20,173**	**21,102**	**21,804**	**22,409**

[1]No field production of NGLs, but production number represents refinery LPG output only.

Sources: Oil & Gas Journal 6/6/2016

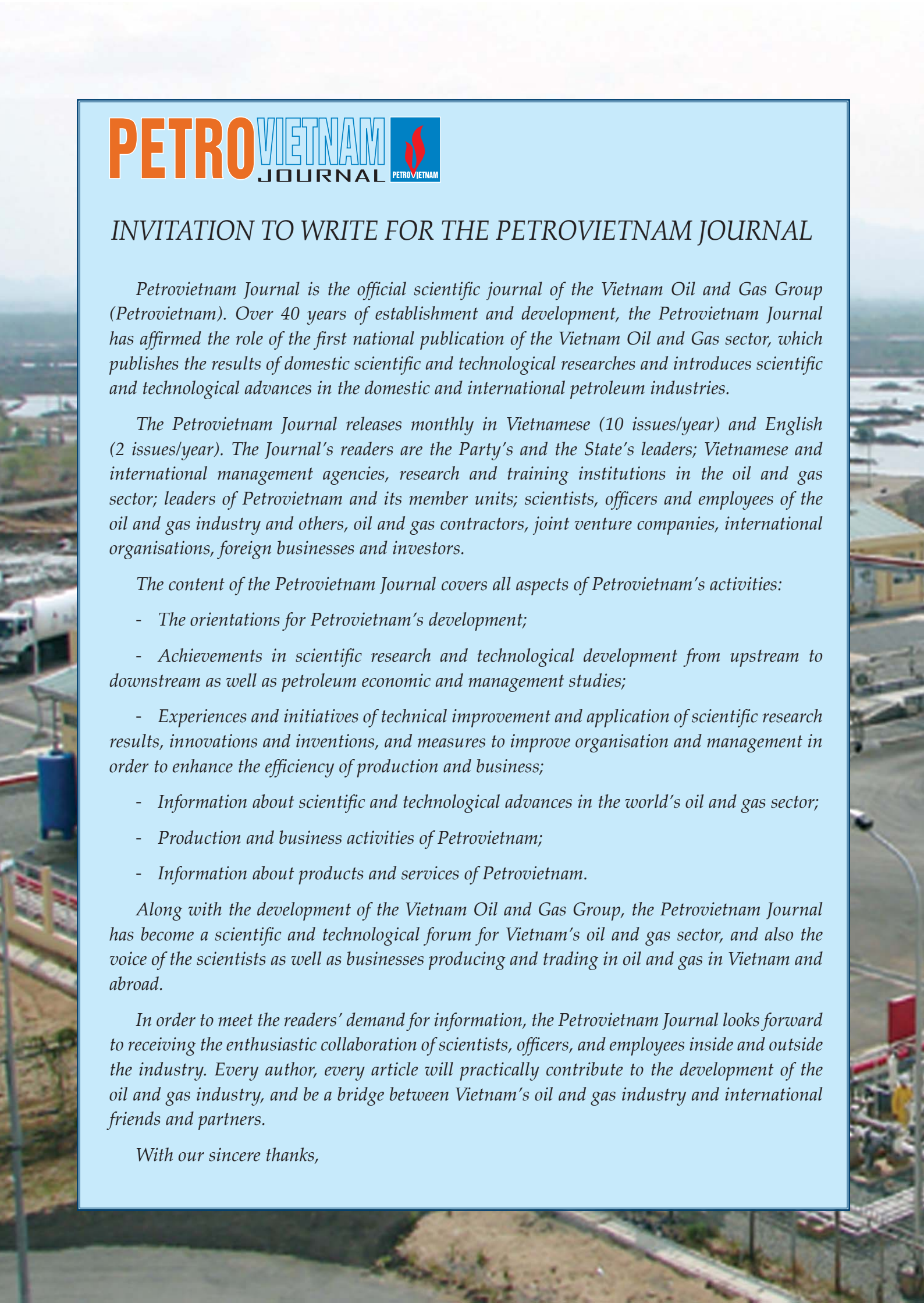

PETROVIETNAM JOURNAL

INVITATION TO WRITE FOR THE PETROVIETNAM JOURNAL

Petrovietnam Journal is the official scientific journal of the Vietnam Oil and Gas Group (Petrovietnam). Over 40 years of establishment and development, the Petrovietnam Journal has affirmed the role of the first national publication of the Vietnam Oil and Gas sector, which publishes the results of domestic scientific and technological researches and introduces scientific and technological advances in the domestic and international petroleum industries.

The Petrovietnam Journal releases monthly in Vietnamese (10 issues/year) and English (2 issues/year). The Journal's readers are the Party's and the State's leaders; Vietnamese and international management agencies, research and training institutions in the oil and gas sector; leaders of Petrovietnam and its member units; scientists, officers and employees of the oil and gas industry and others, oil and gas contractors, joint venture companies, international organisations, foreign businesses and investors.

The content of the Petrovietnam Journal covers all aspects of Petrovietnam's activities:

- *The orientations for Petrovietnam's development;*
- *Achievements in scientific research and technological development from upstream to downstream as well as petroleum economic and management studies;*
- *Experiences and initiatives of technical improvement and application of scientific research results, innovations and inventions, and measures to improve organisation and management in order to enhance the efficiency of production and business;*
- *Information about scientific and technological advances in the world's oil and gas sector;*
- *Production and business activities of Petrovietnam;*
- *Information about products and services of Petrovietnam.*

Along with the development of the Vietnam Oil and Gas Group, the Petrovietnam Journal has become a scientific and technological forum for Vietnam's oil and gas sector, and also the voice of the scientists as well as businesses producing and trading in oil and gas in Vietnam and abroad.

In order to meet the readers' demand for information, the Petrovietnam Journal looks forward to receiving the enthusiastic collaboration of scientists, officers, and employees inside and outside the industry. Every author, every article will practically contribute to the development of the oil and gas industry, and be a bridge between Vietnam's oil and gas industry and international friends and partners.

With our sincere thanks,